Computational modeling of failure in composites under fatigue loading conditions

Latifi, Mohammad

DOI
10.4233/uuid:bdf9afef-48b6-460a-bcd3-91c2e29a196c

Publication date
2017

Document Version
Final published version

Citation (APA)
Latifi, M. (2017). *Computational modeling of failure in composites under fatigue loading conditions*. [Dissertation (TU Delft), Delft University of Technology]. https://doi.org/10.4233/uuid:bdf9afef-48b6-460a-bcd3-91c2e29a196c

COMPUTATIONAL MODELING OF FAILURE IN COMPOSITES UNDER FATIGUE LOADING CONDITIONS

COMPUTATIONAL MODELING OF FAILURE IN COMPOSITES UNDER FATIGUE LOADING CONDITIONS

Proefschrift

ter verkrijging van de graad van doctor
aan de Technische Universiteit Delft,
op gezag van de Rector Magnificus prof. ir. K.C.A.M. Luyben,
voorzitter van het College voor Promoties,
in het openbaar te verdedigen op woensdag 31 mei 2017 om 10:00 uur

door

Mohammad LATIFI

Master in Mechanical Engineering,
geboren te Kerman, Iran

Dit proefschrift is goedgekeurd door de

promotor: Prof. Dr. Ir. L. J. Sluys
copromotor: Dr. F. P. van der Meer

Samenstelling promotiecommissie:

Rector Magnificus,	voorzitter
Prof. Dr. Ir. L. J. Sluys,	Technische Universiteit Delft
Dr. F. P. van der Meer	Technische Universiteit Delft
Onafhankelijke leden:	
Prof. Dr. N. Moës	Ecole Central de Nantes
Dr. B. Chen	Technische Universiteit Delft
Prof. Dr. W. van Paepegem	Universiteit Gent
Prof. Dr. Ir. R. Benedictus	Technische Universiteit Delft
Dr. A. Turon	Universitat de Girona
Prof. Dr. Ir. M. Veljkovic	Technische Universiteit Delft, reservelid

This thesis was accomplished with financial support from Ministry of Science, Research and Technology (MSRT), I.R. IRAN.

ISBN 978-94-92516-52-7

An electronic version of this dissertation is available at
http://repository.tudelft.nl/.

The clear eyes of the wise;
Beholds in every green tree, in every leaf;
A book of the wisdom of God.
(Saadi, 1184-1283)

To my wife for her support and unconditional love

CONTENTS

SUMMARY

Composite materials are increasingly used as a replacement for metals in different industrial applications such as automotive and aerospace structures, and wind turbine blades. Two main design approaches exist for these structures: One aims to prevent any damage from occurring during service life and the other allows cracks to propagate before reaching to a critical size. The latter design approach exploits the damage tolerance of composite structures. It provides a lighter and cheaper product; however, it requires a deep knowledge of the failure process in these structures. This knowledge is needed to evaluate the possibility for the occurrence of defects and to estimate the load carrying capability of a damaged structure. This highlights the importance of numerical models which can simulate the behavior of these structures under different loading conditions. In this context numerical models have been successfully applied for quasi-static analysis of structures; however, to account for fatigue due to cyclic loading is more challenging.

Fatigue models commonly describe crack growth using the Paris law which links the energy released due to delamination to the crack growth rate. Developing a fatigue model using the Paris law needs an accurate method for computing the Paris law input values of energy release rate and a method capable of representing the 3D crack front to impose the crack growth. It is difficult to satisfy these requirements with the available numerical fatigue models developed based on either fracture mechanics or damage mechanics. In the context of fracture mechanics the virtual crack closure technique (VCCT) is used for computing the energy release rate. The requirement of the VCCT that the crack front must be aligned with the element boundaries limits the application of these models especially for problems with non-self similar crack growth. On the other hand, in the context of damage mechanics, cohesive fatigue models lack an accurate computation of energy release rate and the possibility to directly impose the crack growth rate computed from the Paris law.

This thesis aims to propose a 3D mixed-mode model for simulating crack growth in laminate composites under high-cycle fatigue. The focus in this study is primarily on delamination which is an important cause of failure in composite structures. For modeling delamination under fatigue a recent fracture mechanics approach developed for quasi-static analysis with large finite elements is applied to fatigue. In this model the level set method is used to describe the crack front location and a modified version of the VCCT is employed to compute the energy release rate. Using the level set method provides an alternative approach for available fatigue models. In contrast with the classical fracture mechanics based models, this level set model does not require the front to be aligned with the element boundaries which enables simulating non-self-similar growth of delamination under fatigue.

The idea of using the level set method for modeling crack growth is further explored by developing a more general model which can be applied to the failure process other than delamination (e,g. splitting or transverse matrix cracking) under quasi-static and

fatigue loading conditions. The thick level set method, previously developed as non-local continuum damage method, is translated to a discontinuous damage model for use with interface elements. For this approach a new definition for damage in the constitutive law of interface elements is introduced. Similar to cohesive methods, there is a damage variable which varies between 0 and 1, but in contrast with the damage variable in cohesive methods which is a function of displacement jump, the damage is introduced as a function of the level set field. This definition of damage results in a band of damage with a predefined length l_c between sane and fully damaged material. The non-locality in computing the energy release rate appears by integrating local values of energy across the defined transition zone in the interface.

The developed fracture mechanics based level set model and the thick level set interface model are validated against experimental and theoretical data which proves the accuracy of the computed energy release rate as well as of its decomposition in pure mode contributions. In addition, the demonstration of the 3D capability of the models to capture the delamination front shape shows that both allow to predict the shape of the delamination front.

SAMENVATTING

Composietmaterialen worden in toenemende mate gebruikt in plaats van metalen in verschillende toepassingen zoals auto's, vliegtuigen en windturbines. Er bestaan twee ontwerpbenaderingen voor zulke toepassingen: de eerste is erop gericht alle schade tijdens gebruik te voorkomen, terwijl de tweede scheurgroei toelaat tot een bepaalde kritische grootte. De laatste benadering benut de schadetolerantie van composietmaterialen. Dit leidt tot lichtere en goedkopere producten, maar het vereist diep begrip van het bezwijkproces. Zulk begrip is nodig om de mogelijkheid dat defecten voorkomen te beoordelen en om de draagkracht van beschadigde constructies te kunnen bepalen. Hieruit volgt het belang van numerieke modellen waarmee het gedrag van deze constructies onder uiteenlopende condities gesimuleerd kan worden. Numerieke modellen zijn succesvol toegepast voor quasi-statische analyse van constructies, maar het simuleren van vermoeiing onder cyclische belasting is nog een uitdaging.

Vermoeiingsmodellen beschrijven scheurgroei doorgaans met de Paris relatie, die de beschikbare energie voor scheurgroei relateert aan de snelheid waarmee de scheur groeit. Het ontwikkelen van een vermoeiingsmodel met de Paris relatie vereist een nauwkeurige methode voor het berekenen van de *energy release rate* en een methode die het scheurfront in 3D kan beschrijven zodat de scheurgroeisnelheid opgelegd kan worden. Beschikbare numerieke vermoeiingsmodellen die gebaseerd zijn op breukmechanica of schademechanica voldoen niet geheel aan deze criteria. In de breukmechanica wordt de *virtual crack closure technique* (VCCT) gebruikt om de *energy release rate* te berekenen. De VCCT vereist dat het scheurfront samenvalt met de elementranden, wat de toepasbaarheid van deze techniek beperkt tot gevallen waarin de groeiende scheur niet van vorm verandert. In de schademechanica worden cohesieve modellen gebruikt die geen nauwkeurige berekening van de *energy release rate* bieden en evenmin de mogelijkheid hebben om een scheurgroeisnelheid berekend met de Paris relatie exact op te leggen.

Dit proefschrift is gericht op het ontwikkelen van een 3D model voor simulatie van scheurgroei in composietlaminaten onder hoog-cyclische vermoeiing. De focus in deze studie ligt primair op delaminatie, wat een belangrijk bezwijkproces in composieten constructies is. Voor het modelleren van delaminatiegroei onder vermoeiing is een recent breukmechanica-model, dat ontwikkeld is voor statische delaminatie-analyse met grote elementen, toegepast op vermoeiing. In dit model wordt de level set methode gebruikt om de locatie van het scheurfront te beschrijven en een gemodificeerde versie van de VCCT om de *energy release rate* te berekenen. De level set methode biedt een alternatief voor bestaande vermoeiingsmodellen. In tegenstelling tot andere breukmechanica-modellen vereist dit model niet dat het scheurfront samenvalt met de elementranden, waardoor ontwikkeling van de scheurvorm onder cyclische belasting gesimuleerd kan worden.

Het idee om de level set methode te gebruiken voor het modelleren van scheurgroei is verder uitgewerkt met het ontwikkelen van een alternatief model dat ook toepasbaar

is voor andere bezwijkprocessen dan delaminatie (bijvoorbeeld matrix scheuren) onder quasi-statische en cyclische belasting. De *thick level set* methode, oorspronkelijk ontwikkeld als niet-lokale continuüm-methode, is vertaald tot een discontinue methode voor gebruik in combinatie met interface-elementen. Hiervoor is een nieuwe definitie van schade in interface-elementen ontwikkeld. Zoals in cohesieve methodes is er een schade-variabele waarvan de waarde varieert van 0 naar 1, maar in tegenstelling tot cohesieve methodes is deze schade niet een functie van de scheuropening, maar van het level set veld. Deze definitie van schade leidt tot een band met schade met een vooraf gespecificeerde breedte l_c. Niet-lokaliteit is opgenomen in de berekening van de *energy release rate* doordat lokale waarden van energie over deze band geïntegreerd worden.

De ontwikkelde breukmechanica level set methode en *thick* level set interface methode zijn beide gevalideerd met experimentele en theoretische data, waarmee de nauwkeurigheid van de berekening van de *energy release rate* is aangetoond, evenals de decompositie van deze grootheid in drie fundamentele componenten. De 3D toepasbaarheid van beide modellen in het beschrijven van een evoluerende scheurvorm is aangetoond met extra rekenvoorbeelden.

1

INTRODUCTION

1.1. BACKGROUND

Composite materials are a composition of two or more constituents with different properties. The freedom to choose the constituents of composites allows to improve the thermal and mechanical properties of these materials to inhibit superior quality compared with their constituents. This has made composites popular in a wide range of engineering applications. However, because of the complexity in the material behavior and failure process of composites, prediction of the reliability of composite structures is difficult. Therefore, engineers need to consider high safety factors to design these structures which increases the cost of the final product. Reliable computational models can provide a deeper understanding of failure mechanisms of composites. This allows to consider a smaller safety factor for composite structures that finally leads to a cheaper product.

The composites studied in this thesis are laminated composites which are composed of different layers. Each layer is in turn composed of two materials: fibers (e.g. carbon, glass) and matrix (e.g. epoxy). The fibers with higher stiffness and strength bear the

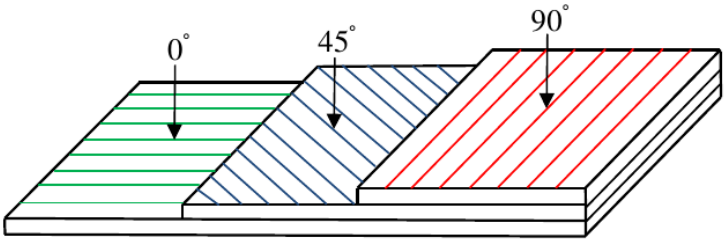

Figure 1.1: Schematic figure of a laminate composite

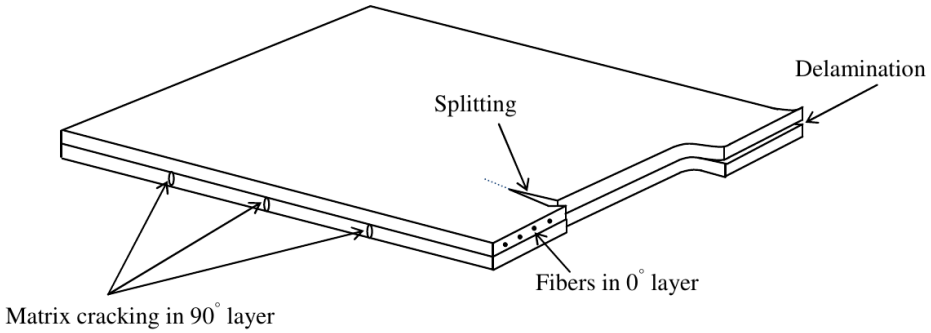

Figure 1.2: Failure mechanisms of composites: Delamination, matrix cracking and splitting

loads applied on a laminate while the matrix with weaker material properties keeps the fibers together. The desired material properties can be achieved by changing the fiber orientation of individual plies.

1.1.1. FAILURE MECHANISMS OF COMPOSITES

Laminate failure may occur due to different failure processes (see Fig. **??**) which can be categorized as failure inside the ply consisting of fiber failure and matrix cracking, and failure between the plies or delamination. The term splitting is used for matrix cracks in loading direction and transverse cracking for matrix cracks perpendicular to the load direction. The focus in this study is primarily on delamination which is an important cause of failure in composite structures.

1.1.2. DELAMINATION

Laminate composites are strong in fiber direction, but their interlaminar strength is low. As a consequence, separation of layers may occur. The delamination can grow under different fracture modes (see Fig. **??**) which are defined as mode I (opening), mode II (sliding) and mode III (tearing). Because delamination follows the ply interface, rather than the direction of the loading, it is typically a mixed-mode phenomenon. Delamination can grow from geometric and material discontinuities inside the laminate (see Fig. **??**). For example, it can start from transverse matrix cracks in one of the plies or develop from the free edge due to the difference between elastic properties of neighboring plies which causes a stress concentration at the ply interface **?**. Delamination decreases the load carrying capacity of laminates; therefore, it is important to predict the occurrence and growth of delamination.

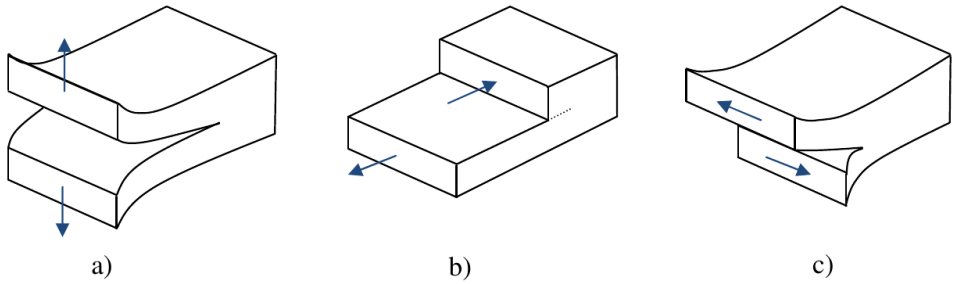

Figure 1.3: Different fracture modes: a) mode I b) mode II c) mode III

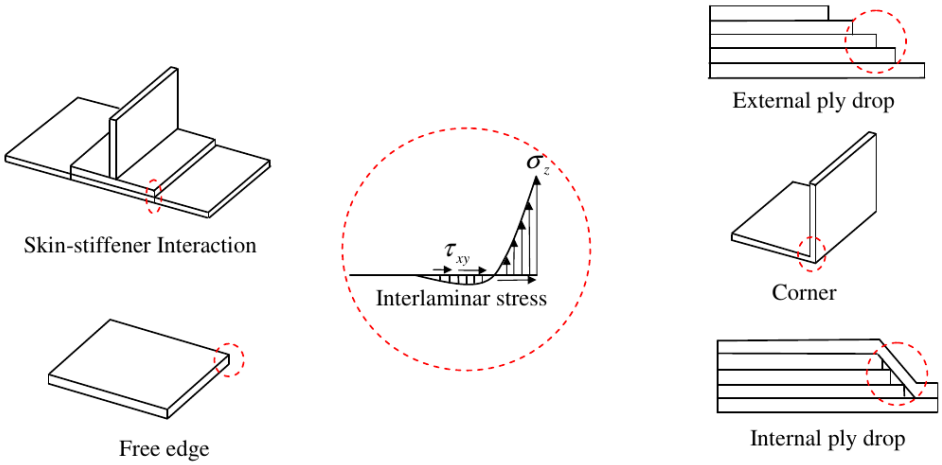

Figure 1.4: Delamination sources in composite structures. Adapted from **?**

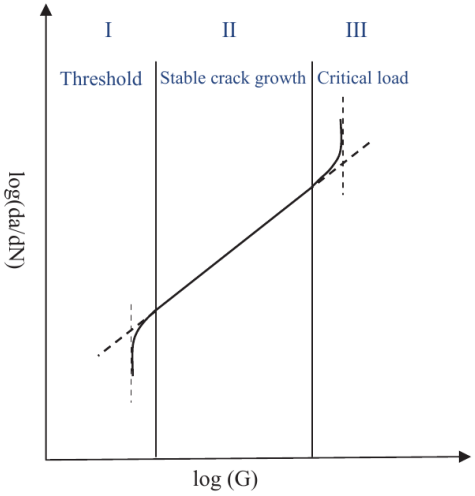

Figure 1.5: Three regions for typical patterns of crack growth rate

1.1.3. FATIGUE

Fatigue loading is usually described as a cyclic load with a given frequency. This cyclic load may initiate a new crack or induce growth of existing defects in the structure. A clear understanding of failure of composite structures under fatigue needs experimental tests which are categorized as: crack propagation, crack onset and crack initiation tests**?**. The crack onset tests are done to determine the number of cycles needed for delamination to start propagating from an existing crack, while in initiation tests the specimen does not have a pre-crack and the number of cycles required to generate a new crack is determined. In crack propagation experiments the crack length a is captured versus the number of cycles N, to determine the crack growth rate. Based on the obtained experimental data from crack propagation the crack growth rate can be plotted as a function of load (see Fig. **??**). Here, the load is typically expressed in terms of energy release rate using analytical formulas based on linear elastic fracture mechanics (LEFM). Figure **??** shows the 3 different regions in crack growth rate that are distinguished from experimental observations. The regions I and III are the near-threshold and the critical load regions respectively and region II defines the stable crack growth regime which can be characterized with the Paris law.

1.1.4. PARIS LAW

The Paris law is a phenomenological formula which describes the delamination growth as a power law function of applied energy release rate. It has been developed to reduce the fatigue experimental data and characterize fatigue crack propagation for a large range of load levels. Paris et al.**?** first introduced this power law to represent the crack growth rate under cyclic loading in metals. The successful application of this power law in metals and its simplicity has led to the extension of its application to composite ma-

terials **???**. The basic form of the Paris law is:

$$\frac{da}{dN} = C(G_{max})^m \tag{1.1}$$

where da/dN is the crack growth rate, G_{max} is the maximum value of the cyclic energy release rate, and the material parameters C and m must be determined experimentally. The exponent m is higher in composites than in metals **?**; therefore, the computed crack growth rate in composites is more sensitive to the error in input values of energy release rate. This reveals the importance of accuracy in the evaluation of the energy release rate for analysis of fatigue in composites. It should be noted that the Paris law was originally expressed in terms of stress intensity factor, but the computation of this quantity for bi-material interfaces is problematic. Therefore, the Paris law is mostly expressed in terms of energy release rate for modeling delamination growth in composite materials **?**.

Different modifications have been proposed to the Paris equation to deal with certain effects such as mode-ratio or load ratio on crack growth rate. Mohlin et al. **?** and Bathias and Laksimi **?** suggested to use the cyclic variation of energy release rate ΔG instead of G_{max} in the Paris law for fiber reinforced polymer (FRP) composites. Wang et al. **?** suggested that the energy release rate in Eq. **??** should be normalized with the fracture energy G_c. Allegri et al. **?** adopted the Paris law to consider the load ratio effect, R, in computed crack growth rate. Brussat et al. **?** suggested an empirical relationship to adopt the value of ΔG based on the mode-mix effects. Benzeggah and Kenane **?** found a dependence between the Paris law parameters on mode-ratio in unidirectional glass/epoxy composites. Based on this experimental observations they proposed the use of the Paris law with ΔG and defining parameters C and m as a function of mode ratio. Blanco et al. **?** improved the formulation developed by Benzeggah and Kenane by adding an extra quadratic form.

1.2. NUMERICAL MODELING OF FATIGUE DELAMINATION

The rise in application of composite materials has increased the demand for fatigue models which can predict the behavior of composite structures. To answer this demand, different fatigue models have been introduced in literature **???**. For a safe-life assessment of a structure fatigue life models which propose a fatigue failure criterion based on S-N curves can be used; however, a design based on the "slow growth" approach which allows some growth of damage under fatigue, leads to a cheaper and lighter production **?**. In order to design the structure based on this approach sufficient understanding of the progressive failure of materials is needed, for instance to plan an inspection schedule for the structure. This highlights the importance of numerical models which can simulate the progression of failure in the material and allows to determine the condition under which damage development in the structure becomes critical. The active research on developing such numerical models is the context for the present work.

Two main approaches exist for numerical modeling of delamination: the fracture mechanics based approach and the cohesive damage approach.

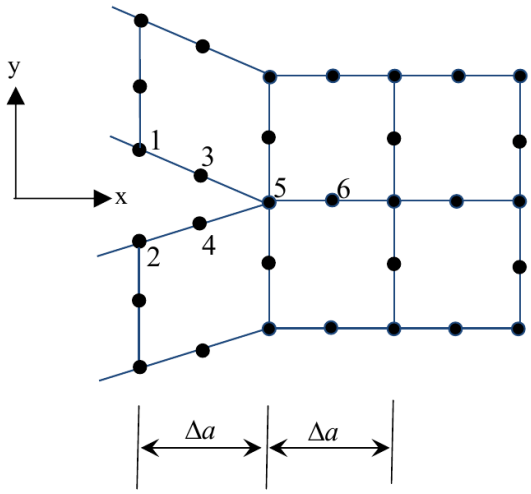

Figure 1.6: VCCT method for 2D application

1.2.1. FRACTURE MECHANICS BASED MODELS

The central thesis of the fracture mechanics theory is considering the fracture toughness as a material property **?**. Fracture mechanics is based on the work by Irwin and Griffith for crack growing in isotropic materials **?**. Griffith introduced the concept that a crack will grow if the total energy of the system is lowered. He assumed energy balance between the decrease in elastic strain energy of a system and the energy needed to propagate an existing crack **?**. Based on this theory Irwin defined the energy release rate as the energy released per unit area of crack extension. As the fracture mechanics approach assumes a pre-existing crack in the structure; the models developed based on this approach can only be used for modeling crack propagation. Crack propagation is related to a fracture mechanics property like energy release rate or stress intensity factor. The strain energy release rate is computed from the derivative of potential energy of the system, with respect to the crack extension area:

$$G = \frac{\delta(W-U)}{\delta A} \tag{1.2}$$

where W is the external work done, U is the strain energy, and δA is an infinitesimal crack extension. When the value of G reaches the critical value G_c, the crack will propagate. Another important fracture mechanics quantity is the stress intensity factor, K, which was introduced by Irwin. This factor describes the stress state around the crack tip. For fatigue analysis, the concepts of energy release rate or stress intensity factor are related to the crack growth rate using the Paris law. As it is explained in **??**, for modeling fatigue in composite materials, the application of the energy release rate is more preferable than the stress intensity factor.

In the context of numerical modeling of delamination, the energy release rate can be

computed from finite element methods like the virtual crack closure technique (VCCT) **??**. In the VCCT the energy release rate and its pure mode components are computed from nodal forces and displacements along the delamination front (see Fig. **??**) **?**:

$$G_I = \frac{1}{2\Delta a}[Y_5(v_1 - v_2) + Y_6(v_3 - v_4)] \tag{1.3}$$

$$G_{II} = \frac{1}{2\Delta a}[X_5(u_1 - u_2) + X_6(u_3 - u_4)] \tag{1.4}$$

where Δa is the assumed finite growth of the crack, X and Y are the nodal force components, and u and v are the nodal displacement components in the x and y directions, respectively. This formulation has been extended to 3D analysis by Shivakumar et al. **?**. The VCCT is well suited to assess the growth of a given crack where the front is aligned with the element boundaries. However, in a progressive failure analysis keeping the crack at element boundaries is only provided in case of self-similar delamination growth. In case of non-self similar delamination growth remeshing of the finite element model is needed which is not straightforward to implement, especially for complex geometries. The VCCT is also suitable for predicting crack growth rates in fatigue analysis. The computed energy release rate can be used directly in Paris law **??**. However, the limitation coming from the requirement that the crack front should be aligned with element boundaries also applies to the case of progressive fatigue analysis.

1.2.2. COHESIVE DAMAGE MODELS

The second approach for the numerical modeling of delamination is the cohesive damage method. The cohesive crack concept was first introduced by Dugdale **?** who considered a thin plastic zone in front of the notch. Hillerborg et al.**?** developed the first finite element model based on this approach for analysis of the initiation and growth of a crack under mode I loading. In this model the cohesive traction is considered a function of the crack opening (see Fig. **??**). This model is a base for current cohesive models which consider a cohesive law that relates the tractions to the displacement jump across the crack plane (see Fig. **??**). A damage parameter progressively decreases the stiffness and reduces the traction to zero which effectively creates a new crack surface. The area under the cohesive law is equal to the fracture energy G_c which links the damage definition to fracture mechanics theory.

For modeling delamination cohesive damage models are mostly applied in combination with interface elements (see Fig. **??**). Interface elements are commonly used in numerical models to define the discontinuity along a predefined crack path. In the context of delamination modeling, interface elements were first used by Schellekens and De Borst **?**. Later, Mi et al. **?** proposed a mixed-mode bilinear softening law for interface elements. Camanho et al. **?** related the fracture energy of interface elements using a phenomenological function of the mode-mixity developed by Benzeggah an Kenane **?**. Turon et al. **?** improved this model to a thermodynamically consistent damage model with mixed-mode capability for quasi-static analysis.

For fatigue analysis different cohesive damage models have been proposed, mostly as an extension of a quasi-static formulation. Foluk et al. **?** developed one of the first cohesive fatigue models by adding a loading/reloading path to Tvergaard's traction-separation

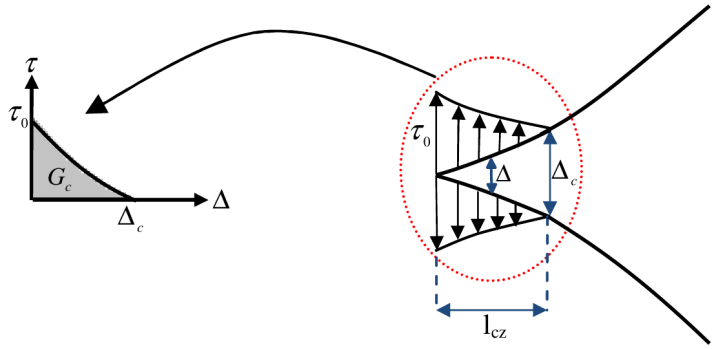

Figure 1.7: Cohesive zone and possible traction-separation curve

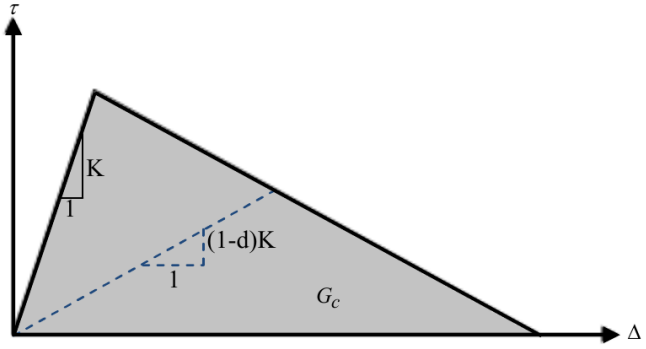

Figure 1.8: Bilinear cohesive law with a damage variable d and initial stiffness K

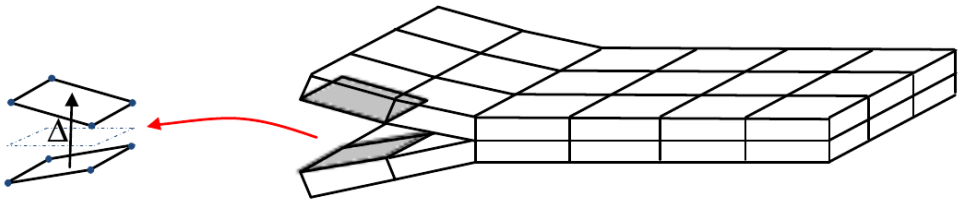

Figure 1.9: Plane interface element with displacement jump Δ

law **?**. Following the cycle by cycle analysis approach several models have been proposed in literature for low-cycle fatigue analysis **??????**.

In high-cycle fatigue the introduced cycle by cycle approach is computationally impractical. Here, the viable alternative is to follow the loading envelope approach which means that instead of the complete cyclic load, a constant load equal to the maximum value of the cyclic boundary conditions is applied. In early studies on the cohesive fatigue modeling **??**, phenomenological formulas were used to compute the development of the damage parameter under cyclic loading. Calibration of the model parameters is then needed to match the experimental crack growth rate from basic tests**?**. To improve the results and reduce the number of parameters that need to be adjusted, Turon et al. **?** proposed a link between damage growth and the Paris law. The provided link avoids the introduction of additional material parameters except the common Paris law parameters. The energy release rate is computed locally by integrating the traction-separation relation. However, for this integration an idealization of the cohesive law must be performed, because the actual response is unknown (see Fig. **??**). This idealization can cause inaccuracy in the computed energy release rate. Furthermore, in cohesive fatigue models the crack growth rate obtained from Paris law can not be imposed directly; therefore, it is linked to the damage growth rate. This link requires information on the the length of cohesive zone (l_{cz}) which can only be estimated based on the geometry and loading conditions. This dependency restricts the applicability of these models in complex 3D simulations **?**. Moreover, the analytical formulas for computing the length of cohesive zone are only proposed for standard fracture toughness tests and they are not validated in more complex geometries **?**. Several studies have been conducted to improve the accuracy of computed energy release rate and to remove the dependency of the crack growth on the length of cohesive zone. Harper and Hallett **?** divided the cohesive zone into two equal zones: static and fatigue damage zone to improve the accuracy of extracted energy release rate from the cohesive law. Kawashita and Hallett **?** developed a method to apply fatigue damage only to the crack tip element. In this way the cohesive response is closer to the idealized cohesive law in Fig. **??**. However, for 3D analysis a crack tip tracking algorithm is needed. Xu and Wang **?** extended this method to be applicable for

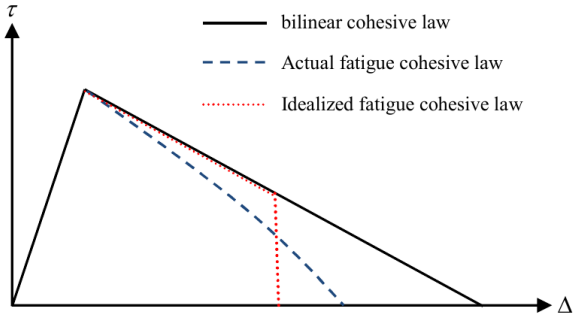

Figure 1.10: The actual shape of cohesive law under fatigue is different from predefined bilinear cohesive law

both orthogonal and non-orthogonal meshes. Recently, Bak et al. **?** used the J-integral for computing the energy release rate in a cohesive fatigue model. This results in a more precise prediction of the crack growth rate under fatigue; however, it is not obvious how this approach can be extended for 3D analysis. For 3D fatigue analysis using a crack tip tracking algorithm is, so far, the most applicable method for improving the accuracy of cohesive fatigue models. However, these algorithms are not developed for general finite element formulations. Especially when the aspect ratio of elements differs from unity the predicted front shape shows oscillations **?**.

1.2.3. PROBLEM STATEMENT

In sections **??** and **??**, two main approaches for modeling fatigue delamination have been discussed. In the context of the fracture mechanics approach, the VCCT is used for computing the energy release rate which limits the application of these models for problems with non-self similar crack growth. On the other hand, in the context of the damage mechanics approach, cohesive fatigue models lack an accurate computation of energy release rate and the possibility to directly impose the crack growth rate computed from the Paris law.

1.3. APPROACH

The objective for the work presented in this thesis is to propose a 3D mixed-mode fatigue model for simulating delamination propagation in laminate composites. The strategy pursued is to develop alternative approaches for fatigue models, rather than to improve the current cohesive or fracture mechanics based models. Based on a literature review and critical evaluation of existing approaches, the following requirements for developing a new approach for fatigue modeling have been formulated:

- The Paris law should be used for computing the local values of crack growth rate. Because it is a reliable formula which has less input parameters than other imple-

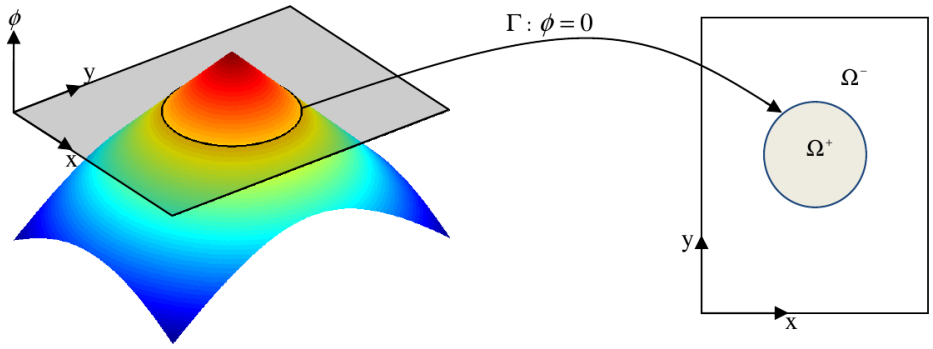

Figure 1.11: 2D level set field extended over the domain Ω

mented phenomenological formulas.

- An accurate method for computing the energy release rate is needed due to the high sensitivity of the Paris law to the input values of energy release rate.
- It should be possible to describe and update of the crack front with arbitrary shape that may move in non self-similar fashion with a certain crack growth rate. This requires a mesh-independent representation of the crack front.
- The solution algorithm of the new model should be robust and efficient.

Based on the third requirement, the level set method is selected to define crack growth. The level set method provides a robust capability to track the arbitrary shape of a moving front. For the other requirements, the level set method needs to be combined with accurate methods for computing the energy release rate. In the remainder of this section, the level set method is introduced and two existing level set based methods for crack growth are reviewed.

1.3.1. LEVEL SET METHOD

The common feature between fatigue models proposed in this thesis is that they use the level set method **?** to define crack growth. With this method a moving front is described in an implicit way that allows to define the front inside the finite elements. Using this method enables the proposed fatigue models to predict the delamination growth pattern based on the mechanics of the problem without prior knowledge of the delamination shape. In the level set method an auxiliary field $\phi(x, y)$ is considered over the domain where the zero level set of this field describes the front (see Fig. **??**). To define the level set field, ϕ is considered as a signed distance function to the front Γ:

$$|\nabla\phi| = 1 \quad on \quad \Omega_\phi \tag{1.5}$$

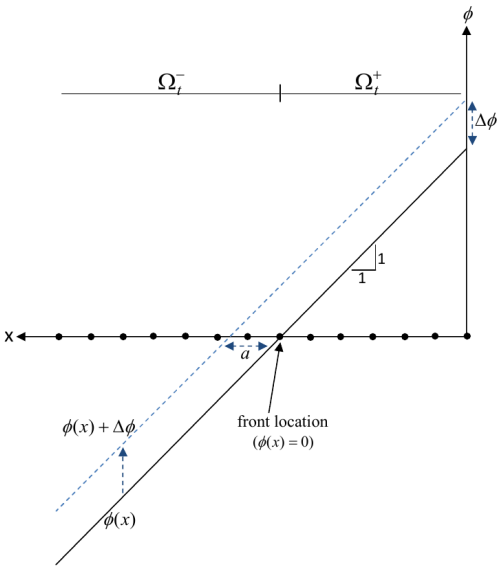

Figure 1.12: 1D level set field extended over the domain Ω

$$\phi = 0 \quad on \quad \Gamma_\phi \tag{1.6}$$

Figure **??** shows a 1D level set field which has a positive sign in one sub-domain (Ω^+) and a negative sign in the other sub-domain (Ω^-). The absolute value of ϕ at every point of the domain is equal to the nearest distance to the front from that point. To describe a moving front, the level set field needs to be updated:

$$\phi_{t+\Delta t} = \phi_t + \Delta\phi \tag{1.7}$$

When the field ϕ is updated with the level set increment $\Delta\phi$, the boundary between the sub-domains advances with the same distance of $\Delta\phi$. In 1D, the condition **??** implies that there is a slope of 1. It can be observed that an increase in the level set with $\Delta\phi$ leads to movement of the point where $\phi = 0$ with a distance a. Because the slope of $\phi(x)$ equals one, the values of $\Delta\phi$ and a are equal and Eq. **??** can be rewritten as

$$\phi_{t+\Delta t} = \phi_t + a \tag{1.8}$$

where the front advance a can be related to a the velocity (V_n) of the front as:

$$a = V_n \Delta t \tag{1.9}$$

where Δt is the increment of time. For a 2D level set field the method works similarly except that the velocity may vary along the front ($V_n(s)$). The front location changes by updating the level set field with the front advance $a(s)$. For the finite element implementation, ϕ is defined with the nodal values over a discretized domain which is interpolated

using the standard shape functions. To update this field over the discretized domain the nodal front advance $a(s)$ can be extended over the domain efficiently using the fast marching method. To apply this method for a fatigue model, considering the variation of energy release rate along the front $G(s)$, the crack growth rate obtained form the Paris law (da/dN) can be used to update the level set field:

$$V_n = \frac{da}{dN} \tag{1.10}$$

With this definition of velocity, the time increment Δt in Eq. **??** is considered to be equal to the number of passed cycles ΔN.

1.3.2. A LEVEL SET MODEL FOR DELAMINATION

A level set method for delamination modeling was first introduced by Van der Meer et al.**?** for quasi- static analysis. The original motivation was to be able to use elements that are larger than the length of the cohesive zone. In this approach, the domain Ω (see Fig. **??**) coincides with the plane of the interface, the moving front is the crack front and the negative and positive sub-domains represent the cracked and uncracked interface respectively. This model is comprised of two main components. The first component provides a kinematic description of a cracked laminate, and the second component represents the crack growth. To adapt this model for the arbitrary definition of the crack front with the level set method innovative solutions were presented for both components. For the first component a special element formulation was developed which allows to represent the kinematic of a partially cracked element. In the second part the energy release rate is computed with either the jump in Eshelby tensor **?** or a modified version of the VCCT **?**, which in contrast with the original VCCT, allows the front to be located inside the elements. This model can deal very well with non-self-similar crack growth.

1.3.3. THICK LEVEL SET METHOD

The thick level set method (TLS) is a method for modeling damage and fracture in solids. This method has been introduced by Möes et al. **??** in the context of continuum damage models for quasi-static loading. In this method similar to other continuum damage models a damage variable progressively reduces the stiffness of the material. However, in classical continuum models this damage variable is defined as a function of the local strain, while in the TLS it is a function of the distance to a moving front described with the level set method. This results in a moving band of damage with a predefined length l_c. Considering the length scale l_c for the damaged band removes the problem of mesh size dependency in local damage methods with softening. Moreover, compared with other regularized damage methods which have addressed this problem like the non-local integral damage method **?**, the TLS is more efficient **??**, because the computational work regarding the regularization is limited to the damaged band. Another advantage of the TLS compared with other continuum damage models is the algorithmic robustness of this method **?**. This is due to the staggered solution scheme in which displacements and damage are computed sequentially rather than iteratively. This solution scheme avoids common convergence problems related to the negative tangent during softening or to sign-change in the tangent because of loading-unloading behavior **?**.

Aside from the capabilities of the TLS as a quasi-static continuum damage model, some characteristics of this method are very suitable for 3D fatigue analysis. It offers a framework for accurate non-local computation of the energy release rate and for imposing a crack growth rate. However, for delamination analysis, the continuum approach is not very suitable. Therefore, a discontinuous version of the TLS is developed in this thesis for crack growth modeling under quasi-static and fatigue loading conditions.

1.4. OUTLINE

Two different approaches have been developed, each with its own merits and drawbacks. In chapter **??** a 3D mixed-mode fatigue model is proposed in the context of the fracture mechanics theory. In this model the level set method is used to describe the crack front location and the modified version of the VCCT is employed to compute the energy release rate. The level set method allows to define the arbitrary shape of the delamination front and extends the application of fracture mechanics towards simulating non-self-similar crack growth.

Although it is demonstrated that the proposed model in chapter **??** is accurate for fatigue analysis, the model uses a special element formulation which restricts the application of the model to a single delamination in thin structures. To develop a more general fatigue model using the standard finite element formulations which keeps the advantage of using the level set method for definition of the delamination front, an alternative model is developed in chapters **??** and **??**. A discontinuous version of the TLS is formulated which allows for an automatic coupling between fracture and damage mechanics. The model is first developed and validated for quasi-static loading in chapter **??** and then extended to fatigue analysis in chapter **??**. It is demonstrated that the proposed models are capable of dealing with non-trivial geometries and mixed-mode conditions.

2

A LEVEL SET MODEL FOR SIMULATING FATIGUE-DRIVEN DELAMINATION IN COMPOSITES

ABSTRACT

This chapter proposes a level set model for simulating delamination propagation in composites under high-cycle fatigue loading. For quasi-static loading conditions, interface elements with a cohesive law are widely used for the simulation of delamination. However, basic concepts from fatigue analysis such as the notion that the crack growth rate is a function of energy release rate cannot be embedded in existing cohesive laws. Therefore, we propose a model in which the cohesive zone is eliminated from the computation while maintaining the flexibility that the crack shape is not bound to element edges. The model is able to predict the delamination growth rate and its front shape accurately. To demonstrate the validity of the model, several tests under different fracture modes are conducted and the results are compared with experimental data, analytical solutions and results from cohesive zone analysis.

2.1. INTRODUCTION

Composite materials are increasingly used in engineering structures such as wind turbines and aircrafts where fatigue is a common cause of failure. Delamination is one of the most important modes of failure because of the relative weakness of the interface between the layers of composite laminates. Therefore, computational tools are needed to predict fatigue-driven delamination in composites. Experimental observations from fatigue tests can generally be described well with the phenomenological Paris law (see Fig. **??**) which formulates the crack growth rate as a function of the energy release rate.

This chapter is based on **?**: Latifi, M.; van der Meer, F.P.; Sluys, L.J: A level set model for simulating fatigue-driven delamination in composites. International Journal of Fatigue, 80:434–442, 2015.

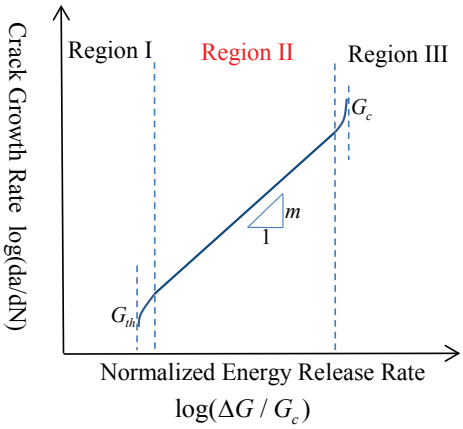

Figure 2.1: Typical pattern of crack growth rate: Paris law is valid in region II

The Paris law relates the load and material-dependent notion of crack growth under cyclic loading to the strain energy release rate with a power law:

$$\frac{da}{dN} = C\left(\frac{\Delta G}{G_c}\right)^m \tag{2.1}$$

where da/dN is the crack growth rate, G_c is the fracture energy, and ΔG is the cyclic variation of energy release rate. The material parameters C and m must be determined experimentally. The main subject in implementing the Paris law in a model is computing the energy release rate due to crack growth. Two main approaches to crack growth modeling, namely damage mechanics and fracture mechanics, provide different solutions for this issue.

The first approach is damage mechanics. In this context interface elements with a cohesive law have been commonly used to simulate delamination under quasi-static loading conditions. Due to the successful application of these models, researchers have tried to extend cohesive laws to high-cycle fatigue analysis. However, cohesive laws do not define the energy release rate and crack growth rate explicitly. Therefore, a straightforward implementation of the Paris law in a cohesive law is not possible.

In **?????**, the cohesive law has been modified to incorporate the effect of cyclic loading. These models add a new damage variable to the quasi-static damage variable to account for fatigue degradation. The rate of this fatigue parameter is related to the crack growth rate computed from the Paris law. The strain energy release rate in the Paris law formulation is extracted from cohesive interface elements by integrating the traction-displacement response of these elements. However, this integration must be performed before the actual response is known. Therefore, idealization of the cohesive fatigue response is needed. This idealization of the cohesive law and the lack of an accurate analytical formula for estimating the fatigue cohesive zone make them imprecise in fatigue analysis. Recently, Kawashita et al. **?** proposed an updated method which is independent

of estimating the cohesive zone length. This method provides a more accurate extraction of the energy release rate; however, this improvement comes at the cost of implementing crack tip tracking algorithms for interface elements.

In the second approach, fracture mechanics, the virtual crack closure technique (VCCT) has been widely used to compute energy release rates for delamination modeling. With this technique, the energy released during a virtual crack extension Δa, is computed as the energy required to close the crack over the same distance. This method is not valid in bimaterial interfaces **?**; therefore, a thin homogeneous interphase layer should be considered at the interface **?**, and a very fine mesh is needed around the crack front. Zou et al. **?** have solved the problem of VCCT in bimaterials without assuming an interphase layer. This method applies the kinematic formulation of shell theory; which has a consequence, that the stress singularity around the crack tip is transformed into a discontinuity in stress resultants over the plane through the thickness of the laminate. The total energy release rate can be computed from these discontinuities. Later, Van der Meer et al. **?** improved the accuracy of this method for coarse meshes by including concentrated bending moments in the expression for mode I dissipation.

The VCCT requires the crack front to be positioned along element boundaries which leads to a poor estimate of energy release rates when the crack growth is not self-similar. This problem does not apply to the level set model presented in **?**, because this model computes the energy release rate from local quantities instead of nodal values. In this method, which also belongs to the category of fracture mechanics, the crack front location is implicitly described with the level set method **?**; therefore, this method allows for representing arbitrary shape of the crack front and continuous growth of the crack. The method was extended for full crack growth analysis with out-of-plane deformations by modeling a laminate as a stack of shell elements for small deformations in **?**.

In this chapter, the level set model for delamination is applied to high-cycle fatigue analysis. Because the model is based on fracture mechanics, it is very suitable for the implementation of the Paris law. To define the crack front location and compute the energy release rate, the level set approach developed in **?** and the modified formulation of Zou's method **?** are used, respectively.

This chapter is structured as follows. Section **??** describes the formulation of the level set model for fatigue analysis, and in section **??**, to validate the level set model, numerical predictions are compared with experimental data.

2.2. METHODS

In high-cycle fatigue applications which may involve more than 10^6 cycles, tracking loading/unloading and stiffness degradation on a cycle-by-cycle basis is computationally impractical; therefore, instead of the real cyclic load which is oscillating between minimum and maximum of applied load, a load envelope is considered (see Fig. **??**). In this loading envelope strategy, a constant numerical load or displacement is applied which is equal to the maximum value of the cyclic boundary conditions. In every time step, a certain number of cycles ΔN is passed. The crack growth per time step is therefore computed by multiplying the crack growth growth rate da/dN from Eq. (**??**) with the time step size ΔN.

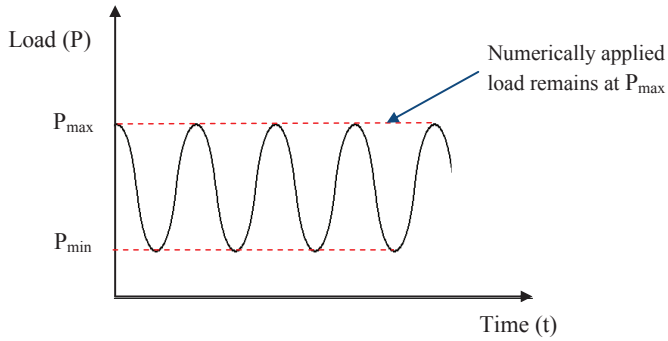

Figure 2.2: Actual cyclic load and numerically applied load based on loading envelope strategy

The model is comprised of two submodels, the cracked laminate model and the crack growth model, which are solved with a staggered solution scheme. The cracked laminate model computes the displacement field of a partially delaminated plate, where the elements containing the crack front have a special kinematic formulation, which is explained in section **??**. The second submodel takes the displacement field from the cracked laminate model and computes the energy release rate for delamination growth. The computed energy release rate is used to compute a velocity field at the crack front. Based on this velocity, the level set field is updated and a new front location is obtained. The second submodel, from computation of energy release rate to the level set update, is explained in section **??**.

2.2.1. CRACKED LAMINATE MODEL

The central idea in the level set model for delamination is that the location of the crack front is described with the level set method. This means that there is a sharp front that does not have to be aligned with the finite element boundaries. In other words, the front can be located inside the finite elements. In the current implementation a laminate is represented with shell elements for small displacements. In this model (see also Van der Meer et al.**?**), there are two layers of elements in the cracked and uncracked subdomains which are connected in the uncracked part. Each layer is composed of five parameter shell elements (two rotational and three displacement on each node). In order to achieve the connection between the layers of elements in the uncracked subdomain, a displacement-only version of five parameter shell is used. The resulting mesh is similar to a mesh with solid-like shell elements, except that all connected nodes with the same (x,y) coordinate share a single z-displacement degree of freedom**?**. The potential energy of the laminate (Π) based on First-order Shear Deformation Theory (FSDT) is given by **?**:

$$\begin{aligned}\Pi_{FSDT}(\hat{\mathbf{u}}, u_3, \boldsymbol{\phi}) = \tfrac{1}{2}\int_\Omega \mathrm{A}\nabla_s\hat{\mathbf{u}}\cdot\nabla_s\hat{\mathbf{u}}\mathrm{d}\Omega + \int_\Omega \mathrm{B}\nabla_s\hat{\mathbf{u}}\cdot\nabla_s\boldsymbol{\phi}\mathrm{d}\Omega + \tfrac{1}{2}\int_\Omega \mathrm{D}\nabla_s\boldsymbol{\phi}\cdot\nabla_s\boldsymbol{\phi}\mathrm{d}\Omega \\ + \tfrac{1}{2}\int_\Omega \mathrm{H}(\nabla u_3+\boldsymbol{\phi})\cdot(\nabla u_3+\boldsymbol{\phi})\mathrm{d}\Omega - \Pi_{ext}(\hat{\mathbf{u}}, u_3, \boldsymbol{\phi})\end{aligned} \tag{2.2}$$

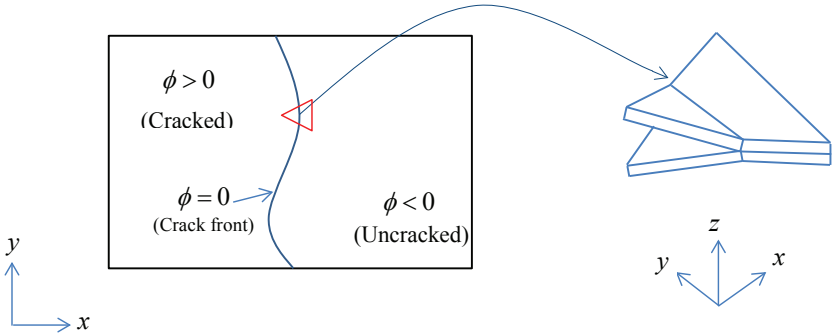

Figure 2.3: Definition of crack front with level set field and schematic deformation of triangle shell element containing the crack front

where $\hat{\mathbf{u}}$ is the in-plane displacement vector of the mid-surface, $\boldsymbol{\phi}$ collects the rotation components, and u_3 is the out-of-plane displacement. A, B and D reflect the effects of membrane, and bending deformations and their coupling respectively, while H is the corrected shear stiffness. The symbol ∇_s indicates the symmetric part of the gradient operator and Π_{ext} accounts for the external load potential. In the current displacement-only formulation, $\hat{\mathbf{u}}$ and $\boldsymbol{\phi}$ are linearly related to displacement degrees of freedom on the top and bottom surface of the element.

In order to model the kinematics of a partially cracked element (see Fig. **??**), a weak discontinuity is inserted at the location of the front. The weak discontinuity (see Fig. **??**), embedded in the formulation of the partially cracked elements, is derived from a strong discontinuity formulation, because compatibility between top and bottom displacements fields at the uncracked part of elements cannot be achieved by direct enrichment of cracked elements with weak discontinuities **?**. For representing the strong discontinuities in the displacement field, the phantom node method is applied **?**. Following this method, each of the cracked elements at the top and bottom layers is replaced with two new elements which are partially active.

The phantom node version of the extended finite element method introduces the possibility of a jump in displacements across the configurational interface (see Fig. **??**). This jump $[\![\mathbf{u}]\!]$ is closed using a penalty method. Therefore, a penalty term is added to the definition of the potential energy in Eq. (**??**):

$$\Pi = \Pi_{FSDT} + \frac{1}{2}\theta \int_{\Gamma} [\![\mathbf{u}]\!] \cdot [\![\mathbf{u}]\!] \, \mathrm{d}\Gamma \tag{2.3}$$

where θ is a penalty parameter and $[\![\mathbf{u}]\!]$ is the three dimensional displacement jump vector. Adding the penalty term results in a continuous displacement field across the configurational interface; however, stress and strain fields are discontinuous. In other words, a weak discontinuity is achieved. The finite element equations are the discretized form of the minimization of Eq. (**??**).

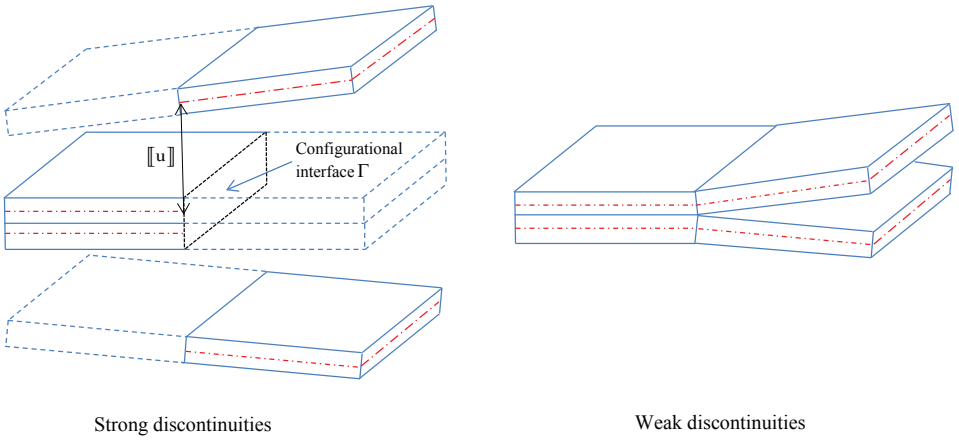

Figure 2.4: Two weakly discontinuous displacement fields are derived by closing the jumps $[[u]]$ in two strongly discontinuous fields

2.2.2. CRACK GROWTH MODEL

The cracked laminate model described in the previous section provides a mechanical analysis of a partially delaminated structure. In order to perform crack growth analysis, the level set function needs to be updated in each time step. In the quasi-static version of the level set model for delamination **?**, crack growth is defined with a velocity that is computed along the front as a function of energy release rate. This framework is very suitable for fatigue analysis. In the fatigue model, the Paris law is embedded in this framework. In general, the Paris law (Eq. **??**) can be expressed as

$$\frac{da}{dN} = C(\beta, R)\left(\frac{\Delta G(R)}{G_c(\beta)}\right)^{m(\beta,R)} \tag{2.4}$$

where the fracture energy G_c is a function of mode ratio (β), C and m are material constants that depend on the mode ratio and load ratio R, and the cyclic variation of energy release rate ΔG is a function of stresses and displacements at peak cyclic load level and of load ratio. In this equation the load ratio R is considered as the minimum over the maximum of cyclic load(P_{min}/P_{max})(see Fig. **??**). For completeness, it should be noted that C and m can also be made a function of loading frequency.

The dependence of fracture energy on the mode ratio is defined using an expression introduced by Benzeggagh and Kenane **?**:

$$G_c = G_{Ic} + (G_{IIc} - G_{Ic})(\beta)^{\eta} \tag{2.5}$$

where G_{Ic} and G_{IIc} are fracture energy in modes I and II, and η is a mode interaction parameter. The parameter β is the ratio between shear dissipation (mode II and mode III taken together) and total energy release rate. Following Turon et al. **?** this parameter is defined as

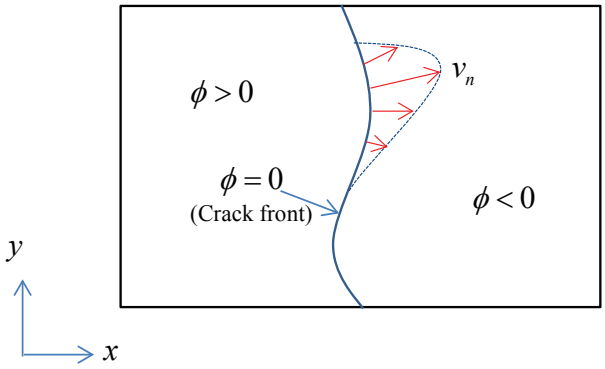

Figure 2.5: Velocity is defined as a function of the crack front location

$$\beta = \frac{G_{II} + G_{III}}{G} \tag{2.6}$$

where G_{II} and G_{III} are pure mode contributions to the energy release rate and G is the sum of all three pure mode contributions (see Section **??**). With this expression for β, it is assumed that the fracture energy is the same for mode II and mode III. In contrast with the cohesive zone method, the pure mode energy release rates G_{II} and G_{III} can be computed with the present method. However, introducing a relation for G_c as function of independent shearing contributions G_{II} and G_{III} lies outside the scope of this chapter.

The definitions of m and C under mixed mode conditions at constant load ratio, are considered to be a function of mode ratio following Blanco et al. **?**:

$$\log C = \log C_I + (\beta) \log C_{mix} + (\beta)^2 \log \frac{C_{II}}{C_{mix} C_I} \tag{2.7}$$

$$m = m_I + m_{mix}(\beta) + (m_{II} - m_I - m_{mix})(\beta)^2 \tag{2.8}$$

where C and m are crack growth rate parameters and subscripts I, II and mix define mode I, mode II, and mixed mode loading conditions, respectively. These parameters can be obtained by curve-fitting mixed-mode experimental data. Further investigation is needed for developing a general formula which considers the effects of all three mode contributions on fatigue parameters C and m.

By assuming a tension-tension fatigue loading, the maximum of strain energy release rate in each cycle ($G = G_{max}$) can be used for computing the cyclic variation of energy release rate:

$$\Delta G = (1 - R^2) G \tag{2.9}$$

The value of G and β can vary along the crack front; consequently, the crack growth rate is a function of the location along the front (see Fig. **??**).

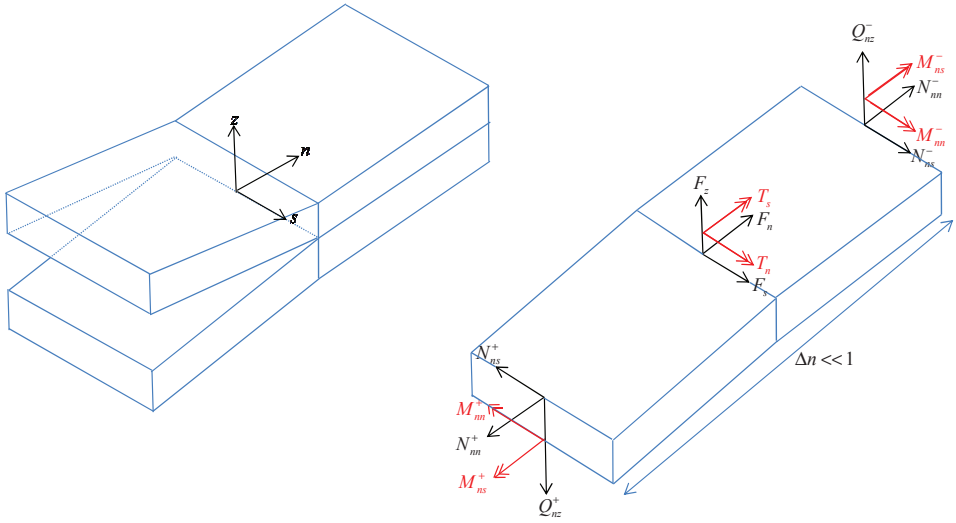

Figure 2.6: Free body diagram of an infinitesimal extension of the bottom sublaminate around the front

ENERGY RELEASE COMPUTATION

The energy release rate G used in the Paris law, is computed from a modified virtual crack closure technique **??** that is based on local quantities at the location of the configurational interface. The energy release rate G is partitioned into three individual parts which are related to the classical fracture modes:

$$G = G_I + G_{II} + G_{III} \tag{2.10}$$

The energy release rate contributions are computed along the crack front using the following definitions **?**:

$$G_I = F_z \left[\left[u_{z,n}\right]\right] + T_n \left[\left[\phi_{n,n}\right]\right] + T_s \left[\left[\phi_{s,n}\right]\right] \tag{2.11}$$

$$G_{II} = F_n \left[\left[u_{n,n}\right]\right] \tag{2.12}$$

$$G_{III} = F_s \left[\left[u_{s,n}\right]\right] \tag{2.13}$$

where F_z, F_s and F_n are the jumps in stress resultants, while T_n and T_s are distributed moments acting on the crack front(see Fig. **??**).

The differences in displacement gradients $u_{z,n}$, $u_{n,n}$ and $u_{s,n}$ are defined as

$$\left[\left[u_{j,n}\right]\right] = u_{j,n}\big|_{n=0^-,z=0^+} - u_{j,n}\big|_{n=0^-,z=0^-} \tag{2.14}$$

where $j = z, n, s$.

DISCRETIZATION

For the level set update, the velocity needs to be known at the nodes. However, as Fig. **??** shows, the distributed force vectors and the differences in displacement gradients are computed at the front, and consequently, G and the velocity field da/dN are defined along the front. Therefore, to define the velocity degrees of freedom $\mathbf{V}_n$ on the nodes, Eq. (**??**) is discretized with the shape functions $\overline{\mathbf{N}}$, on the nodes whose support is intersected by the front.

Satisfying Eq. (**??**) in an integral form and following Galerkin's method **?** results in

$$[\mathbf{M}+\mathbf{K}]\cdot\mathbf{V}_n = \mathbf{f} \tag{2.15}$$

$$\mathbf{M} = \int_{\Gamma} \overline{\mathbf{N}}\otimes\overline{\mathbf{N}} d\Gamma \tag{2.16}$$

$$\mathbf{K} = \kappa h^2 \int_{\Gamma} (\nabla\overline{\mathbf{N}}\cdot\mathbf{s})\otimes\left(\nabla\overline{\mathbf{N}}\cdot\mathbf{s}\right) d\Gamma \tag{2.17}$$

$$\mathbf{f} = \int_{\Gamma} \overline{\mathbf{N}}\left(C\left(\frac{\Delta G}{G_c}\right)^m\right) d\Gamma \tag{2.18}$$

where $\mathbf{K}$ is added to stabilize oscillations on the front, κ is a stabilization parameter, and h is the typical element size. It should be noted that the Paris law is used to define right hand side vector $\mathbf{f}$ (Eq. **??**), and it includes the dependence of the model on the load ratio and mode ratio.

LEVEL SET UPDATE

The nodal velocity around the crack front is obtained by solving equation (**??**). In order to update this level set field, the velocity is first extended over the whole domain, using a fast marching method **?**. The obtained velocity field is normal to the level sets; therefore, the level set field can be updated with a standard level set update procedure **?**:

$$\phi + v_n \Delta N \rightarrow \phi \tag{2.19}$$

where ϕ is the level set field, ΔN is the number of cycles in the time step and v_n is the extended velocity field.

2.3. RESULTS AND DISCUSSION

In this section the proposed fatigue level set model is applied to several cases of delamination growth under cyclic loading. Numerical examples include the simulation of a basic test with different mode ratios (see Fig. **??**) and load ratios. Furthermore, the prediction of delamination front shape in a more complex test is examined. The obtained results are compared with experimental data from literature to prove that the level set model can accurately reproduce the response of composite laminates under fatigue loading conditions.

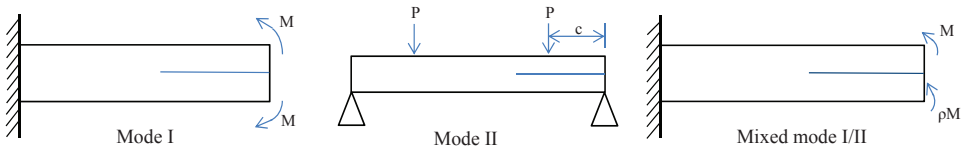

Figure 2.7: Loading conditions in three different fracture modes

2.3.1. SIMULATION OF A DCB TEST UNDER FATIGUE LOADING

A double-cantilever beam under mode I loading was modeled, following the experiments by Asp et al. **?**. The specimen was 150 mm long, 20 mm wide, with two 1.55 mm thick arms, with an initial crack of 35 mm. In order to obtain a constant crack growth rate, the specimen's arms were loaded with two constant opposite moments (see Fig. **??**-left). Table **??** presents the material properties of this specimen fabricated with carbon/epoxy HTA/6376C. The specimen lay-up was $[0_{12}//(\pm 5/0_4)_S)]$ where the sign // specifies the plane of delamination.

Table 2.1: Material properties for HTA/6376C carbon/epoxy **??**

E_{11}	E_{22}=E_{33}	G_{12}=G_{13}	G_{23}
120.0 GPa	10.5 GPa	5.25 GPa	3.48 GPa
$\nu_{12} = \nu_{13}$	ν_{23}	G_{Ic}	G_{IIc}
0.3	0.51	0.260 kJ/m^2	1.002 kJ/m^2

The fatigue material properties which were used in these simulations are taken from **?** and summarized in Table **??**. The crack growth rate in the specimen was evaluated in a post-processing step from dividing the growth of the crack along one of the free edges by the number of elapsed cycles. The obtained crack growth rates in simulations were compared with experimental data from **?**.

Table 2.2: Fatigue material properties for HTA/6376C carbon/epoxy laminate **?**

C_I(mm/cycle)	C_{II}(mm/cycle)	C_{mix}(mm/cycle)	η
0.0616	2.99	458087	2.73
m_I	m_{II}	m_{mix}	
5.4	4.5	4.94	

The laminate was modeled as an assembly of sublaminates which are governed by the shear-deformable laminate theory. To discretize the laminate, 6-node triangular shell elements with 5 degrees of freedom for each node were used; where, one layer of elements was considered in each arm. Size of the smallest finite element in these simu-

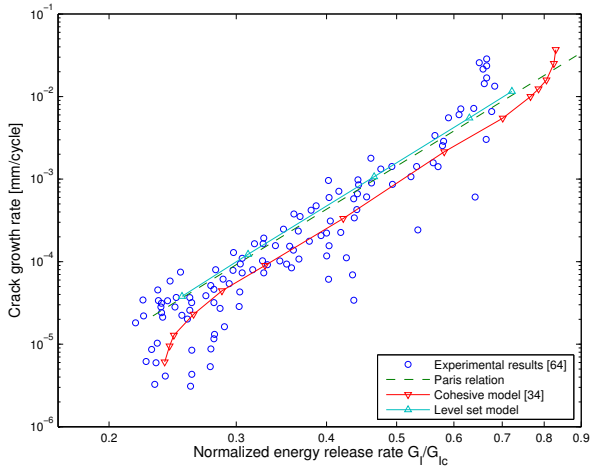

Figure 2.8: Comparison of crack growth rate from level set model with experimental data and cohesive model results for DCB tests

lations was 2.7 mm. Several simulations with different values of applied moments were conducted and the computed crack growth rate in each test is plotted versus energy release rate in Fig. **??**. This energy release rate is obtained from an analytical formula which relates the energy release rate to the applied moment M **?**:

$$G_I = \frac{M^2}{bEI} \tag{2.20}$$

where b is the specimen width, E is the longitudinal Young's modulus and I is the second moment of area of the specimen's arm. It should be noted that with the applied load envelope strategy, the moment M is equal to the maximum cyclic moment, and the computed value for the energy release rate is therefore equal to the maximum value in the cycle ($G = G_{max}$).

Fig. **??** compares numerical results obtained from the level set model, experimental data **?**, and cohesive model results **?**. Excellent agreement is found between level set results and Paris curve fitted through experimental results. This Paris curve was input for both level set and cohesive model **?** and it is reproduced more accurately by the level set model. For the mixed mode fracture energy parameters and the Paris law parameters, which are input parameters in the cohesive zone method as well as in the level set model, the same values were used in both analysis. Parameters that are required for the cohesive zone method but not for the level set method are the cohesive strength parameters. In contrast, the level set model has one additional parameter, which is the stabilization parameter κ. For κ, a value of 0.5 was default in all simulations.

The level set model does not predict the limit behavior in regions I and III of fatigue crack growth (see Fig. **??**). In the current implementation, the level set model just covers

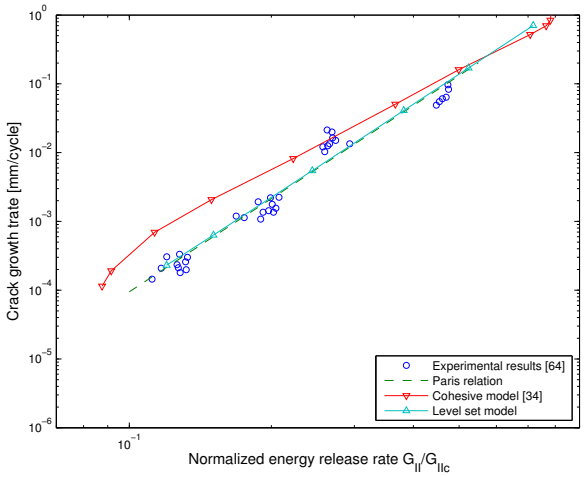

Figure 2.9: Comparison of crack growth rate from level set model with experimental data and cohesive model results for 4ENF tests

the Paris law, which is only valid in region II. Nevertheless, it is possible to redefine the relation between v and G as a piecewise function covering the three regions. This can be implemented by adapting Eq. **??**.

2.3.2. SIMULATION OF 4ENF TEST UNDER FATIGUE LOADING

A similar validation exercise was performed for the mode II case of the four point end-notched flexure (4ENF) test (Fig. **??**-center). The geometry and material were the same as in the previous section, but the boundary conditions were different. In these simulations the size of the smallest element was 1.73 mm. In this case the energy release rate is related to the applied load P as **?**

$$G_{II} = \frac{3c^2 P^2}{16bEI} \tag{2.21}$$

where c is the distance between load and support (see Fig.**??**). The results of the simulations are presented in Fig. **??**. The Paris relation that served as an input for the model is again retrieved with high accuracy. This does not hold for the cohesive model results **?** due to aforementioned difficulties to implement the Paris law in the framework of the cohesive law and damage mechanics.

2.3.3. SIMULATION OF MIXED-MODE TEST UNDER FATIGUE LOADING

In the simulated mixed-mode test the material and geometry of the specimen were the same as in the DCB and 4ENF tests, and the same approach was followed for validating the numerical results. Size of the smallest finite element in the following simulations was 1.8 mm. In this test the specimen was loaded with two unequal moments (Fig. **??**-right).

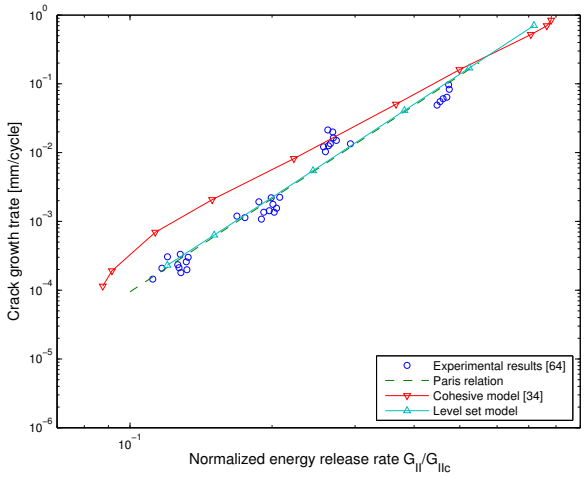

Figure 2.10: Comparison of crack growth rate from level set model with experimental data and cohesive model results for mixed-mode tests

The ratio between them ρ, is given by **?**

$$\rho = \frac{1 - \frac{\sqrt{3}}{2}}{1 + \frac{\sqrt{3}}{2}} \tag{2.22}$$

The relationship between applied moments M results in a mode ratio of 50 %, with pure mode energy release rate contributions defined as **?**

$$G_I = G_{II} = \frac{3}{4\left(1 + \frac{\sqrt{3}}{2}\right)^2} \frac{M^2}{bEI} \tag{2.23}$$

The total energy release rate is computed from pure mode contributions using Eq. (**??**), and the fracture energy (G_c) is obtained from Eq. (**??**) using the mixed-mode values provided in tables **??** and **??**. The results from the simulations are shown in Fig.**??**. Once again, the results demonstrate a perfect match with the Paris law, proving the suitability of the approach.

2.3.4. CAPTURING LOAD RATIO EFFECTS ON CRACK GROWTH RATE

The fatigue level set model presented in this chapter has the potential to take into account load ratio effects on crack propagation. To test this ability, several DCB simulations on a GFRP laminate under different R-ratios were conducted and the model predictions were verified using the experimental results reported by Shahverdy et al. **?**. The experiments by Shahverdi et al. **?** were performed on a complex composite system. In order to keep the simulations simple, an equivalent isotropic material is used in this

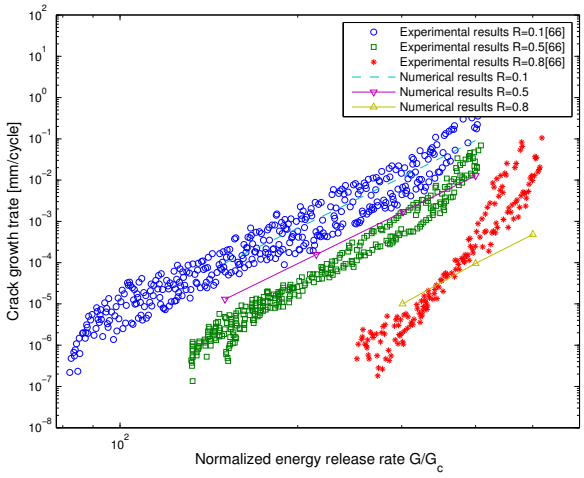

Figure 2.11: Comparison between model predictions and experimental results for different level of load ratio

chapter with elastic properties given in **?**. For our current purpose, we are not so much interested in capturing all the physics of the experiments correctly, but rather in investigating how the influence of load ratio on fatigue crack growth can be included in the model. The laminate Young's modulus and Poisson ratio were 25.0 GPa and 0.23, respectively. The specimen length, width and thickness were 250 mm, 40 mm and 6 mm, respectively, and an initial crack of 50 mm was considered at the mid-height of the beam. The type of elements and mesh size were the same as in section **??**. Three different load ratios, namely $R = 0.1$, $R = 0.5$ and $R = 0.8$ were considered in these simulations. The fracture toughness and Paris law parameters obtained from **?** were $G_c = 0.6$ kJ/m^2, $C = 1.0321 \times 10^{-21}$ mm/cycle and $m = 7.072$.

Fig. **??** presents a comparison between the model predictions and experimental results which shows a good agreement. These results prove the sensitivity of the model to the load ratio. However, there is a notable difference between the slope of numerical plots and the experimental results. This difference is due to the assumption of constant values of m and C for different load ratios. Fig. **??** shows an improvement in numerical results achieved by considering the effect of load ratio on these parameters. The new values of C and m for a different level of load ratio are presented in table **??** which show a rise in the values of m (the slope in log scale) and a decline in the values of C (the intercept in log scale) by increasing the value of load ratio R from 0.1 to 0.8. These values were extracted from the experimental graph provided in **?**.

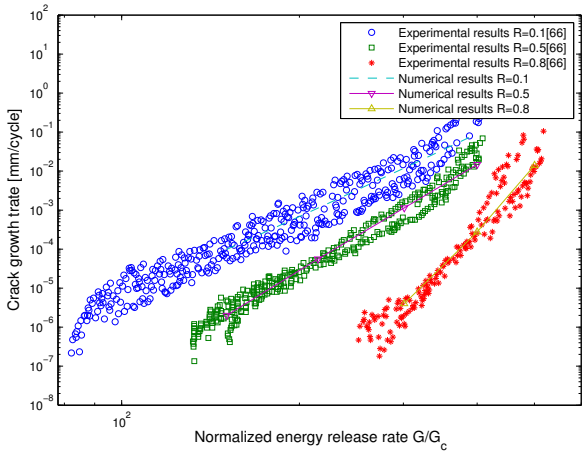

Figure 2.12: Comparison between model predictions and experimental results by considering load ratio effect on Paris law parameters C and m

Table 2.3: Fatigue material properties for hybrid laminate, extracted from experimental data in **?**

R	C(mm/cycle)	m
0.1	1.031×10^{-21}	7.072
0.5	8.143×10^{-27}	8.987
0.8	2.007×10^{-42}	16.066

The results show that the model reproduces the sensitivity of crack growth rate to the load ratio accurately. The experiments indicate that at the same energy release level, by increasing the load ratio the crack growth rate decreased. As this is shown in Fig. **??**, the simulations reproduced this relation between load ratio and crack growth rate correctly. In addition, the improvement observed in model predictions provided in Fig. **??** demonstrates the importance of the load ratio effect on the Paris law constants. Moreover, it highlights the need for a general formulation which can predict the load ratio effects on Paris law constants. To the best of our knowledge, a formulation that accounts for this as well as for mode ratio effects is not available.

2.3.5. SIMULATION OF A SINGLE EDGE NOTCH TEST UNDER FATIGUE LOADING CONDITION

In the previous simulations we dealt with nearly self-similar crack growth. However, as a 3D model the level set model is able to predict the delamination growth pattern in more complex cases. To demonstrate this capability of the model, facesheet delamination growth in a titanium-graphite hybrid laminate was simulated, after single edge

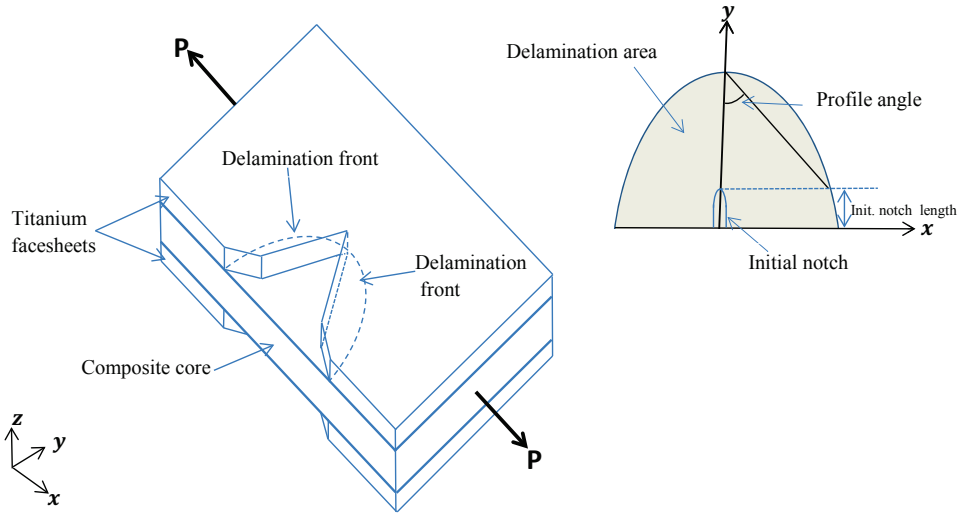

Figure 2.13: Schematic of $[\mathrm{Ti}/0/90/0_2]_s$ laminate in SENT

notch test (SENT) experiments by Burianek et al. **?**. Fig. **??** shows a schematic diagram of the problem.

The experimental procedure is described in **?**. The test specimen was a 152×38 mm^2 rectangular coupon and the lay-up was $[\mathrm{Ti}/0/90/0_2]_s$. Table **??** presents properties of the composite core plies and the titanium facesheets. The values are taken from **?**, with the exception of ν_{23}, which we assumed to be equal to ν_{12}. The thickness of the titanium layers and each composite ply were 0.127 mm and 0.142 mm, respectively. The experimental specimen had a 2 mm long notch which was cut using a 0.64 mm diameter mill **?**, and this starter notch was considered in the finite element model as the initial delamination front.

Table 2.4: Material properties of Titanium graphite laminate **?**

Material properties	Ti 15-3	IM-7/PIXA-M
E_1 (GPa)	107	155
E_2 (GPa)	112	6.9
G_{12} (GPa)	41.4	5.1
ν_{12}	0.33	0.35
ν_{23}	0.33	0.35

In the finite element model, due to the symmetry of the laminate and the assumed symmetry of delamination growth, a quarter of the laminate is modeled. In order to represent the facesheet crack we assumed that the crack tip exactly coincides with the

delamination front. Therefore, the facesheet boundary on the plane of symmetry is free in the delaminated part, while symmetry boundary conditions are applied on the undelaminated part of the facesheet as well as on the core. This simulation was carried out under load control with an applied stress level of 419 MPa. The fatigue material parameters are provided in Table **??**. In this table the Paris law parameters (C, m) and the values for fracture energy (G_{Ic}, G_{IIc}) are taken from **?** and **?** respectively. The value of η is our assumption. Because of the mixed-mode nature of the tests, proper mode-dependent Paris law parameters (Eq. **??**) are needed; however, due to the lack of experimental data the values for C and m are assumed constant. For κ a value of 3 is considered in this simulation.

Table 2.5: Fatigue material properties considered for hybrid laminate in simulation

C(mm/cycle)	m	G_{Ic} (N/mm)	G_{IIc}(N/mm)	η
6.1574×10^{-4}	2.15	0.21	0.45	3.5

The experimental results **?** from the SENT revealed that the stiffness reduction of the laminate is due to a combination of facesheet crack and delamination growth. Consequently, the energy release that is computed along the delamination front near the facesheet crack tip belongs to both of these failure mechanisms. For this reason, the energy release rate computed near the facesheet crack tip can not be used for computing the delamination growth rate. Burianek et al. **?** observed a steady state behavior of facesheet crack growth rate; therefore, to tackle the problem of delamination growth at the vicinity of the crack tip, in this simulation the experimental crack growth rate is taken to be the value of delamination growth rate at the plane of symmetry ($y = 0$). Away from the facesheet crack, delamination is the only failure mode and the delamination growth rate was computed with the energy release rate obtained from the modified virtual crack closure technique described in section **??**. The delamination shape obtained from the simulation was compared with experimental results (see Fig. **??**). The predicted profile is consistent with experimental observations. Unlike the previous analysis of delamination growth in this test **?**, in our model there is no assumption about the delamination shape. Its evolution is predicted by the model.

Burianek et al.**?** reported a change in orientation of the delamination front as the crack progressed. A similar phenomenon is found in the level set model results. The experimental and predicted evolution of the delamination profile angle (see Fig. **??**) are presented in Fig. **??**. Given the fact that the sudden drop in profile angle around a crack length of 20 mm is not to be expected in simulations with homogeneous properties, the results match reasonably well. It is concluded that the level set model for delamination can capture the evolution of the delamination shape during non-self-similar fatigue crack growth.

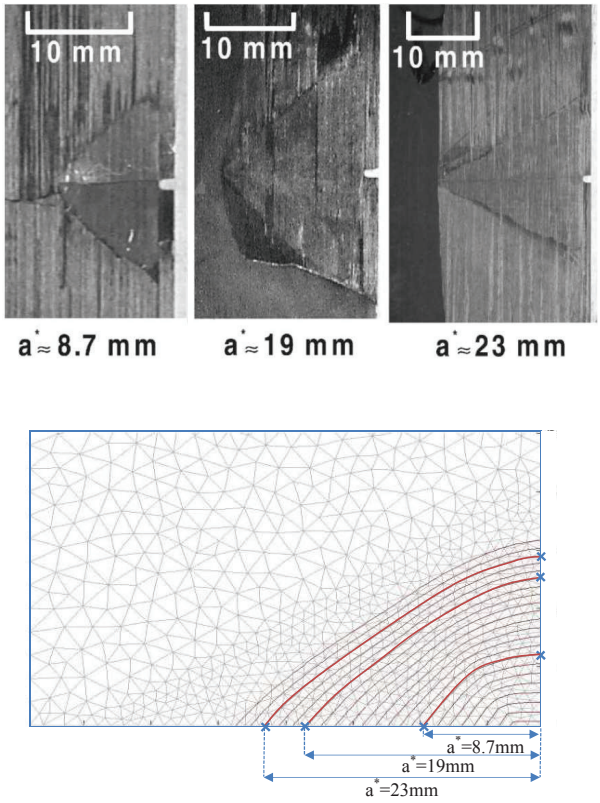

Figure 2.14: Comparison of experimental **?** (top) and numerical delamination (bottom) profiles for $[\mathrm{Ti}/0/90/0_2]_s$ laminate in SENT

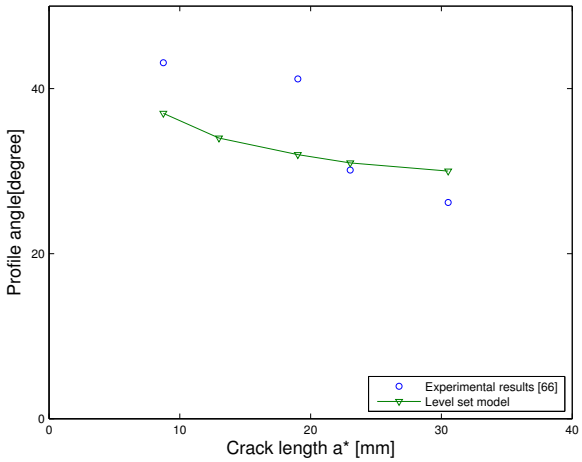

Figure 2.15: Comparison of experimental **?** and numerical delamination profile for $[\mathrm{Ti}/0/90/0_2]_s$ laminate in SENT as a function of crack length

2.4. CONCLUSIONS

A level set model is proposed which introduces a new approach to simulating delamination propagation under fatigue loading conditions. Unlike other recent fatigue models, which follow damage mechanics and the cohesive zone approach, the level set model is developed based on fracture mechanics theory. The crack front location is described implicitly with a level set field and this field is updated according to the velocity computed from the Paris law. The model predicts the crack growth rate in different modes of fracture precisely. This was demonstrated by simulating the propagation rates of mode I, mode II and mixed-mode tests and comparing results with experimental measurements and direct evaluation of the Paris law. The results reveal a higher accuracy of the level set model compared with the cohesive zone approach.

The load ratio effect on fatigue crack propagation was captured in the simulation of DCB tests on a GFRP laminate. These results reveal the dependence of Paris law parameters on the load ratio which affects the accuracy of the model predictions. The model can deal with effects of mode ratio and load ratio on crack growth rate, provided that sufficiently rich Paris law parameters are available.

The fatigue level set model captures the delamination growth pattern without any predefined front shape. This is due to a specific enrichment scheme of cracked elements which allows the crack front to intersect the elements at arbitrary locations. This special representation of the kinematics of delamination allows for a continuous and smooth progression of the front during the analysis. The ability of the model to represent non-self-similar crack growth was demonstrated by simulating a single edge notch test in a hybrid laminate. The predicted trend in the delamination shape has good agreement with experimental observations.

3

AN INTERFACE THICK LEVEL SET MODEL FOR SIMULATING DELAMINATION IN COMPOSITES

ABSTRACT

This chapter presents an interface thick level set model for modeling delamination initiation and propagation in composites. Interface elements are widely applied in delamination models to define a discontinuity between layers of a laminate. In this chapter the common damage definition in the constitutive relation of interface elements is replaced with a new definition developed using the thick level set approach. Following this approach a band of damage with predefined length is considered where the damage is defined as a function of distance to the damage front. The specifications of suitable damage functions for the developed method are investigated and an efficient damage function is introduced. A sensitivity analysis of numerical input parameters is performed which proves that the model is not sensitive to the length of the damage band. Since the required element size is linked to the length of the damage band, the insensitivity to this length provides freedom to use coarser meshes. Furthermore, the model provides a direct link between fracture mechanics and damage mechanics which enables further development of the model for fatigue analysis. Validation of this model is presented by conducting three-dimensional mode I, mode II and mixed-mode simulations and comparing the results with analytical solutions.

3.1. INTRODUCTION

Delamination is one of the main causes of failure in composite structures. To simulate delamination, several numerical models have been developed in the framework of

This chapter is based on **?**: Latifi, M.; van der Meer, F.P.; Sluys, L.J: An interface thick level set model for simulating delamination in composites. International Journal for Numerical Methods in Engineering (In press)

damage mechanics. These damage models are mostly formulated based on the cohesive crack approach which considers a small fracture process zone around the crack tip **???**. Cohesive tractions are defined as a function of displacement jumps using a cohesive traction-separation law. Cohesive models are conveniently implemented in finite element programs using interface elements that define the discontinuity at the interface between layers of a laminate.

A critical aspect in using cohesive models is the number of interface elements applied in the model **?**. The load displacement response of the simulated structure is smooth when the mesh is fine enough, otherwise oscillations may appear in the response, leading to inaccurate results and convergence difficulties. Satisfying this mesh size requirement for analysis of a structure or component on industrial scale needs excessive computational work **?**. To tackle this problem, Turon et al. **?** proposed to reduce the maximum interfacial strength which results in a larger process zone at the interface. This larger process zone enables an accurate simulation with an almost 10 times coarser mesh compared to an analysis with the nominal interface strength **?**. However, a lower interfacial strength also affects the criterion for the initiation of delamination which may lead to an overestimation of the predicted delamination area. Van der Meer et al.**?** have introduced a level set model for delamination that allows the use of elements which are larger than the cohesive zone; however, this method is only applicable for modeling a single delamination in thin structures.

The second open issue concerning cohesive models is related to extending these damage models to fatigue analysis. This extension needs an accurate extraction of energy release rate to link damage growth to the fracture mechanics based Paris law. Computing the energy release rate in a damaging cohesive law is not straightforward. In earlier work **?**, we have shown that level set based methods provide a better match with the Paris law.

In this chapter a new method for delamination modeling is proposed that is promising for overcoming these two issues associated with the cohesive zone method. The new method is developed around a definition of damage using the thick level set (TLS) approach. The thick level set approach to model damage growth in solids was first introduced by Möes et al. **?** as a continuum damage model. The model contains a non-local treatment to avoid spurious localizations. This non-local treatment appears when the energy release rate is computed by integrating local values of a configurational force over the width of the damaged zone. This zone has a predefined width, l_c, over which the damage variable is computed as an explicit function of a level set field. The signed distance function is used for the level set field, which means that the distance to a moving front is known throughout the domain. Damage changes from 0 to 1 as the distance behind the front increases from 0 to l_c. Bernard et al. **?** improved this model to a robust and easy to implement model with an explicit damage growth algorithm. Van der Meer and Sluys **?** extended this continuum model by introducing a special interphase material and a strength-based initiation parameter for simulating cusp formation at the core of a sandwich loaded in shear.

In contrast with the earlier continuum damage implementation of the thick level set method, the new model proposed in this chapter is a discontinuous damage model for modeling delamination. Damage is now applied to an initially stiff interface and the con-

figurational force is computed from the displacement jump. The discontinuity is defined using interface elements. The model results are not sensitive to the chosen width of the damaged zone and this width can be increased to allow for the use of larger elements. An independent stress-based initiation criterion is introduced for the proposed model. Therefore, in contrast with cohesive zone models, the size of the numerical fracture process zone can be increased to alleviate mesh requirements without causing spurious initiation of damage. The new method has the potential to be easily extended to fatigue analysis, because it provides a link between fracture mechanics and damage mechanics.

In section **??** the solution scheme and the formulation of the model will be introduced. A sensitivity study of input parameters as well as the validation of the model will be presented in section **??**.

3.2. METHODS

Before details of the formulation are given, the solution algorithm is briefly discussed (see Fig. **??**). The TLS method provides a staggered solution algorithm in which in each time step displacements and damage growth are computed sequentially **?**. The same is adopted in the proposed interface version of the TLS approach. The solution starts with a given level set field $\phi(x, y)$. The iso-zero of this field implicitly defines the damage front location. The damage distribution follows from the level set field through a predefined damage function $d(\phi)$. Using a standard finite element computation the displacement jump (Δ) and traction (τ) are obtained.

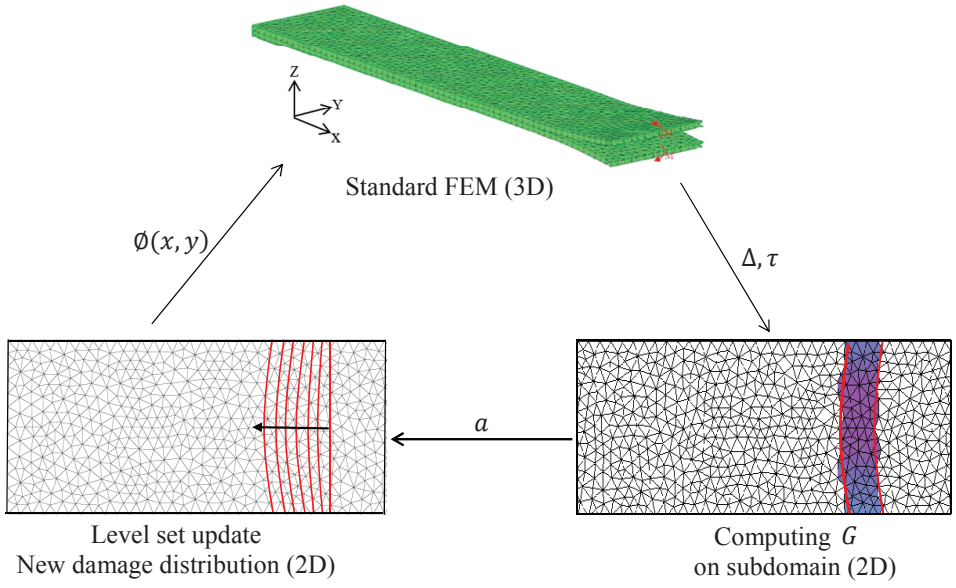

Figure 3.1: Solution algorithm in interface version of the thick level set method

Next, this displacement jump is used for computing the energy release rate along the damage front (G). This is done by solving an additional system of equations over a subdomain in the 2D mesh at the interface. Solving the extra system of equations is not expensive, because it is linear and restricted to the damaged band. The computed energy release rate allows to compute the front movement (a) which is used to update the level set field. These new level set values are used to define the front location and damage distribution for the next time step.

3.2.1. LOCAL GOVERNING EQUATIONS

The constitutive law of an interface element that relates the displacement jump Δ to the traction τ in a material discontinuity is derived from the definition of free energy. The free energy per unit surface of interface is expressed as

$$\varphi(\boldsymbol{\Delta}, d) = (1-d)\varphi_0(\boldsymbol{\Delta}) \tag{3.1}$$

where $\boldsymbol{\Delta}$ is a vector that contains the displacement jump in local coordinate frame and d is a damage parameter that is a function of level set field (ϕ) which will be introduced in section **??**. This definition of damage is significantly different from the cohesive zone approach, where the damage is a function of displacement jump ($\boldsymbol{\Delta}$). The variable φ_0 in Eq.(**??**) is defined as

$$\varphi_0(\boldsymbol{\Delta}) = \frac{1}{2}\Delta_i K \delta_{ij} \Delta_j \quad i = 1,2,3; \quad j = 1,2,3 \tag{3.2}$$

where K is the dummy stiffness and δ_{ij} is the Kronecker delta. This expression for free energy φ is valid for tension dominated cases; however, in compression negative values of the displacement jump in normal direction Δ_3 represent unphysical interpenetration at the contact surface. Therefore, to prevent significant interfacial interpenetration, damage is deactivated in normal direction if the normal displacement jump is negative and Eq. (**??**) is modified into

$$\varphi(\boldsymbol{\Delta}, d) = (1-d)\varphi_0(\Delta_i) - d\varphi_0(\delta_{3i}\langle -\Delta_3 \rangle) \tag{3.3}$$

where the MacAuley bracket is defined as $\langle x \rangle = \frac{1}{2}(x + |x|)$. The traction-displacement law at the material discontinuity is obtained by differentiation of the free energy with respect to the displacement jump:

$$\tau_i = \frac{\partial \varphi}{\partial \Delta_i} = (1-d)K\delta_{ij}\Delta_j - dK\delta_{ij}\delta_{3j}\langle -\Delta_3 \rangle \tag{3.4}$$

The local driving force for damage growth is obtained by differentiating the free energy with respect to the damage variable:

$$Y = -\frac{\partial \varphi}{\partial d} = \varphi_0(\Delta_i) - \varphi_0(\delta_{3i}\langle -\Delta_3 \rangle) \tag{3.5}$$

3.2.2. DAMAGE DEFINITION IN THE TLS APPROACH

In the TLS method a length scale (l_c) is defined in the wake of a damage front which determines the size of the damaged zone between the sane and fully damaged material (see

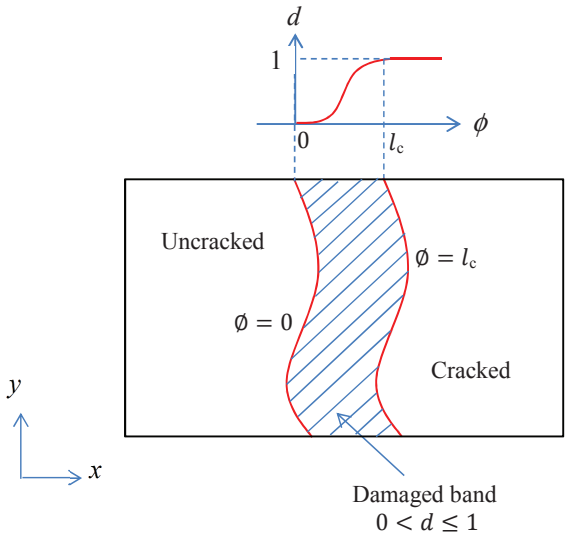

Figure 3.2: Damaged zone between cracked and uncracked material

Fig.**??**). The level set method provides the shortest distance of every point in the domain to the front using a signed distance function. The iso-zero of this function is the damage front. The damage is defined as a function of distance to the front which increases from 0 to 1 as the level set field rises from 0 to l_c. The mathematical interpretation of the introduced damage parameter is expressed with $d(\phi) = f(\phi)$ where $f(\phi)$ is a continuous function that is differentiable on the domain $(0 < \phi < l_c)$ and satisfies

$$\begin{cases} f(\phi) = 0 & (\phi = 0) \\ f(\phi) = 1 & (\phi = l_c) \\ f'(\phi) > 0 & (0 < \phi < l_c) \end{cases} \tag{3.6}$$

3.2.3. COMPUTATION OF ENERGY RELEASE RATE

In the TLS approach the front energy release rate is obtained as a non-local quantity by integrating the local driving force over the damaged zone. When the damage front moves infinitesimally from $A(0,\alpha)$ (see Fig. **??**) to a new location A' in the damaged band, the distance of any point $P(\phi,\alpha)$ to the front will change. Therefore, damage in these points which is defined as a function of shortest distance to the front will be updated which results in variation of free energy in these points. The energy released due to the movement of point A can be computed by integrating the local variation of free energy inside the damaged band:

$$G = -\int_0^l \frac{\partial \varphi}{\partial \phi} d\phi = -\int_0^l \frac{\partial \varphi}{\partial d}\frac{\partial d}{\partial \phi} d\phi \tag{3.7}$$

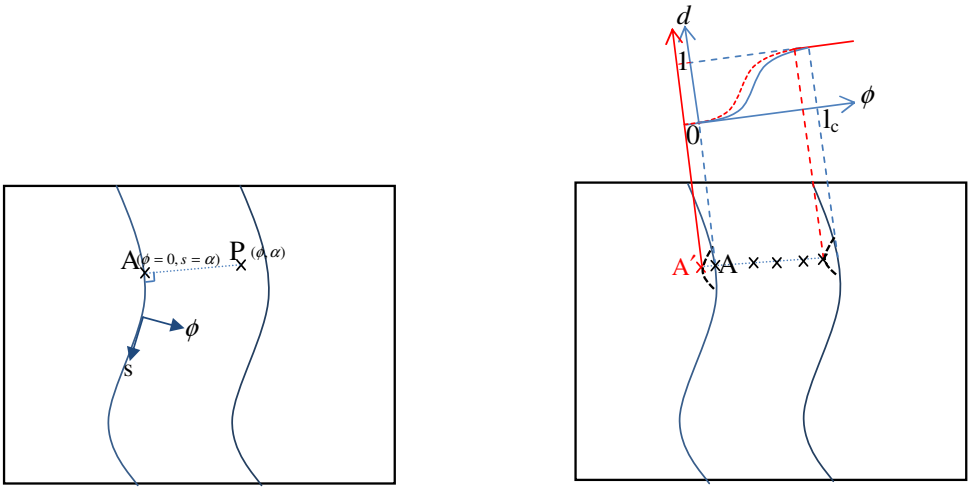

Figure 3.3: Updating damage distribution inside damage band due to an infinitesimal movement of point A

where l is the length of the damaged band which is equal to l_c for a fully developed damaged band. Using the definition of local driving force in Eq.(**??**), we can rewrite above equation based on Y:

$$G(s) = \int_0^l d'(\phi)\, Y(\phi, s) \left(1 - \frac{\phi}{\rho(s)}\right) d\phi \tag{3.8}$$

where $d'(\phi)$ is the spatial derivative of the damage function and ρ is the front curvature **?**. Eq.(**??**) enables us to compute the energy release rate along the damage front. Practically to update the level set field, values for G need to be known on nodes along the front. For this reason, an average value of the local driving force, $\bar{Y}$ is introduced which is defined as

$$\int_0^l d'(\phi)\, \bar{Y}(s) \left(1 - \frac{\phi}{\rho(s)}\right) d\phi = \int_0^l d'(\phi)\, Y(\phi, s) \left(1 - \frac{\phi}{\rho(s)}\right) d\phi \tag{3.9}$$

The field $\bar{Y}$ is discretized over the nodes of the elements inside the damaged band; however, following Bernard et al.**?** the constraint that $\bar{Y}$ is constant in ϕ direction ($\nabla \bar{Y} \cdot \nabla \phi = 0$) is weakly enforced using Lagrange multipliers. For this reason, a variational approximation of $\bar{Y}(s)$ is introduced ($\bar{\bar{Y}}$) which is not only a function of s, but a function of s and ϕ. Then, Eq.(**??**) becomes

$$\int_0^l d'(\phi)\, \bar{\bar{Y}}(s,\phi) \left(1 - \frac{\phi}{\rho(s)}\right) d\phi = \int_0^l d'(\phi)\, Y(\phi, s) \left(1 - \frac{\phi}{\rho(s)}\right) d\phi$$
$$\text{subject to} \quad \nabla \bar{\bar{Y}} \cdot \nabla \phi = 0 \tag{3.10}$$

The Galerkin method is employed to find nodal values for $\bar{\bar{Y}}$ from a discretized version of Eq.(**??**) subject to the constraint with Lagrange multipliers with the following system of equations **?**:

$$\begin{bmatrix} \mathbf{K} & \mathbf{L} \\ \mathbf{L} & \mathbf{0} \end{bmatrix} \begin{Bmatrix} \bar{\bar{\mathbf{Y}}} \\ \mathbf{I} \end{Bmatrix} = \begin{Bmatrix} \mathbf{f^y} \\ \mathbf{0} \end{Bmatrix} \tag{3.11}$$

The matrices and the right hand side vector are defined as

$$K_{ij} = \int_{\Omega^d} d' N_i N_j + \frac{\kappa h^2}{l_c} \frac{\partial N_i}{\partial x_k} \frac{\partial N_j}{\partial x_k} d\Omega \tag{3.12}$$

$$L_{ij} = \int_{\Omega^d} l_c \left(\frac{\partial N_i}{\partial x_k} \frac{\partial \phi}{\partial x_k} \right) \left(\frac{\partial N_j}{\partial x_k} \frac{\partial \phi}{\partial x_k} \right) d\Omega \tag{3.13}$$

$$f_i^Y = \int_{\Omega^d} N_i d' Y d\Omega \tag{3.14}$$

where Ω^d is the domain of the damaged band, κ is a stabilization parameter which affects the smoothness of $\bar{\bar{Y}}$ along the damage front, h is the typical element size, and N_i and N_j are standard linear shape functions associated with nodes i and j. The necessity and influence of the stabilization term in Eq.(**??**) which was not present in Eq.(**??**) will be studied in section **??**.

3.2.4. DAMAGE GROWTH

To update the damage distribution, advance of the level set front should be related to the computed values for the energy release rate $\bar{\bar{Y}}$. In the proposed TLS model following **?** and **?** $\bar{\bar{Y}}$ is obtained from unit load analysis. The actual value of configurational force ($\bar{\bar{Y}}_{actual}$), corresponds to $\bar{\bar{Y}}$ multiplied with the square of the yet unknown load factor λ: $\bar{\bar{Y}}_{actual} = \lambda^2 \bar{\bar{Y}}$. To compute the load factor λ we introduce the material resistance against damage growth as Y_c. The damage develops when in at least one point of the front the value of $\bar{\bar{Y}}_{actual}$ is equal to Y_c. The load factor is therefore defined as the value for which the maximum nodal value $\bar{\bar{Y}}_i$ at the elements that contain the damage front becomes equal to Y_c:

$$\lambda^2 (\bar{\bar{Y}}_i)_{max} = Y_c \tag{3.15}$$

To obtain the movement of the front, the value of actual configurational force ($\lambda^2 \bar{\bar{Y}}$) is related to the nodal increase in the level set field (a_i) at nodes of elements that contain the damage front (see Fig.**??**), using the formula provided in **?**:

$$a_i = \frac{a_{max}}{r-1} \left\langle \frac{r \lambda^2 \bar{\bar{Y}}_i}{Y_c} - 1 \right\rangle \tag{3.16}$$

where the parameter r defines the spread of the front movement and a_{max} is the maximum of a_i values along the front. It should be noted that in the level set method the damage front moves only in normal direction; therefore, the damage front advance can

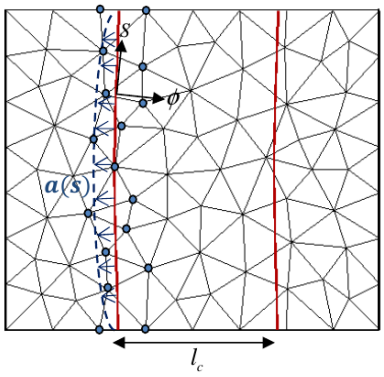

Figure 3.4: Profile of front movement

be expressed with a scalar field. The stability of the method requires to choose a value for a_{max} smaller than the size of an element **?**. In this chapter the value of $a_{max} = 0.25 h_{min}$ is used where h_{min} is defined as the characteristic size of the smallest element. The characteristic size of an element is equal to the length of the diagonal of the smallest rectangle around the element. In order to define the damage distribution for the next time step we need to update the level set field throughout the domain. However, the values obtained from Eq.(**??**), just belong to the nodes around the front. Therefore, these values are extended over the whole domain using a fast marching method **?**. The nodal values of the level set field are then updated from time step n to time step $n+1$ with:

$$\phi_i^{n+1} = \phi_i^n + a_i \tag{3.17}$$

The updated level set field defines the new damage distribution for the next time step. The new damage front location is implicitly defined as the iso-zero of this new level set field.

The presented loading scheme based on unit load analysis is only valid for cases where apart from damage growth the response of the structure is linear. For other cases different loading schemes have to be defined with a closed form relation between energy release rate and crack growth rate such as adopted in **??**.

3.2.5. CRACK PROPAGATION

In case of a mature damaged band, movement of the damage front implies crack propagation. The resistance against damage growth, Y_c, should then be related to the material resistance against crack growth, or the fracture energy G_c. Using the equalities provided in Eqs. (**??**) and (**??**) the relation between G and $\bar{Y}$ is more straightforward than in the continuum version of the TLS method:

$$G = \bar{Y} \int_0^{l_c} d'(\phi) d\phi = \bar{Y} \tag{3.18}$$

Based on this definition the computed values $\bar{\bar{Y}}_i$ stand for the energy release rate upon crack growth and Y_c in Eq. (**??**) can be replaced directly with G_c. The dependence of G_c on the fracture mode is taken into account using the expression introduced by Benzeggagh and Kenane **?**:

$$G_c = G_{Ic} + (G_{IIc} - G_{Ic})(\beta)^{\eta} \tag{3.19}$$

where η is a mode interaction parameter, G_{Ic} and G_{IIc} are fracture energy in modes I and II, and the mode ratio β is defined as

$$\beta = \frac{G_{II} + G_{III}}{G} = \frac{G_{shear}}{G} \tag{3.20}$$

where, G_{shear} is the value of the shear part of the energy release rate. The dependence of G_c on β and G_{shear} means that, apart from evaluation of G, we also need to compute G_{shear} for damage update. To obtain the nodal values of shear contribution of the averaged configurational force, Eq.(**??**) is solved once more in slightly updated form:

$$\begin{bmatrix} \mathbf{K} & \mathbf{L} \\ \mathbf{L} & \mathbf{0} \end{bmatrix} \begin{Bmatrix} \bar{\bar{\mathbf{Y}}}_{shear} \\ \mathbf{I} \end{Bmatrix} = \begin{Bmatrix} \mathbf{f}^{\mathbf{y}} \\ \mathbf{0} \end{Bmatrix} \tag{3.21}$$

where at the right hand side in Eq.(**??**), the shear component of the local driving force, Y_{shear}, is used instead of the complete local driving force Y:

$$f_i^Y = \int_{\Omega^d} N_i d' Y_{shear} d\Omega \tag{3.22}$$

where Y_{shear} is defined as

$$Y_{shear} = \frac{1}{2} \Delta_i K \delta_{ij} \Delta_j, i = 1,2; j = 1,2 \tag{3.23}$$

It should be recalled that Δ_3 is the jump in normal direction; therefore, Δ_1 and Δ_2 represent the shear part of the displacement jump.

Note that with the level set formulation it is possible to transform the displacement jump in the local ϕ and s frame and compute mode II and mode III contributions separately from Δ_1 and Δ_2. Due to the absence of established phenomenological relation between G_c and independent G_{II} and G_{III}, this is not done in this chapter, but distinction between mode II and III energy release rates is an additional potential advantage of the present approach over classical cohesive methods.

3.2.6. INITIATION

To handle damage initiation for the proposed model a strength based material property is considered as a criterion for damage initiation. This criterion is local because when the length of the damaged band tends to zero, the average of energy release rate $\bar{Y}$ tends to the local value Y. The delamination initiates when the norm of the interfacial traction exceeds τ_{max}:

$$\lambda \sqrt{\tau \cdot \tau} \geq \tau_{max} \tag{3.24}$$

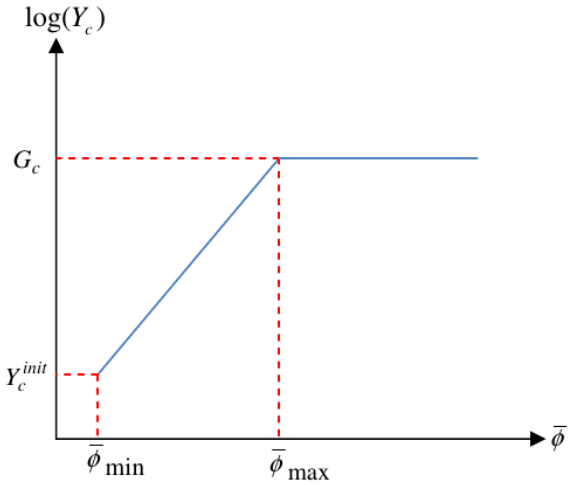

Figure 3.5: Interpolation of Y_c between Y_c^{init} and G_c

where the value of τ_{max} is computed using this formula **?**:

$$(\tau_{max})^2 = (\tau^I_{max})^2 + \left((\tau^{II}_{max})^2 - (\tau^I_{max})^2\right)\beta^\eta \tag{3.25}$$

where τ^I_{max} and τ^{II}_{max} are interfacial strength corresponds with mode I and mode II loading. It is assumed in this formula that the interfacial strength of mode II and mode III are equal ($\tau^{II}_{max} = \tau^{III}_{max}$).

When the criterion introduced in Eq.**??** is met in any point along the boundary, a small damaged band with the size smaller than l_c is placed in front of this point. The size of this band increases according the same methodology as introduced in sections **??** and **??**. The value of critical energy (Y_c) in Eq.**??** increases from an initial value Y_c^{init} for the initial damaged band to G_c for a fully damaged band. The initial resistance against damage growth corresponds to the value of Y at initiation (cf. Eq.(**??**):

$$Y_c^{init} = \frac{(\tau_{max})^2}{2K} \tag{3.26}$$

where K is the dummy stiffness. To provide a smooth transition between damage initiation ($Y_c = Y_c^{init}$) and crack propagation ($Y_c = G_c$) the intermediate values of Y_c are related to the size of the damaged zone similar to what was proposed for the continuum TLS in **?**, using a new interpolation function for $\log(Y_c)$ (see Fig **??**):

$$\log(Y_c) = \log(Y_c^{init}) + \frac{\bar{\bar{\phi}} - \bar{\phi}_{init}}{\bar{\phi}_{max} - \bar{\phi}_{init}}(\log(G_c) - \log(Y_c^{init})) \tag{3.27}$$

where $\bar{\phi}_{init}$ and $\bar{\phi}_{max}$ represent a measure of the initial size of damaged band and the size of a fully developed damaged band. $\bar{\phi}$ is a measure for the size of a damaged zone

defined as the averaged value of ϕ inside a contiguous damaged domain. Its nodal counterpart $\bar{\bar{\phi}}$ is computed in each time step in a similar way as $\bar{\bar{Y}}$ by inserting $\bar{\bar{\phi}}$ instead of $\bar{\bar{Y}}$ in Eq.(**??**) and the value of level set field ϕ instead of Y in the right hand side vector. Furthermore the factor d' is omitted from left hand side and right hand side expressions (cf., Eqs. **??** and **??**). Variations of $\bar{\bar{\phi}}$ in s direction are removed by considering a high value of κ for computing $\bar{\phi}$ values. The value of $\bar{\phi}$ for the damaged band of length l ($l_0 < l < l_c$) can vary from $l/3$ for a band with a circular front to $l/2$ for a straight front. In this chapter in mode I, mode II and mixed-mode simulations for an initial damage band with a length l_0 and a straight front the value of $\bar{\phi}_{init}$ is equal to $l_0/2$, where l_0 is chosen based on the shape of damage function $d(\phi)$ and introduced at the end of section **??**. The value of $0.465 l_c$ is considered for $\bar{\phi}_{max}$ in this chapter.

The solution algorithm for the proposed model is summarized in Fig. **??**. It shows when the initiation criterion is evaluated and also when the systems of equation, associated with $\bar{Y}$, $\bar{Y}_{shear}$ and $\bar{\phi}$ are solved. If there is no initial damage defined, in the first time step the load scale factor can not be computed. The elasticity solution from this time step is used to identify the point with maximum traction and λ is set to a very high value to force initiation to take place.

3.2.7. INTEGRATION SCHEME

The three point Gauss integration scheme is used for the triangular elements in the mesh in the interface to evaluate the integral in Eqs.(**??**)-(**??**). However, to improve the accuracy of the model, a sub-triangulation method is used in the finite elements that are intersected by the bounds of the damaged zone. This is done on both bounds of the zone, at the iso-zero and iso-l_c of the level set field. It is shown in Fig. **??** how this method provides 6 more integration points for partitioned elements. The effect of the integration scheme on the accuracy of results is investigated in section **??**. Integration points in sub-triangulated elements that are outside the band are kept for implementation simplicity. These points do not contribute to the relevant terms in the integral, because the derivative of damage function (d') is equal to 0 in the areas where $d = 0$ or $d = 1$.

3.3. RESULTS AND DISCUSSION

In this section first the influence of input parameters on the efficiency of the model is investigated by comparing the amount of oscillations in the load displacement responses in double cantilever beam (DCB) simulations. In these comparisons, the values of the input parameters are varied, with constant mesh size. Quasi two-dimensional DCB simulations with a structured mesh (see Fig. **??**) are considered to investigate the effect of input damage function ($d(\phi)$). The 2D analysis enables us to visualize the variation of relevant fields along the length with simple 1D plots. Full 3D DCB simulations with an unstructured mesh are done in order to investigate the effect of the length of the damaged band (l_c), integration scheme and stabilization parameter (κ). After this sensitivity analysis, the model is validated by comparing the numerical results from mode I, mode II and mixed-mode 3D simulations against analytical solutions.

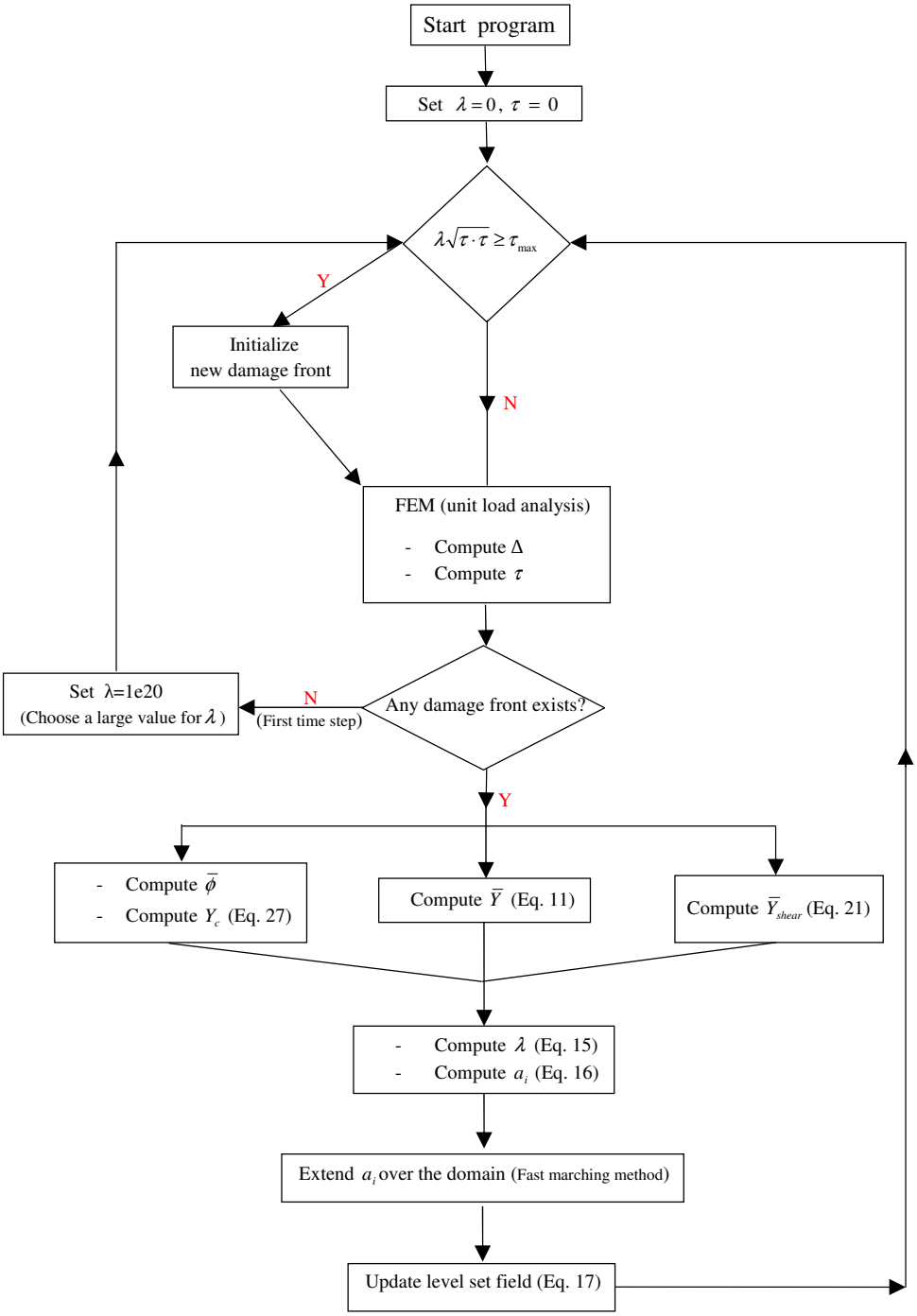

Figure 3.6: The solution algorithm for the thick level set interface model

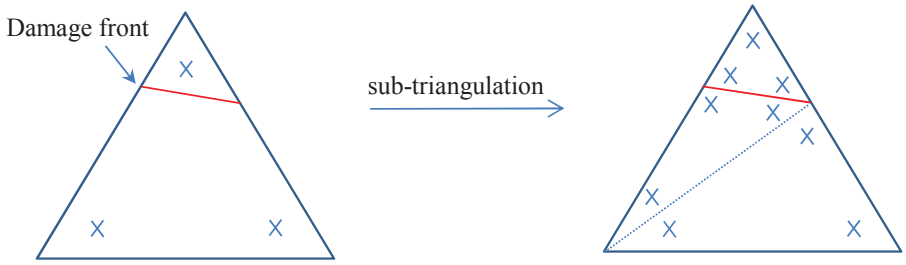

Figure 3.7: Sub-triangulation provides 6 more integration points at elements which contain damage front or the iso-l_c

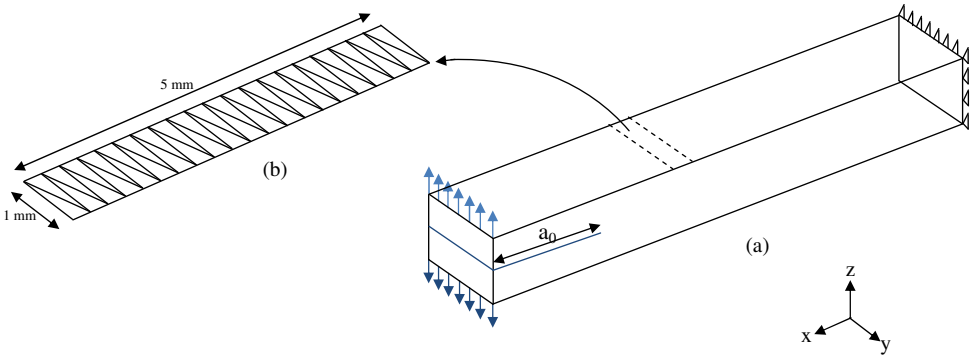

Figure 3.8: Quasi 2D DCB model to test different damage functions: a) loading and boundary conditions (not in scale) b) structured mesh used in simulations

3.3.1. EFFECT OF INPUT DAMAGE FUNCTION

In order to investigate the sensitivity of results to the shape of the damage profile, a DCB test was modeled. This test is common to determine the mode I fracture toughness. The boundary conditions of simulations are shown in Fig. **??**. The material properties used for these simulations are presented in Table **??** in which index 1 refers to the fiber direction, which is aligned with the x axis in Fig. **??**. The specimen was 100 mm long and 1 mm wide with arms of 0.525 mm thick and an initial crack of 26.5 mm. A structured mesh with a single element over the width of the specimen and input values $l_c = 3$ mm and $\kappa = 20$ were used for this analysis. Three different damage functions d_1, d_2 and d_3 were considered (see Fig. **??**). The initiation is not considered for these simulations, because the length of initial damage band (l_0) can be dependent on the type of damage function that is used. Here, the different damage functions are compared regarding crack propagation only. All simulations start with a fully damaged band with a length of $l_c = 3$ mm.

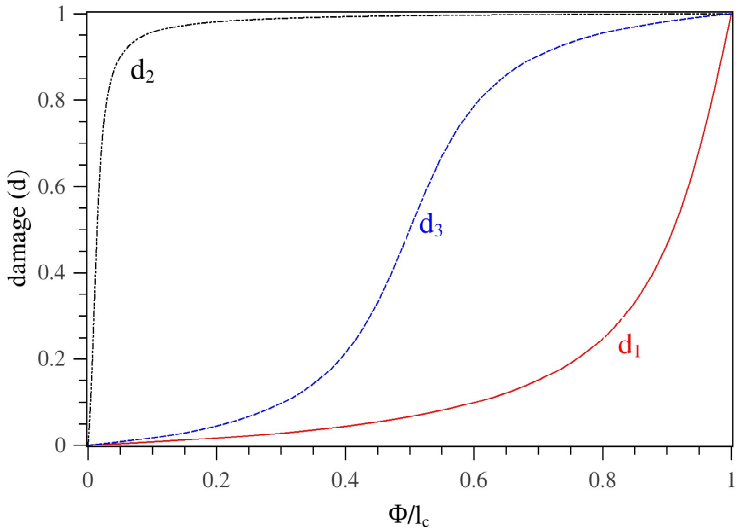

Figure 3.9: Three different shapes of possible damage functions

Table 3.1: Material properties for AS-4/3501-6 graphite/epoxy **?**

E_1	E_2	G_{12}	G_{23}	ν_{12}	G_{Ic}	τ^I_{max}
138000 MPa	8960 MPa	7100 MPa	3446 MPa	0.3	0.222 kJ/m^2	51.7 MPa

The damage profiles were obtained from an arc-tangent formula **?**:

$$f(\phi) = c_2 \text{atan}\left(c_1\left(\frac{\phi}{l_c} - c_3\right)\right) + c_4 \tag{3.28}$$

where satisfying the conditions for the damage function $d(\phi) = f(\phi)$ as given in Eq. (**??**), determines c_2 and c_4 respectively:

$$c_2 = (\text{atan}(c_1(1-c_3)) - \text{atan}(-c_1 c_3))^{-1} \tag{3.29}$$

$$c_4 = -c_2 \text{atan}(-c_1 c_3) \tag{3.30}$$

The values of user defined parameters c_1 and c_3 for different damage functions were ($c_1 = 10$, $c_3 = 1$) for d_1, ($c_1 = 100$, $c_3 = 0.01$) for d_2 and ($c_1 = 10$, $c_3 = 0.5$) for d_3. The damage function d_3 was used earlier for simulation in continuum level set models in **??**. Fig. **??** compares the DCB response related to each damage function. The observed difference between the computed stiffness of the structure before propagation with different damage functions is due to the fact that the initial condition for these simulations

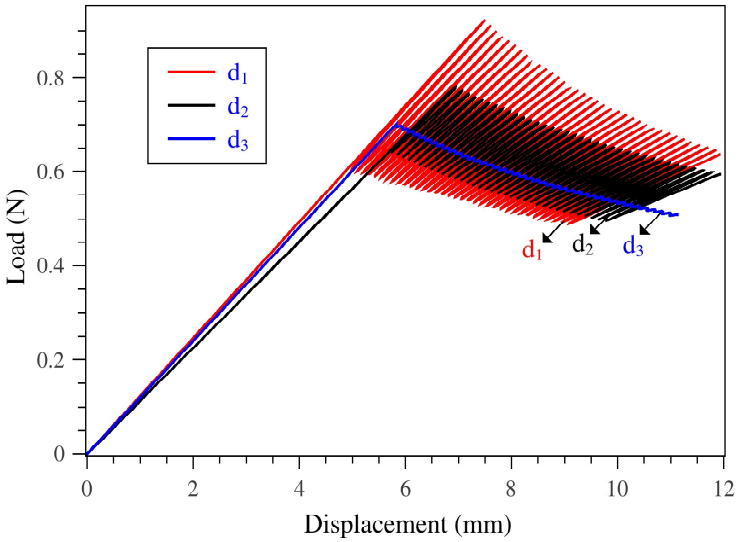

Figure 3.10: Comparison between the load displacement response of the specimen with different shapes of damage function

was a notch with a given length a_0 plus a complete damaged band with the width of l_c. Therefore, the effective initial notch length was equal to a_0 plus a certain portion of l_c, where the size of this portion is dependent on the shape of the damage function. A significant difference is observed between the amount of oscillations in descending branch of the load displacement responses. However, they all have the same averaged trend which is independent of $d(\phi)$. The response corresponding to damage function d_3 is relatively smooth while the oscillations are most extreme for function d_1. The poor performance of d_1 is as expected, because it is at least similar to the typical damage distribution found in cohesive methods. However, the better performance of d_3 over d_2 is surprising in that light. Nevertheless, this can also be explained through detailed examination of the evaluation of the integrals in equations **??** and **??**. Considering the given number of integration points inside the damaged band, the accuracy of these integrals is related to the smoothness of their integrands $d'Y$ and d'. Fig. **??** shows the distribution of product $d'Y$ over the length of the damaged band for each damage function. The product $d'Y$ related to d_1 is distributed only over 10% of the elements inside the damage zone which means that only 10% of the elements contribute towards the integration of this product. This small number of elements means less integration points and less accuracy for computing the integral which explains the severe oscillations in the results corresponding to d_1. The fraction of contributing elements for computing the integral of product $d'Y$ is 57% and 27% for d_2 and d_3, respectively. With these percentages of element contribution, the relatively large oscillations using d_2 are still not expected. To explain this further, we look at the left hand side integral in Eq. **??** which contains d'

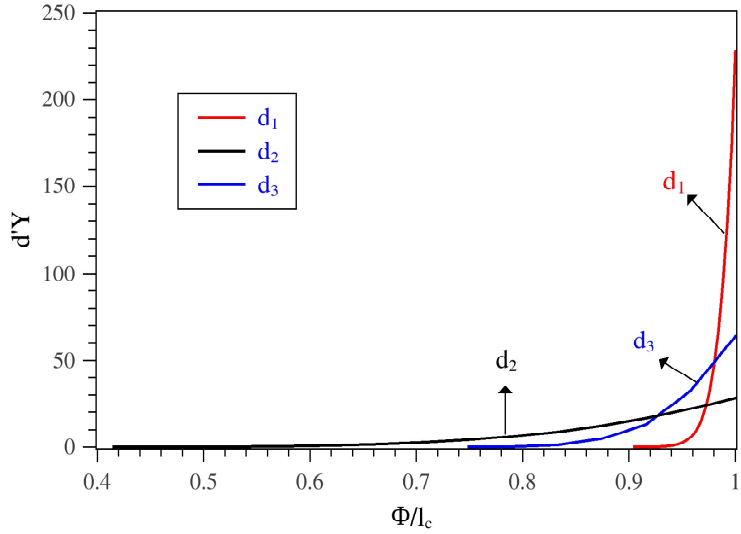

Figure 3.11: Variation of product $d'Y$ along the damaged band for different damage functions

rather than $d'Y$. Fig. **??** illustrates the derivatives of the introduced damage functions. It can be observed that the profile of d_3' is more widely distributed than that of d_1' and d_2'. This smooth shape of d_3' provides a smooth and easy to integrate function and this reveals the reason of the smaller amount of oscillations in the DCB response using function d_3. Based on this investigation on the role of damage function in the thick level set interface model, two specifications have been found for an optimal damage function for this model: a function which has a long zone with damage values close to 1 (like d_2) and of which the derivative is widely distributed over l_c (like d_3). These two specifications are at odds; therefore, to meet these criteria we developed a compound damage function as follows (see Fig. **??**):

$$d(\phi) = \begin{cases} g(\phi) & \phi \leq m l_c \\ f(\phi) & \phi > m l_c \end{cases} \tag{3.31}$$

where the function $f(\phi)$ is the expression from Eq.(**??**) and the new polynomial function $g(\phi)$ is defined as

$$g(\phi) = c_5 \left(\frac{\phi}{l_c}\right)^2 + c_6 \left(\frac{\phi}{l_c}\right) \tag{3.32}$$

where c_5 and c_6 are defined as follows to satisfy continuity of $d(\phi)$ and $d'(\phi)$ at point m:

$$\begin{aligned} c_6 &= 2\left(\frac{f(m l_c)}{m} - \frac{l_c f'(m l_c)}{2}\right) \\ c_5 &= \frac{l_c f'(m l_c) - c_6}{2m} \end{aligned} \tag{3.33}$$

In this chapter the values of $c_1 = 500$, $c_3 = 0.5$, $m = 0.6$ are used to develop damage function d_4.

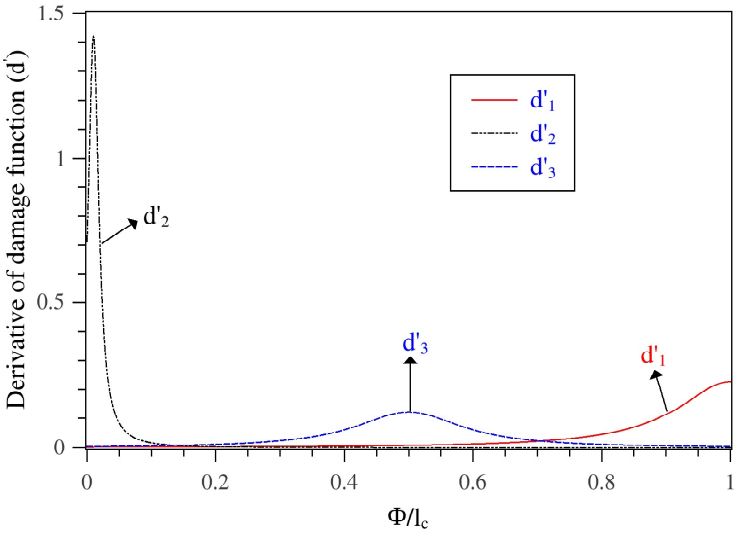

Figure 3.12: The derivative functions of damage functions d_1, d_2 and d_3

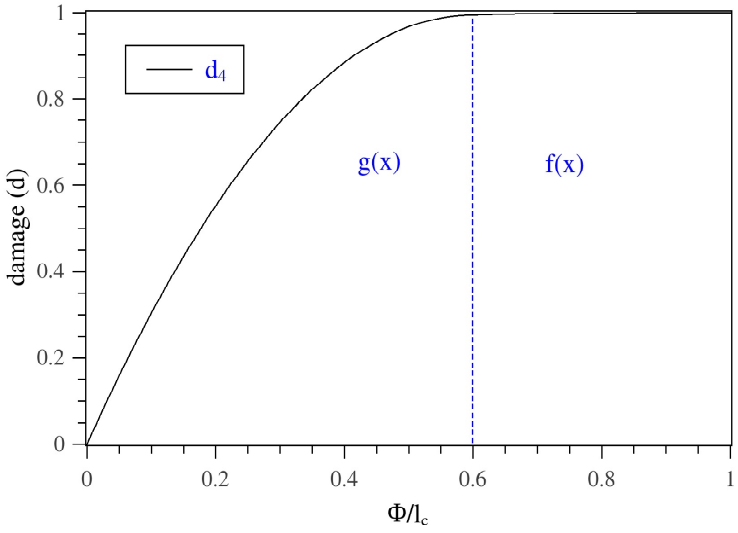

Figure 3.13: Improved damage function d_4(m=0.6)

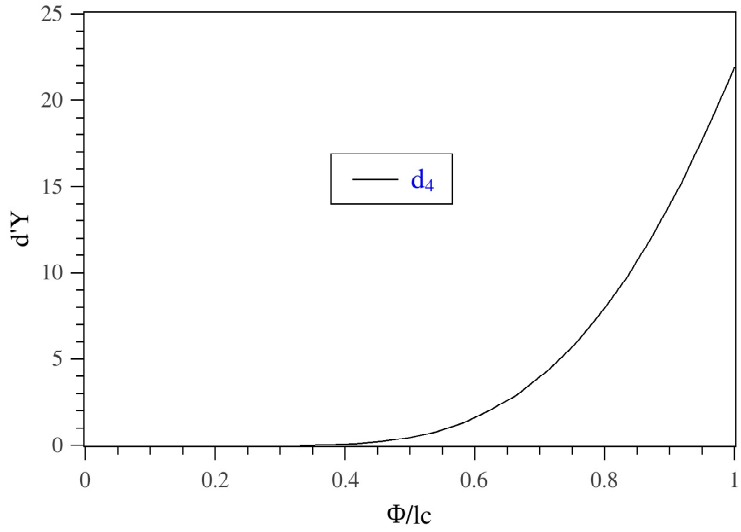

Figure 3.14: Variation of product of $d'Y$ along damage front for damage function d_4

To evaluate the performance of new damage function d_4, the DCB simulation is repeated where the mesh size and l_c were the same as in previous simulations. It is shown in Fig. **??** that around 65% of elements contribute to the computation of the integral of product $d'Y$. The derivative of the function also has a profile with a wide distribution (see Fig. **??**). Fig. **??** compares the results of the DCB simulation obtained using d_3 and d_4, which shows smoother results with d_4. We should stress that with the proper size of mesh the results of the simulations related to different damage functions all converge to the same smooth response. However, choosing a proper damage function allows to use a coarser mesh leading lower computational costs. The damage function d_4 is used in all other simulations presented in this chapter.

Because the initial part of the damage function does give rise to large stiffness loss or significant release of energy, in this chapter the value of $l_0 = ml_c$ is considered for the initial size of the damage band after initiation.

3.3.2. EFFECT OF LENGTH OF THE DAMAGED ZONE (l_c)

The length of the damaged band l_c is an important input parameter of the model. From numerical point of view, l_c determines the number of elements inside the band for a given mesh. To investigate the sensitivity of the results to the value of l_c, 3D simulations of the DCB test were conducted with three different values for l_c. The specimen was 150 mm long, with a width of 25.4 mm, thickness of 3.05 mm and initial notch of 30.4 mm. An unstructured mesh with triangular elements at the interface and six-node wedge element in the arms was used for these simulations. The applied load, boundary conditions and material properties were similar to the simulations presented in the

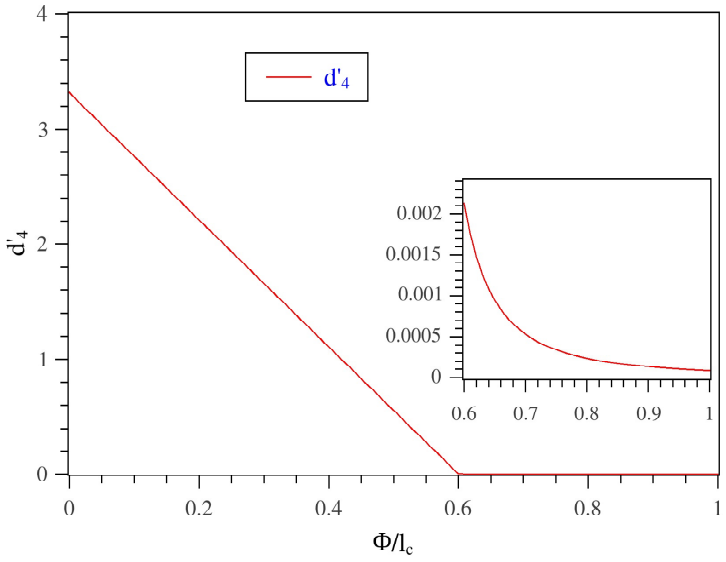

Figure 3.15: Derivative of damage function d_4

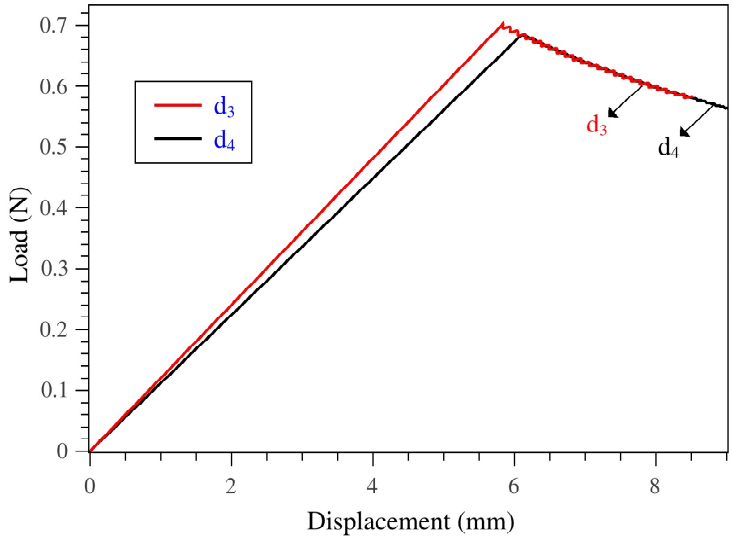

Figure 3.16: Load displacement response of DCB specimen with damage functions d_3 and d_4

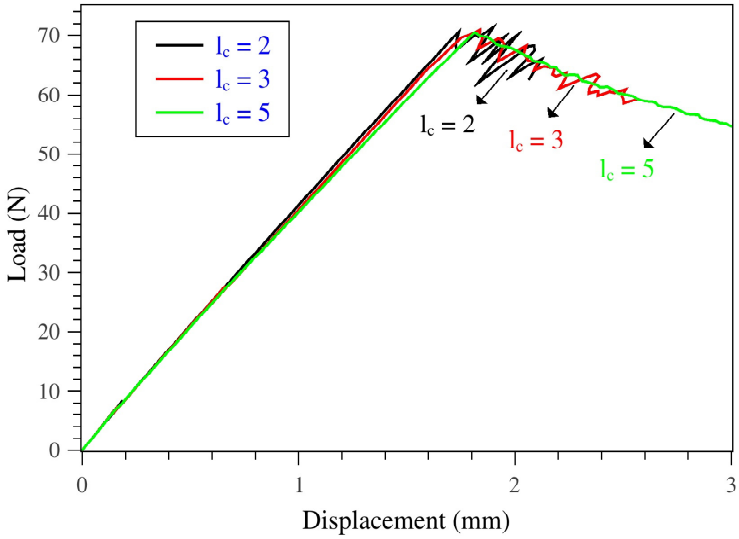

Figure 3.17: Load displacement response of DCB specimen with different length of damaged band l_c

previous section. Fig. **??** presents the load displacement response corresponding to each value of l_c. The figure shows that by increasing l_c from 2 mm to 5 mm the oscillatory response converges to a smooth response. Increasing the number of elements inside the damaged zone results in a higher accuracy of the computation. The freedom to choose l_c is an advantage of the proposed model that provides the possibility of using a coarser mesh which leads to lower computational costs. In these simulations with a characteristic element size of 0.76 mm, for l_c equal to 2 , 3 and 5 mm approximately 3, 4 and 7 elements are placed along the length of l_c.

3.3.3. EFFECT OF INTEGRATION SCHEME

It is mentioned in section **??** that sub-triangulation is used for elements at the bounds of the damaged zone. The effect of this technique on the amount of oscillations in the load displacement response is investigated by repeating the simulations from the previous section. The value of l_c = 5 mm was considered in these simulations. Fig. **??** shows the comparison between DCB results obtained from simulation with and without sub-triangulation. It is shown that with the same size of mesh and l_c, using this technique helps to decrease the oscillations in the results. This is due to the shape of the field $d'Y$ which shows a sharp increase near the front (see Fig. **??**). Sub-triangulation ensures that the numerical integration takes place over the correct domain

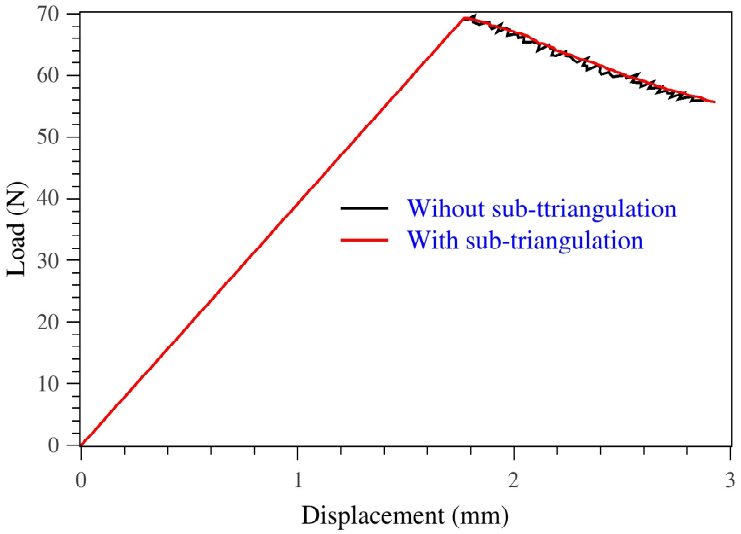

Figure 3.18: Oscillations in load displacement response with and without sub-triangulation technique

3.3.4. EFFECT OF STABILIZATION PARAMETER (κ)

The effect of stabilization parameter κ (see Eq. **??**) on the load displacement response is investigated in this section. The DCB simulations from the previous section were repeated with the same input parameters except for κ. Fig. **??** compares the load displacement results obtained with different values of (κ). It can be observed that with the same mesh size by increasing the value of κ from 5 to 20 the smoothness of response improved clearly. For a value higher than 20 the figure shows little difference. However, due to the role of κ in suppressing variations in energy release rate along the front, the effect of κ on the delamination front shape should also be considered. Fig. **??** illustrates the delamination front shape for five different values of κ.

It is shown that the shape of the front is not very sensitive to the value of κ. However, for the lowest value of κ (5) small oscillations in the front shape can be observed, while for the highest value of κ (1500) the damage front remains a straight line. This is related to the distribution of predicted energy release rate ($\bar{\bar{Y}}$) along the front which is shown in Fig. **??**. It is observed from this figure that raising the value of κ results in a more smooth distribution of energy release rate along the front. For a very high value of κ, the distribution is forced to be uniform which explains the straight front shape observed for high κ in Fig. **??**. It should be noted that in case of using a very fine mesh due to the very small value of element size h the diffusion term ($\frac{\kappa h^2}{l_c}$) provided in Eq. **??** will vanish, and consequently the sensitivity of results to the stabilization parameter κ will disappear.

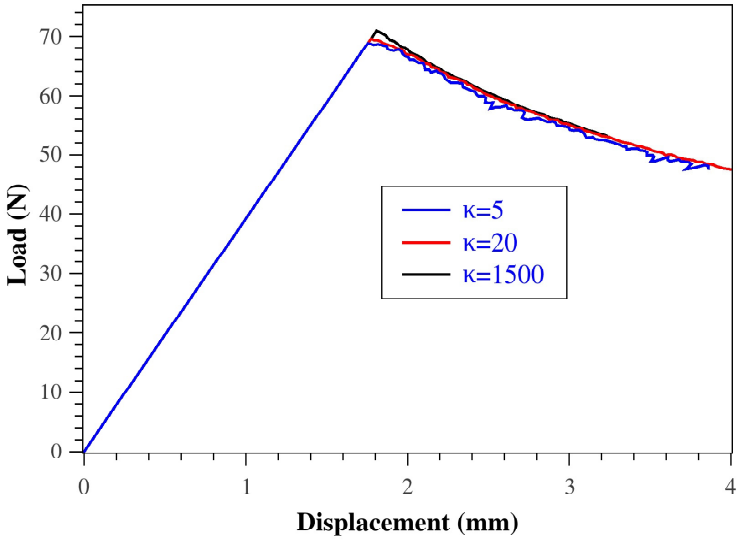

Figure 3.19: Effect of stabilization parameter (κ) on the load displacement response in DCB simulations

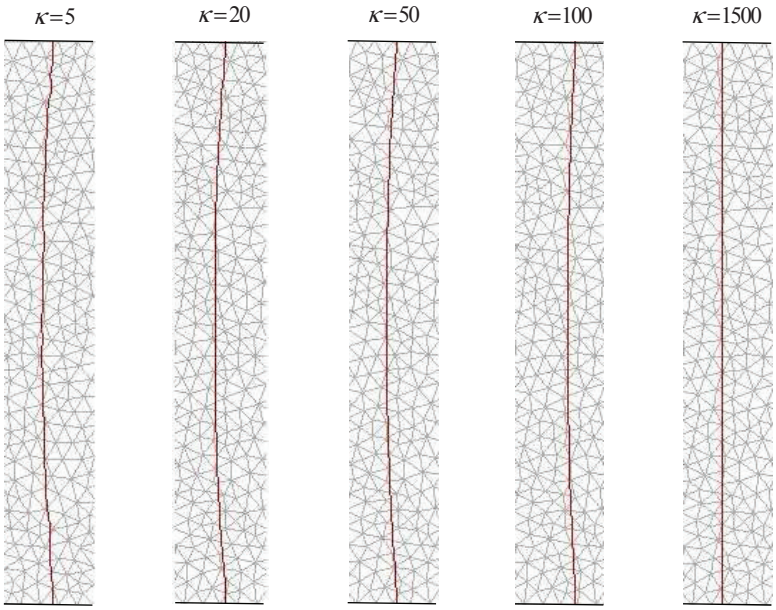

Figure 3.20: Effect of stabilization parameter (κ) on delamination front shape in DCB simulations

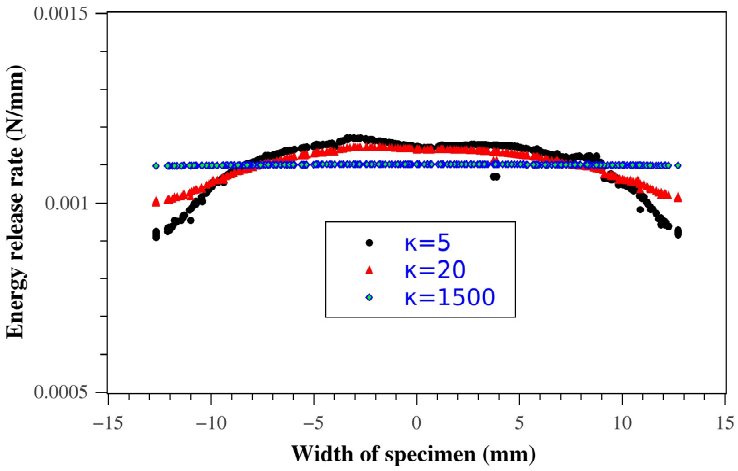

Figure 3.21: Variation of predicted energy release rate ($\bar{\bar{Y}}$) along the delamination front for different values of stabilization parameter

3.3.5. VALIDATION: MODE I

For validation of the model, mode I, mode II and mixed mode simulations were conducted and the obtained response was compared with analytical solutions. The simulated specimen was 102 mm long, and 25.4 mm wide with two arms of 1.56 mm thick and initial notch length of 32.9 mm. The material properties used in the simulations are related to a carbon/PEEK fiber reinforced composite and listed in Table **??**.

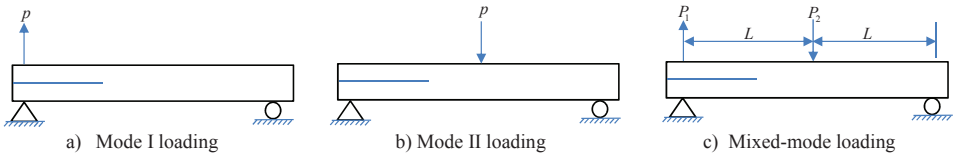

Figure 3.22: Loading conditions in different fracture modes

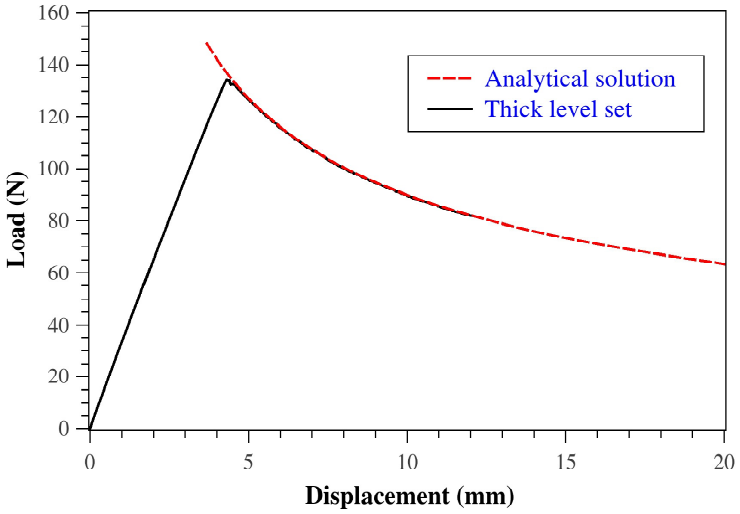

Figure 3.23: Comparison between analytical and numerical results for DCB simulation

Table 3.2: Material properties for carbon/PEEK composite used in mode I, mode II and mixed-mode simulations**?**

E_1	E_2=E_3	G_{12}=G_{13}	G_{23}	η	ν_{12}=ν_{13}
122700 MPa	10100 MPa	5500 MPa	3700 MPa	2.284	0.25
ν_{23}	G_{Ic}	G_{IIc}	τ^I_{max}	τ^{II}_{max}	
0.45	0.969 kJ/m^2	1.719 kJ/m^2	80 MPa	100 MPa	

In these simulations again 3D wedge elements connected with 6-node interface elements were used with a 2D triangular mesh for the level set field. The smallest size of the finite elements in the 2D mesh at the interface (h_{min}) was 0.618 mm. Numerical values l_c = 5 mm and $\kappa = 20$ mm^{-2} were considered for this analysis. The set up for the mode I loading test is shown in Fig. **??**a, where the length of the initial notch was 32.9 mm. The analytical solution for the DCB test is derived from beam theory following Mi et al. **?**. The decreasing part of the analytical load displacement relationship is given by

$$\Delta = \frac{2}{3}\frac{(WG_cEI)^{3/2}}{EIP^2} \tag{3.34}$$

where W is the width of specimen, G_c is the fracture energy, E is the elasticity modulus, I is the second moment of inertia for one arm and Δ is the opening displacement. Fig. **??** compares the analytical and numerical results showing an excellent agreement.

Fig. **??**a illustrates the evolution of the damage front shape. The delamination front

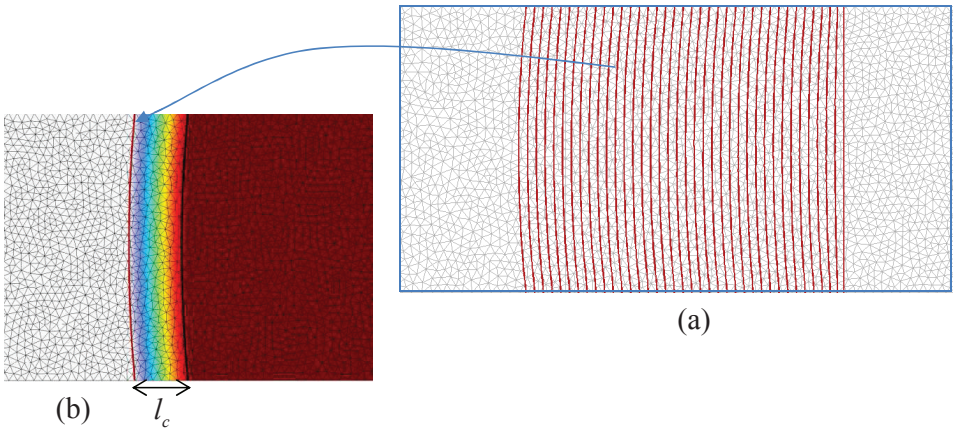

Figure 3.24: DCB simulation: a) delamination front shape b) variation of damage parameter inside the damaged zone

starts from a straight line and develops into a curved shape as the delamination propagates along the interface. The damage distribution from a single time step is presented in Fig. **??**b which shows the variation of the damage parameter inside the damaged band. The presented results of the DCB simulation confirm the accuracy of the computed mode I energy release rate as well as the 3D capability of the model to capture the delamination front shape.

3.3.6. VALIDATION: MODE II

The validation of the model for mode II loading was conducted using the same geometry and discretization as in the previous section. The loading condition for the mode II loading case is illustrated in Fig. **??**b. An initial crack of length 34.1 mm was considered for this simulation. The numerical data were the same as for the mode I simulation. The analytical formula provided in **?** was used for validation. For the line in the region in which the crack length is smaller than half the length of the specimen ($a < L$), this relation between load and displacement is given by:

$$\Delta = \frac{P}{96EI}\left[2L^3 + \frac{(64G_{IIc}WEI)^{3/2}}{\sqrt{3}P^3}\right] \tag{3.35}$$

The load-displacement response for the case in which the crack develops beyond the middle of the specimen ($a > l$) is given by:

$$\Delta = \frac{P}{24EI}\left[2L^3 - \frac{(64G_{IIc}WEI)^{3/2}}{4\sqrt{3}P^3}\right] \tag{3.36}$$

A comparison between numerical results obtained from the thick level set interface model and the analytical solution is presented in Fig. **??**. The comparison shows an excellent match between the simulated response and the analytical solution. It is shown that the

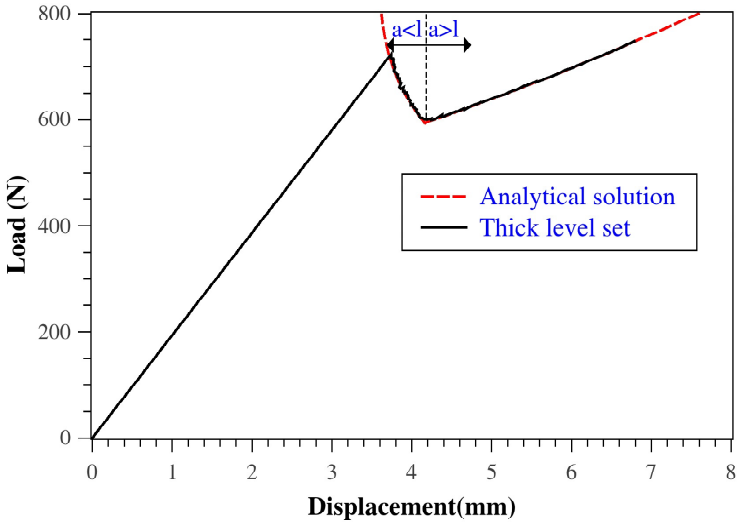

Figure 3.25: Comparison between analytical and numerical results for mode II loading simulation

model can accurately capture the load displacement response during crack propagation in the region with a crack length smaller than half the length of the specimen ($a < L$) as well as in region with $a > L$. The observed accuracy of the numerical result proves the validity of computed mode II energy release rate with the model as well as the suitability of using damage function d_4 for a mode II simulation.

3.3.7. VALIDATION: MIXED-MODE

Finite element analysis of a mixed-mode test was conducted for further validation of the proposed model. The geometry, discretization and numerical input were the same as for the mode I and mode II validation tests. An initial notch with a length of 34.1 mm was considered. The loading condition of the mixed-mode problem is illustrated in Fig. **??**c where values P_1 and P_2 are obtained as

$$P_1 = P\left(\frac{c}{L}\right) \qquad P_2 = P\left(\frac{c+L}{L}\right) \tag{3.37}$$

where the parameter c and P are the lever arm and applied load respectively, (see Fig. **??**) which are related to the experimental set up of mixed-mode bending test (MMB). The ratio between fracture modes G_I and G_{II} for the MMB configuration is defined as **?**

$$\frac{G_I}{G_{II}} = \frac{4}{3}\left(\frac{6c-2L}{2c+2L}\right)^2 \tag{3.38}$$

For a mode-mixity (β) of 50%, which is considered here, the ratio G_I/G_{II} is equal to 1; for which the value of c = 44.596 mm is obtained. The analytical solution is derived using

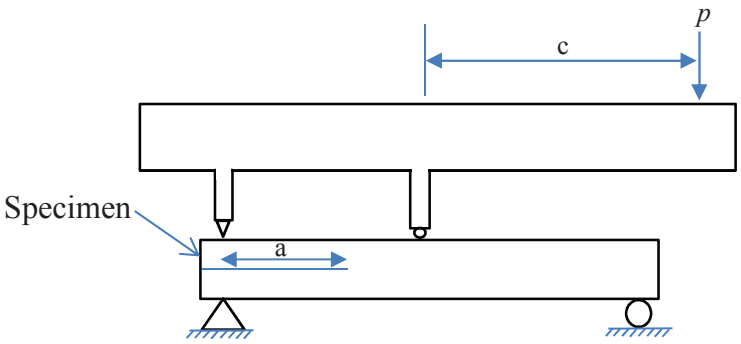

Figure 3.26: Configuration of mixed mode bending experiment

the relations provided in **???**. The pure mode load components are defined as a function of the load applied on the arm, P_1:

$$F_I = P_1 - P_2/4 = \left(\frac{3c-L}{4c}\right)P_1 \tag{3.39}$$

$$F_{II} = P_2 = \left(\frac{c+L}{c}\right)P_1 \tag{3.40}$$

The relationship between crack length a and the reaction force P_1 is derived for $a < L$ as:

$$a = \sqrt{\frac{G_c 64WEI}{64F_I^2 + 3F_{II}^2}} \tag{3.41}$$

and for $a > L$:

$$a = 2L\frac{(7L-9c)(L+c) - 2\sqrt{4\frac{G_c WEIc^2}{(LP_1)^2}(23L^2-50Lc-9c^2) - (5L^2-6Lc-27c^2)(L+c)^2}}{23L^2-50Lc-9c^2} \tag{3.42}$$

The load displacement relationship for the mixed-mode test is obtained by substituting the computed values for crack length a in this equation:

$$\Delta = \frac{(3c-L)a^3}{6cEI}P_1 \tag{3.43}$$

Fig. **??** compares the load-deflection response of the specimen (P_1 vs Δ) obtained from the numerical model with the analytical solution. An excellent match is observed between results in the region where the crack length is smaller than half the length of the specimen; however, the numerical result deviates from the analytical solution as the crack propagates in region $a > L$. This discrepancy is related to the mechanics of the MMB test. The value of the fracture energy (G_c) used in the analytical formula is computed based on the assumption of constant mode-ratio (β). However, β is only independent of the crack length when $a < L$. For region $a > L$ this assumption is not valid **?**;

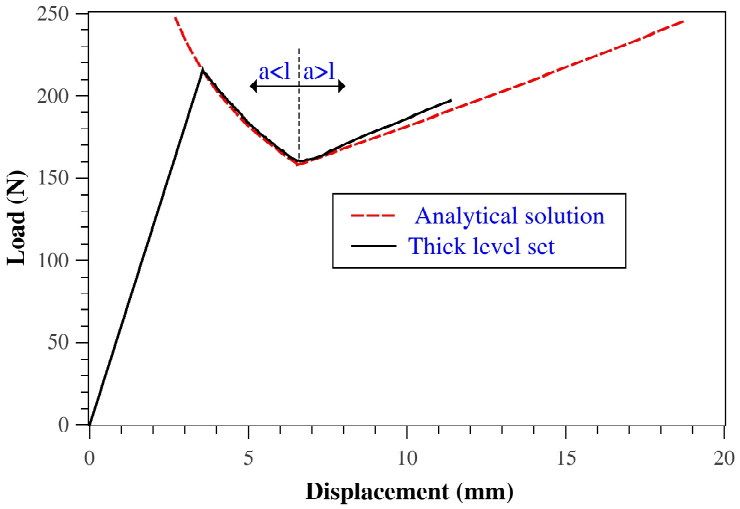

Figure 3.27: Comparison between analytical and numerical results for mixed-mode simulation

therefore, in this region we can expect more accurate results from the numerical model because the effect of mode-ratio variation on fracture energy is considered via Eq.(**??**). Figure **??** presents a contour plot of the distribution of β inside the damaged band for one time step (with $a < l$). It can be seen that the mode-mixity (β) is not constant along the damage front and varies smoothly along the width of the specimen. The value of β increases away from the middle of the damage front which is due to an increase in the shear component of the energy release rate (G_{shear}) close to the free edges. Figure **??** highlights an additional advantage of the TLS over cohesive zone models. Because G and G_{shear} are both computed as integral quantities, β varies only in direction along the front, not perpendicular to it. In the cohesive zone, β is computed locally. A variation in β over the length of the cohesive zone can then be found, which does not have clear physical meaning and which can give rise to undesirable behavior **??**. In the TLS, the mode mixity is computed as a non-local quantity, which is more in line with the usage of β in Eq. (**??**).

The accuracy and smoothness of the obtained mixed-mode result validates the capability of the model to compute the total energy release rate (G) and its shear component (G_{shear}). It also demonstrates the good performance of the damage function d_4 under several loading conditions.

3.4. CONCLUSIONS

In this chapter, a thick level set interface model is proposed for simulating delamination initiation and propagation in composites. Using the thick level set method in combination with interface elements provides a new discontinuous damage model for simulating

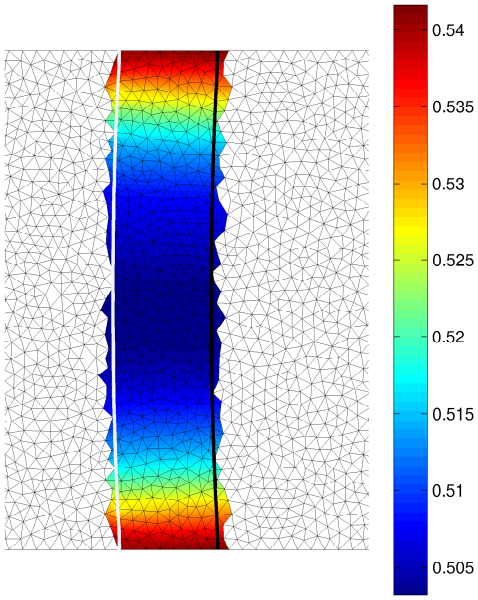

Figure 3.28: Distribution of mode-mixity (β) inside the damaged band

delamination. This 3D model benefits from the convenience of using interface elements for modeling cracks as well as from the new definition of damage provided by the thick level set method. The sensitivity of the model to the numerical input data was investigated. In this investigation the specifications of a suitable damage function for the model were analyzed and an efficient function has been introduced. The analysis of numerical input parameters proves that the model is not sensitive to the predefined length of the damage band. This is an advantage of this model because increasing this length provides the possibility of using a coarser mesh. The model was validated by simulating mode I, mode II and mixed-mode tests and comparing the obtained load displacement responses with analytical solutions. The comparison shows an excellent agreement between the numerical and analytical results, which confirms the accuracy of method. The presented model can easily be extended to a fatigue model, because of the direct link between fracture and damage mechanics offered by the thick level set method.

4

FATIGUE MODELING IN COMPOSITES WITH THE THICK LEVEL SET INTERFACE METHOD

ABSTRACT

This chapter presents a new discontinuous damage model for modeling fatigue crack growth in composites. This new fatigue model is formulated based on the thick level set interface approach which we developed recently. In this approach the thick level set (TLS) method is combined with interface elements for modeling delamination growth. Crack growth under cyclic loading is described with the Paris relation. In contrast with popular cohesive zone methods, this new approach provides an accurate non-local evaluation of the energy release rate as well as a framework in which the crack growth rate can be directly imposed. The proposed 3D mixed-mode model is validated against experimental and theoretical data.

4.1. INTRODUCTION

Delamination is a common mode of failure in laminated composites. Delamination growth is mostly modeled with the cohesive zone method in combination with interface elements. This method was initially developed for modeling crack growth under quasi-static loading and later extended to fatigue analysis **?????**. Yamaguchi et al. **?** used a power law to decrease the residual strength parameter of interface elements under cyclic loading. This model has been used to simulate different damage modes in CFRP layers of a notched hybrid titanium/CFRP laminate. The simulated delamination growth pattern showed a good agreement with experimental observations; however, this method

This chapter is based on : Latifi, M.; van der Meer, F.P.; Sluys, L.J.: Fatigue modeling in composites with the thick level set interface method (Manuscript accepted for publication in Composites Part A: Applied Science and Manufacturing)

requires calibration of 3 different model parameters which can not be directly related to experimental observations. Concerning parameter identification, it is attractive to relate fatigue damage growth directly to Paris law. For implementation of Paris law in a fatigue cohesive model, the energy released due to delamination growth must then be extracted from the cohesive law, and the computed energy can be used to obtain the crack growth rate as proposed by Turon et al. **?**. However, limitations arise from inaccuracy in the local extraction of the energy release rate **?**. Furthermore, imposing the crack growth rate requires information on the length of the cohesive zone ahead of the crack tip which can only be estimated based on geometry and loading conditions **?**. Harper and Hallett **?** proposed the division of the cohesive zone into two equal regions: a static damage zone and a fatigue damage zone, to improve the accuracy of the local energy release rate approximation. Kawashita and Hallett **?** developed a crack tip tracking algorithm to only apply fatigue degradation at the crack tip elements. This method eliminates the dependency of the cohesive fatigue models on the length of the cohesive zone. Xu and Wang **?** proposed an alternative crack tip tracking algorithm which is applicable to both orthogonal and non-orthogonal meshes although the crack front shape is still sensitive to the aspect ratio of elements **?**. Recently, Bak et al. **?** used the J-integral to determine the energy release rate in a cohesive fatigue model. The J-integral method improved the accuracy of computed energy release rate, resulting in more precise prediction of the crack growth rate under fatigue. However, this model has only been validated for 2D simulations and it is not obvious how the approach can be extended to general 3D analysis.

In earlier work on fatigue analysis we have proposed a level set model as an alternative for the cohesive zone method in the framework of fracture mechanics **?**. This 3D model was able to predict fatigue delamination growth rate and its front shape accurately. However, this model is, so far, only applicable for simulating a single delamination in thin structures. This is due to the special element formulation used to describe the crack in this model, which lacks the flexibility of interface elements for modeling crack growth along any predefined path inside a solid material.

In this work a new method for delamination modeling under fatigue is proposed following the thick level set (TLS) approach **???**. The TLS approach was first introduced by Möes et al. **?** as a continuum damage model to simulate damage growth in solids under quasi-static loading conditions. A damaged band with a predefined length l_c is located between sane and fully damaged material. The level set method is used to track the location of a damage front and to provide the distance to that front throughout the domain. The damage variable is computed as an explicit function of the level set field, increasing from 0 to 1 as the distance behind the front increases from 0 to l_c. The TLS method provides a non-local computation of the energy release rate along the damage front. The non-locality appears by integrating a local configurational force across the damaged band. Latifi et al. **?** adapted the TLS method for use in interface elements to develop a 3D discontinuous method for modeling quasi-static delamination in composites. Voormeeren et al. **?** developed a 2D model for fatigue analysis in metals based on the TLS method.

In this chapter, the 3D model from **?** is extended to fatigue analysis. The Paris relation is used to define crack growth rate under fatigue. The proposed model benefits from the convenient properties of interface elements and allows for accurate non-local

computation of the energy release rate. Moreover, the crack growth rate can be directly imposed as front velocity in the level set method. The model allows for accurate simulation of self-similar and non-self-similar interface crack propagation under pure and mixed-mode loading conditions. This is validated by comparing the results from simulations with experimental observations and direct evaluation of the Paris curve. Because the method works with interface elements, it can also be applied to failure processes other than delamination such as splitting. This is demonstrated with the simulation of damage development in a notched laminate with interaction between splitting and delamination.

4.2. METHODS

Before presenting the details of the model the solution scheme is briefly introduced. A staggered solution scheme is used in which in each time step displacement jump and damage are computed sequentially **?**. Each time step starts with a certain damage distribution. The standard finite element method is applied to compute the displacements for given boundary conditions on the mesh composed of interface elements and solid elements. Next, the computed displacement jump is used to update damage distribution. For this purpose, the energy release rate G is computed along the damage front and related to a crack growth rate using the Paris relation. The obtained crack growth rate allows to compute the front movement a, which is used to update the level set field. This new level set field defines the damage distribution for the next time step.

4.2.1. DAMAGE DEFINITION

In the TLS method a damaged band with length l_c is considered between fully damaged and undamaged material (see Fig. **??**). It is similar to the cohesive zone method in the sense that damage changes gradually from 0 to 1. However, it is different in the sense that damage is not a direct function of the displacement jump. Instead, the damage variable is defined as a predefined function of the nearest distance to a moving front. To determine this distance and to describe the location of the front the level set method is used. The absolute value of the level set field at any point inside the domain is equal to the shortest distance to the damage front from that point. Furthermore, the iso-zero (damage front) and the iso-l_c (crack front) of this field determine the boundary of the damaged band. Over this band a predefined damage profile is considered where the damage increases from 0 to 1 as the level set field rises from 0 to l_c (see Fig. **??**). The damage function $d(\phi)$ should be continuous and differentiable on the domain $\langle 0, l_c \rangle$ and satisfy the following conditions:

$$\begin{cases} d(0) = 0 \\ d(l_c) = 1 \\ d'(\phi) > 0 \qquad (0 < \phi < l_c) \end{cases} \tag{4.1}$$

where $d'(\phi)$ is the spatial derivative of the damage function. Generally, each function which satisfies above requirements can be considered as damage function in the TLS method. For a linear bulk material, the crack growth results of the discontinuous TLS are independent of the choice for l_c and $d(\phi)$ **?**. However, the damage function does

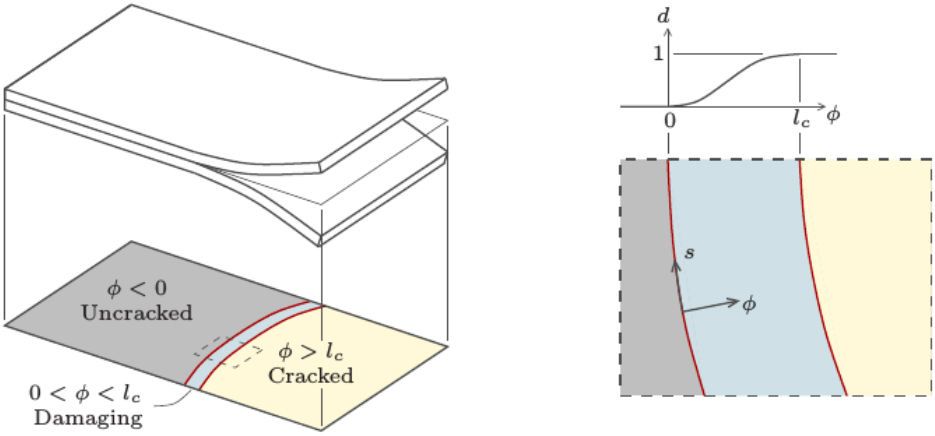

Figure 4.1: The discontinuous TLS method: a damaged band with predefined damage function defined between the cracked and uncracked part of the interface

affect the size of the required mesh and consequently the efficiency of the method. This issue was investigated in **?** where the specifications of an optimal damage function were introduced. In this chapter, following **?** a compound damage function is used for $d(\phi)$ (see Fig. **??**):

$$d(\phi) = \begin{cases} f(\phi) & \phi \geq ml_c \\ g(\phi) & \phi < ml_c \end{cases} \tag{4.2}$$

where m defines the region in which $f(\phi)$ and $g(\phi)$ are active, the function $f(\phi)$ is obtained from an arc-tangent formula **?** and $g(\phi)$ is a polynomial function:

$$f(\phi) = c_2 \text{atan}\left(c_1\left(\frac{\phi}{l_c} - c_3\right)\right) + c_4 \tag{4.3}$$

$$g(\phi) = c_5\left(\frac{\phi}{l_c}\right)^2 + c_6\left(\frac{\phi}{l_c}\right) \tag{4.4}$$

The conditions given in Eq. (**??**) determine c_2 and c_4, while parameters c_5 and c_6 are defined to satisfy the continuity of $d(\phi)$ and $d'(\phi)$ at $\phi = ml_c$ (see Fig. **??**):

$$c_2 = (\text{atan}(c_1(1-c_3)) - \text{atan}(-c_1 c_3))^{-1} \tag{4.5}$$

$$c_4 = -c_2 \text{atan}(-c_1 c_3) \tag{4.6}$$

$$c_5 = \frac{l_c f'(ml_c) - c_6}{2m} \tag{4.7}$$

$$c_6 = 2\left(\frac{f(ml_c)}{m} - \frac{l_c f'(ml_c)}{2}\right) \tag{4.8}$$

Throughout this chapter, similar to **?** the values of $c_1 = 500$, $c_3 = 0.5$, $m = 0.6$ are used.

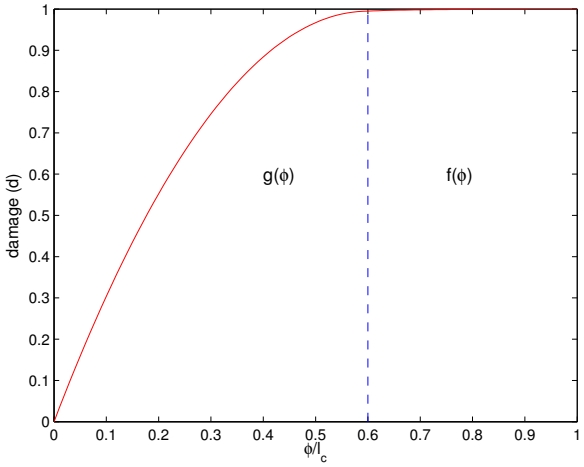

Figure 4.2: The profile of the compound damage function (m=0.6)

4.2.2. CONSTITUTIVE LAW

The constitutive behavior in the interface elements is derived from a free energy definition with isotropic damage:

$$\varphi(\boldsymbol{\Delta}, d) = (1-d)\varphi_0(\boldsymbol{\Delta}) + d\varphi_0(\langle -\boldsymbol{\Delta}\cdot\boldsymbol{n}\rangle\,\boldsymbol{n}) \tag{4.9}$$

where d is the damage parameter and $\boldsymbol{\Delta}$ is the displacement jump vector in local coordinate frame. The MacAuley bracket in the second term in Eq. (**??**) is defined as $\langle x\rangle = \frac{1}{2}(x+|x|)$. This term is added to prevent interfacial interpenetration in normal direction. The variable φ_0 in Eq. (**??**) is defined as

$$\varphi_0(\boldsymbol{\Delta}) = \frac{1}{2}K\boldsymbol{\Delta}\cdot\boldsymbol{\Delta} \tag{4.10}$$

where K is the dummy stiffness. The constitutive law for interface elements is derived from Eq. (**??**):

$$\boldsymbol{\tau} = \frac{\partial\varphi}{\partial\boldsymbol{\Delta}} = (1-d)K\boldsymbol{\Delta} - dK(\langle -\boldsymbol{\Delta}\cdot\boldsymbol{n}\rangle\,\boldsymbol{n}) \tag{4.11}$$

The local driving force for damage growth is obtained by differentiating the free energy with respect to the damage variable:

$$Y = -\frac{\partial\varphi}{\partial d} = \varphi_0(\boldsymbol{\Delta}) - \varphi_0(\langle -\boldsymbol{\Delta}\cdot\boldsymbol{n}\rangle\,\boldsymbol{n}) \tag{4.12}$$

4.2.3. NON-LOCAL COMPUTATION OF ENERGY RELEASE RATE

In the TLS method the energy release rate is defined in a non-local way by integrating the local driving forces obtained from Eq. (**??**) over the damaged band:

$$G(s) = \int_0^{l_c} d'(\phi) Y(\phi, s) \left(1 - \frac{\phi}{\rho(s)}\right) d\phi \tag{4.13}$$

where ρ is the front curvature and $d'(\phi)$ is the spatial derivative of damage. It should be noted that Y is the derivative of free energy with respect to d, while d' is the derivative of damage with respect to the distance to the front (ϕ). This implies that $d'Y$ is the derivative of free energy with respect to ϕ. Because ϕ is defined as the closest distance to the front from a given point, $d'Y$ is equal to the local rate of energy dissipation when the front moves away from this point. The energy release rate for crack growth can be computed from Eq. (**??**) at any point s along the front. However, to evaluate this integral numerically it needs to be discretized over the 2D mesh at the interface. For this purpose, an averaged value of the local driving force, $\bar{Y}$, is defined:

$$\int_0^{l_c} d'(\phi) \bar{Y}(s) \left(1 - \frac{\phi}{\rho(s)}\right) d\phi = \int_0^{l_c} d'(\phi) Y(\phi, s) \left(1 - \frac{\phi}{\rho(s)}\right) d\phi \tag{4.14}$$

In order to compute $\bar{Y}$ along the front, Eq. (**??**) is made into a field equation and the field $\bar{Y}$ is discretized over the nodes of the elements that contain the damaged band. For this discretization following Bernard et al.**?** a variational approximation of $\bar{Y}(s)$ is introduced ($\bar{\bar{Y}}$) which is not only a function of s, but a function of s and ϕ. The constraint that $\bar{Y}$ is constant in ϕ direction ($\nabla \bar{Y} \cdot \nabla \phi = 0$) is enforced on $\bar{\bar{Y}}$ using Lagrange multipliers. The obtained variational form is solved using the Galerkin method to find nodal values for $\bar{\bar{Y}}$:

$$\begin{bmatrix} \mathbf{K} & \mathbf{L} \\ \mathbf{L} & \mathbf{0} \end{bmatrix} \begin{Bmatrix} \bar{\bar{\mathbf{Y}}} \\ \mathbf{I} \end{Bmatrix} = \begin{Bmatrix} \mathbf{f^Y} \\ \mathbf{0} \end{Bmatrix} \tag{4.15}$$

The matrices and the right hand side vector are defined as

$$K_{ij} = \int_{\Omega^d} \left(d' N_i N_j + \frac{\kappa h^2}{l_c} \frac{\partial N_i}{\partial x_k} \frac{\partial N_j}{\partial x_k} \right) d\Omega \tag{4.16}$$

$$L_{ij} = \int_{\Omega^d} l_c \left(\frac{\partial N_i}{\partial x_k} \frac{\partial \phi}{\partial x_k} \right) \left(\frac{\partial N_j}{\partial x_k} \frac{\partial \phi}{\partial x_k} \right) d\Omega \tag{4.17}$$

$$f_i^Y = \int_{\Omega^d} N_i d' Y d\Omega \tag{4.18}$$

where Ω^d is the domain of the damaged band, h is the typical element size, N_i and N_j are standard shape functions associated with nodes i and j, and κ is a stabilization parameter which affects the smoothness of $\bar{\bar{Y}}$ along the damage front. For the stabilization parameter the value of $\kappa = 20$ is used in all simulations.

Based on the equalities provided in Eqs. (**??**) and (**??**) the relation between G and $\bar{Y}$ is defined as

$$G = \bar{Y} \int_0^{l_c} d'(\phi) d\phi = \bar{Y} \tag{4.19}$$

Therefore, nodal values of $\bar{\bar{Y}}$ at nodes of elements containing the damage front can be used directly to represent G along the front.

4.2.4. DAMAGE GROWTH MODEL

To define the damage growth for the proposed model the computed nodal values for the energy release rate (G) should be related to the advance of the level set front. Here, the suitability of TLS method for fatigue analysis becomes evident, because the computed energy release rate can be directly used in the Paris relation to obtain the crack growth rate ($\frac{da}{dN}$):

$$\frac{da}{dN} = C\left(\frac{\Delta G}{G_c}\right)^M \tag{4.20}$$

where C and M are fitting parameters and G_c is the fracture energy. In this equation, the cyclic variation of energy release rate ΔG is defined as

$$\Delta G = (1 - R^2)G \tag{4.21}$$

where the value of G is obtained from solving equation (**??**) and R is the fatigue load ratio. It should be noted that the proposed model in this chapter is for high cycle fatigue analysis where modeling the full loading/unloading cycle is numerically impractical. Therefore, the only viable alternative is a loading envelope approach in which the maximum load is applied and the influence of cyclic loading is incorporated by embedding the Paris relation in the model.

Computing the crack growth rate from Eq. (**??**) allows to obtain the nodal increase in the level set field (a_i) at the nodes of elements which contain the crack front using:

$$a_i = \left(\frac{da}{dN}\right)_i \Delta N \tag{4.22}$$

where ΔN is the number of skipped cycles based on a cycle jump strategy **?**:

$$\Delta N = \frac{a_{\max}}{(\frac{da}{dN})_{\max}} \tag{4.23}$$

where $a_{\max}$ is a numerical parameter that defines the maximum crack growth in a single time step and $(\frac{da}{dN})_{\max}$ is the maximum crack growth rate computed for a time step as evaluated according to Eq. (**??**). Eq. (**??**) ensures that time step size ΔN is selected such that the maximum crack growth along the front is equal to $a_{\max}$. For stability, this parameter has a value that is smaller than the characteristic element size in the mesh. The obtained level set advance from Eq. (**??**) is extended over the whole domain using a fast marching method **?**. Then the level set field is updated from time step n to time step $n+1$ with:

$$\phi_i^{n+1} = \phi_i^n + a_i^n \tag{4.24}$$

The new level set field defines the new damage distribution and the iso-zero of this field implicitly defines the new damage front location.

4.2.5. MIXED-MODE LOADING

In composite materials, none of the parameters in Eq. (**??**) are material constants. In fact, C, G_c and m all depend on the fracture mode. To account for this dependence the mode ratio β needs to be computed:

$$\beta = \frac{G_{II} + G_{III}}{G} = \frac{G_{\text{shear}}}{G} \tag{4.25}$$

where G_{shear} is the shear contribution to the energy release rate. Considering Eq. (**??**), G_{shear} is equal to the shear contribution to the averaged configurational force $\bar{Y}_{\text{shear}}$. To obtain $\bar{Y}_{\text{shear}}$, Eq. (**??**) is solved once more. This time at the right hand side in Eq. (**??**), Y_{shear} is used instead of Y, where the shear component of the local driving force, Y_{shear}, is obtained from Eq. (**??**) after setting the normal component of the displacement jump to zero.

The mode ratio effect on the fracture energy G_c is considered using the expression introduced by Benzeggagh and Kenane **?**:

$$G_c = G_{Ic} + (G_{IIc} - G_{Ic})\beta^{\eta} \tag{4.26}$$

where G_{Ic} and G_{IIc} are fracture energy in modes I and II, and η is a mode interaction parameter. The dependence of the Paris relation parameters C and M on the mode ratio is introduced following **?**

$$\log C = \log C_I + (\beta) \log C_{\text{mix}} + (\beta)^2 \log \frac{C_{II}}{C_{\text{mix}} C_I} \tag{4.27}$$

$$M = M_I + M_{\text{mix}}(\beta) + (M_{II} - M_I - M_{\text{mix}})(\beta)^2 \tag{4.28}$$

where subscripts I, II and mix indicate values obtained from mode I, mode II, and mixed-mode tests, respectively.

4.3. RESULTS

4.3.1. VERIFICATION OF THE MODEL FOR FUNDAMENTAL LOAD CASES

The proposed model has been validated for mode I, mode II and mixed-mode loading cases. For this purpose the double cantilever beam (DCB), four point end-notched flexure (4ENF) and mixed-mode loading tests have been simulated and the obtained results are compared with experimental data as well as with the Paris curve. A load ratio (R) equal to 0.1 is considered. In all simulations the specimen was 150 mm long, 20 mm wide with two arms of 1.5 mm thick and an initial crack length of 35 mm. For each arm one layer of three dimensional 6-node wedge elements were used, which were connected with 6-node interface elements. Furthermore, a conforming two-dimensional triangular mesh was defined on the interface for the level set field. The used algorithm of the fast marching method is designed for triangular elements and this is the reason that wedge elements are used for the bulk material. There exists a fast marching method

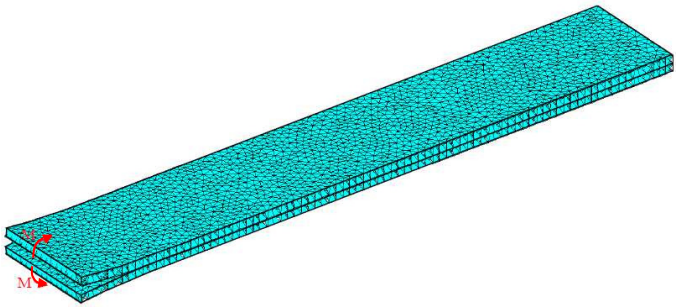

Figure 4.3: Finite element model of the DCB test

for quadrilateral elements. It is therefore possible to use the presented model with brick elements. The value of $l_c = 5$ mm was considered in combination with a mesh that provided approximately 7 elements inside the damaged band were considered. CFRP input properties used in these simulations are listed in Table **??**.

Table 4.1: Input properties for verification cases

Elastic properties**??**			
E_{11}	E_{22}=E_{33}	G_{12}=G_{13}	G_{23}
120000 MPa	10500 MPa	5250 MPa	3480 MPa
$\nu_{12} = \nu_{13}$	ν_{23}	G_{Ic}	G_{IIc}
0.3	0.51	0.260 kJ/m^2	1.002 kJ/m^2
Fatigue properties **?**			
C_I	C_{II}	C_{mix}	η
0.0616 mm/cycle	2.99 mm/cycle	458087 mm/cycle	2.73
M_I	M_{II}	M_{mix}	
5.4	4.5	4.94	

DCB SIMULATION

Figure **??** shows the finite element model of the DCB test. To provide a constant crack growth rate, the arms were loaded with constant opposite moments. The simulation was repeated with different values of applied moments. In each simulation the crack growth rate was evaluated in a post-processing step by dividing the growth of the crack along one of the free edges by the number of elapsed cycles. Figure **??** compares the results obtained from the thick level set model with experimental data **?** and the Paris curve. The energy release rate along the horizontal axis of the figure is computed from the applied load with beam theory:

$$G_I = \frac{M^2}{bEI} \tag{4.29}$$

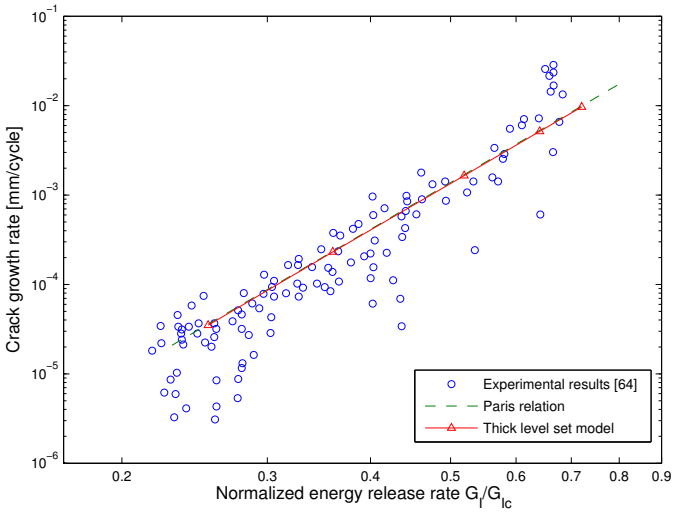

Figure 4.4: Comparison of crack growth rate from level set model with experimental data and Paris relation for DCB tests

where b is the specimen width, E is the longitudinal Young's modulus and I is the second moment of area of the specimen's arm. A perfect match is observed between the results. It should be noted that the Paris curve parameters were obtained by fitting through the same experimental data set and that these parameters were direct input for the TLS simulation. The agreement should therefore not come as a surprise. Nevertheless, for cohesive methods reproducing an input Paris curve has proven to be less successful. The good agreement demonstrates the accuracy of the computed energy release rate under mode I loading using the thick level set interface model.

4ENF SIMULATION

Similarly, a series of simulations with different load levels was conducted to validate the proposed model under mode II loading conditions. Figure **??** shows the boundary conditions of the 4ENF test which provide a constant crack growth rate. The analytical crack tip energy release rate for mode II is related to the applied load P as **?**

$$G_{II} = \frac{3c^2 P^2}{16bEI} \tag{4.30}$$

where c is the distance between load and support (see Fig. **??**). Figure **??** shows a comparison between the simulation results, experimental data and the Paris curve. Again, a very good match is observed, which proves the accuracy of the computed energy release rate under mode II loading.

MIXED-MODE SIMULATION

Figure **??** shows the finite element model for mixed-mode simulations.

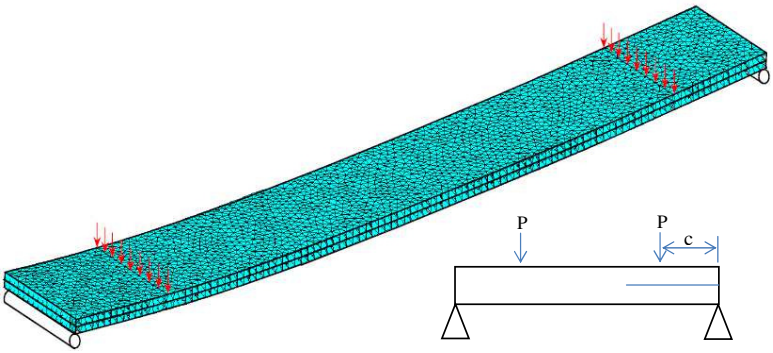

Figure 4.5: Finite element model of 4ENF test

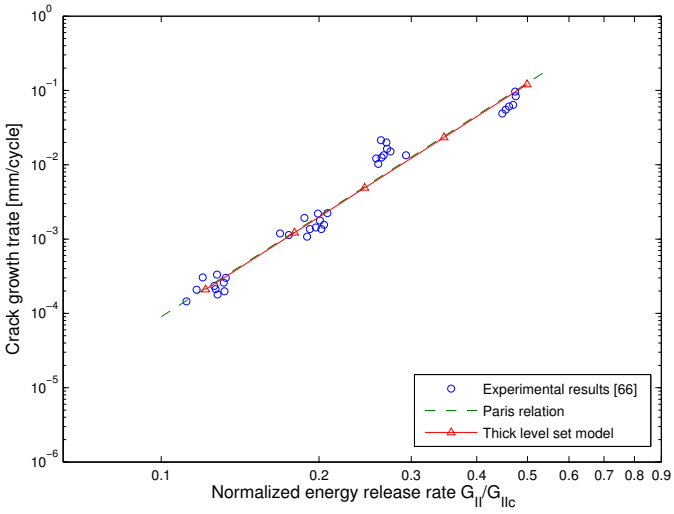

Figure 4.6: Comparison of crack growth rate from thick level set model with experimental data and Paris relation for 4ENF tests

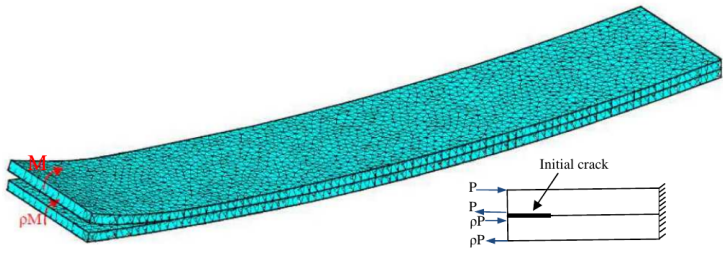

Figure 4.7: Finite element model of mixed-mode test

Two unequal moments were applied on the specimen with a fixed ratio ρ **?**:

$$\rho = \frac{1-\frac{\sqrt{3}}{2}}{1+\frac{\sqrt{3}}{2}} \tag{4.31}$$

which results in a mode ratio of 50 %, with analytical pure mode energy release rate contributions defined as **?**

$$G_I = G_{II} = \frac{3}{4\left(1+\frac{\sqrt{3}}{2}\right)^2}\frac{M^2}{bEI} \tag{4.32}$$

The results of the simulations are again compared with experimental data and the fitted Paris curve (see Fig. **??**). An excellent agreement is observed between the results demonstrating that the thick level set interface approach does not only allow accurate computation of the energy release rate, but also accurate decomposition of this quantity into pure-mode contributions.

4.3.2. CIRCULAR DELAMINATION TEST

The simulation of delamination propagation at the interface of an isotropic circular plate under mode II loading was performed. The radius of the plate was 100 mm with a total thickness of 4 mm and a non-circular pre-crack at the interface of the plate. Considering the symmetry of the plate with homogenized properties, only one quarter of the specimen was simulated (see Fig. **??**). Two layers of 6-node wedge elements were connected with interface elements. Table **??** presents the input values for this simulation.

Table 4.2: Material properties **?** and numerical inputs for circular plate simulation

ν	E	G_{IIc}	C_{II}	M_{II}	l_c	η
0.3	60000 MPa	0.8 N/mm	0.0669 mm/cycle	6.37	5 mm	2.73

The Paris law parameters were taken from **?**. A single point load was applied at the center of the plate. It has been demonstrated in **?** that due to the large displacement of

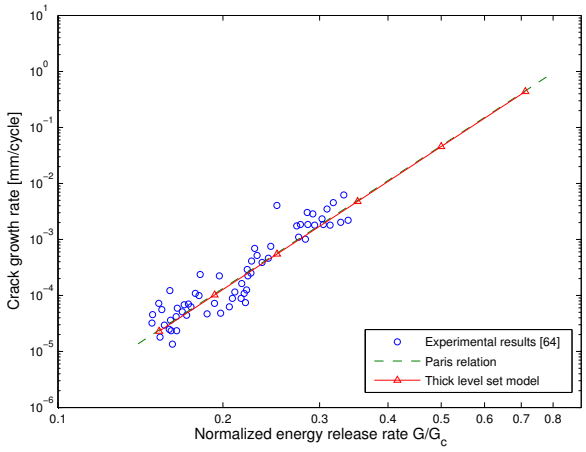

Figure 4.8: Comparison of crack growth rate from thick level set model with experimental data and Paris relation for mixed-mode tests

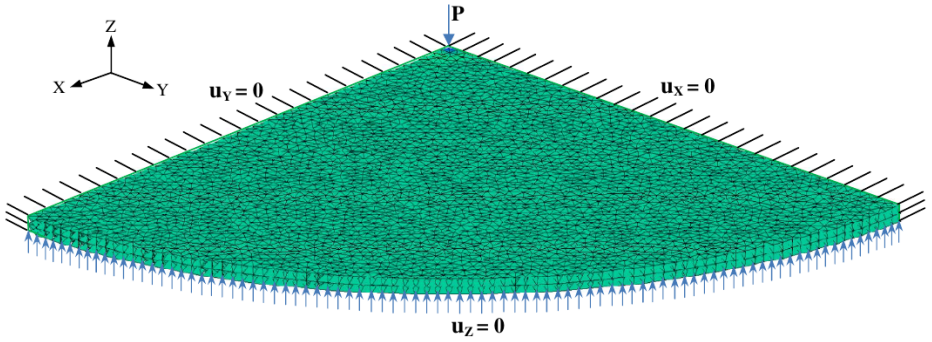

Figure 4.9: Boundary conditions in circular delamination simulation

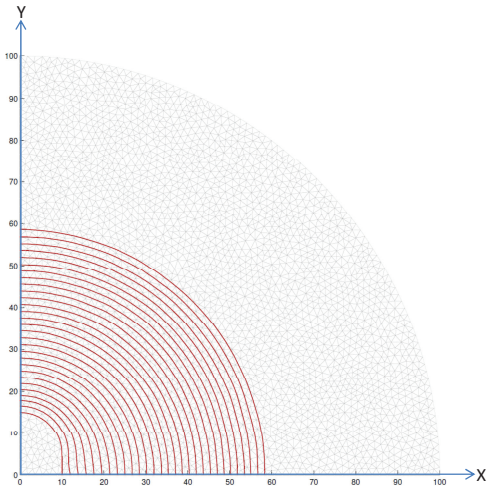

Figure 4.10: Evolution of damage front in circular delamination simulation

the laminate, a geometrically nonlinear analysis needs to be performed for this problem. To show the ability of the model to track non-self-similar crack growth a non-circular pre-crack is used as initial condition. Figure **??** shows crack propagation at the interface of the plate. It can be observed that the crack develops into a circular shape. This circular shape corresponds to experimental observations in the quasi-static NAFEMS benchmark **?** and the simulation in **?**. Figure **??** shows the location of the damage front along X and Y axes versus the number of elapsed cycles. At the beginning of the delamination process the growth rate is higher in X direction and it becomes equal with the growth rate in Y direction as the crack front tends to the circular shape. It is also observed that the crack growth rate decreases rapidly as delamination develops away from the center of the laminate which can only be captured by considering geometrical nonlinearity. The presented results demonstrate the 3D capability of the model to capture the evolution of the delamination front shape.

4.3.3. DELAMINATION AND SPLITTING IN A NOTCHED LAMINATE

To illustrate the capability of the model to capture the delamination front shape in more complex cases, the damage growth in a CFRP $[90/0]_s$ laminate with a central notch under tensile fatigue loading is studied. Figure **??**a shows a schematic figure of this laminate. Figure **??** illustrates the schematic picture of the damage pattern in a notched laminate based on the experimental results, presented by Spearing et al. **??**. The failure mechanisms consists of delamination between 0° and 90° layers around the notch, a split in the 0° layer and transverse cracks in 90° plies. Three planes of symmetry were used to reduce the size of the computational model. The model of 16 mm long and 12 mm wide was composed of one 0° and one 90° layer with thickness of 0.125 mm. Each ply was modeled with one layer of 2D triangular plane stress elements, bonded with interface elements to model delamination. In absence of out-of-plane displacement degrees of

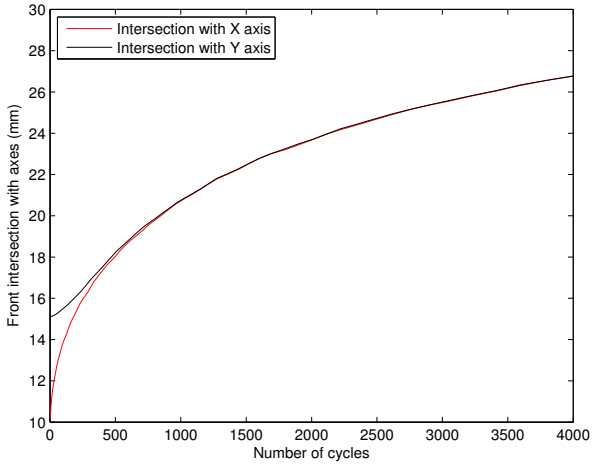

Figure 4.11: Damage front location versus number of cycles in circular delamination simulation

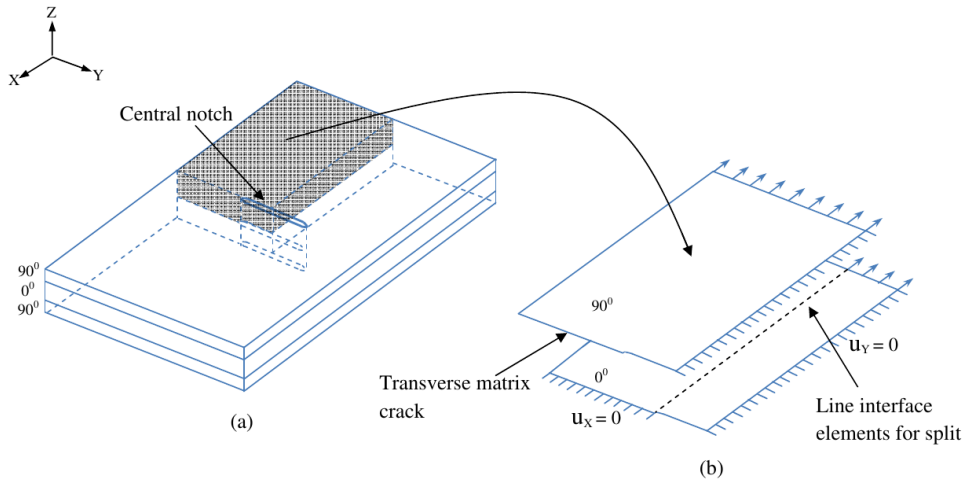

Figure 4.12: Notched laminate: a) laminate geometry b) loading and boundary conditions (interface elements between plies are not visualized)

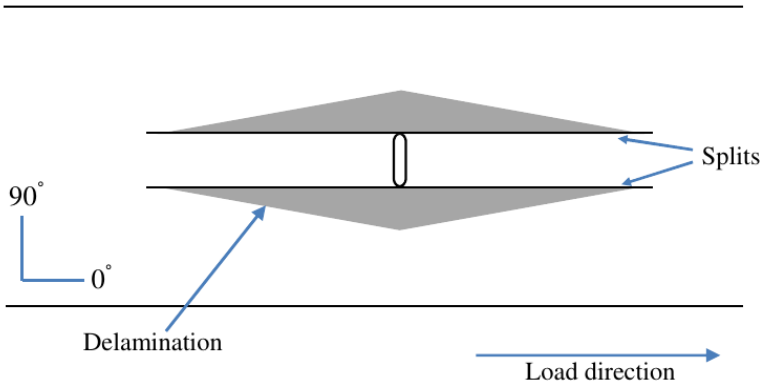

Figure 4.13: Schematic of the damage pattern in a notched laminate based on the experimental results, adapted from Spearing et al. **??**

freedom, possible opening of the interface is ignored. This is reasonable for the present case in which delamination growth is dominated by shear loading. The same strategy has been applied successfully to the simulation of a similar case under quasi-static loading **??**.

Additionally, line interface elements were inserted in the 0° ply perpendicular to the notch (see Fig. **??**b) to model the split in this layer. The formulation for the interface thick level set model on a line is a simplification of the surface model formulation presented in section **??**. For the split the energy release rate can be computed from the closed form integral in Eq. (**??**); therefore, an additional system of equations in Eq. (**??**) is not needed for the split. This is because at the interface of the 2D elements instead of a damage front only a damage tip grows, and consequently in 2D the nodal values along the front obtained from Eq. (**??**) do not exist anymore.

Because the transverse crack in the 90° ply is expected to develop before the delamination **?** it is assumed to be present from the start of the simulation. The transverse crack was modeled by not applying the symmetry boundary conditions to the 90° ply in the plane of the notch (see Fig. **??**b).

The specimen was loaded with a maximum tensile stress of 300 MPa. The input values of the parameters used in this simulation are presented in Table **??**.

Table 4.3: Input values for simulation of notched laminate

E_1 **?**	E_2 **?**	G_{12} **?**	ν_{12} **?**	l_c
135000 MPa	9600 MPa	5800 MPa	0.31	0.3 mm
G_{II}(delamination)**?**	G_{II}(split)**?**	M_{II}	C_{II}	η
0.6 kJ/m^2	0.36 kJ/m^2	7	0.8 mm/cycle	2.73

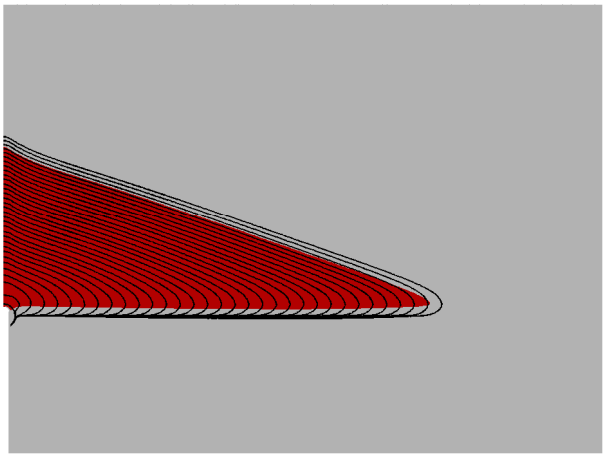

Figure 4.14: Simulation of notched laminate: The final shape of the fully damaged zone corresponds with experimental observations (red area), the damage front evolution visualized with black lines

The delamination in this test is dominated by mode III and mode II and the split is governed by mode II shear loading. Therefore, assuming $G_{II_c} = G_{III_c}$, only the values of mode II fracture energy for delamination and splitting are needed. These values are assumed the same as the values used in **?**.

Figure **??** illustrates the evolution of the predicted delamination front shape. The figure shows that the delamination starts from a small predefined circular damage front around the notch and develops into a self-similar triangular pattern which is in agreement with experimental observations. The fact that the delamination front is completely different from the initial shape of the damage front indicates the suitability of the thick level set method for modeling delamination in complex cases. Due to the lack of experimental data for fracture energy and Paris law parameters, the validation for this case is limited to a qualitative comparison in the delamination growth pattern, which agrees well with the experimental observations.

4.4. CONCLUSIONS AND DISCUSSION

In this chapter a 3D mixed-mode model is proposed for modeling delamination and splitting under fatigue loading. To develop the model the thick level set method is combined with interface elements for a new definition of damage in the constitutive law of interface elements. In this model, the thick level set method provides an accurate nonlocal computation of energy release rate and allows to track the arbitrary shape of the

damage front, while the interface elements are used to define the discontinuity. The Paris relation is used to define the cyclic effect of fatigue loading for which the thick level set method is very suitable. The validation of the model against mode I, mode II and mixed-mode tests proves the accuracy of the computed energy release rate as well as of its decomposition in pure mode contributions. The 3D capability of the model to capture the delamination front shape was proved with simulating a circular delamination test and a notched laminate. It is observed from these simulations that the level set method allows to predict the shape of the delamination front without any prior knowledge of the final front shape.

5

CONCLUSIONS AND RECOMMENDATIONS

5.1. CONCLUSIONS

The main objective of this work was developing a 3D model for simulating delamination in laminate composites under high-cycle fatigue loading. This requires embedding the Paris law for computing the local values of crack growth rate and using an accurate method for computing the Paris law input values of energy release rate. Moreover, a method capable of representing crack propagation is needed to impose crack growth. Meeting these requirements is problematic for existing numerical fatigue models. Fracture mechanics based models have difficulties with arbitrary representation of the crack front through the elements which is because of using the VCCT for computing the energy release rate. On the other hand, damage mechanics based cohesive models lack an accurate computation of energy release rate and the possibility to directly impose the crack growth rate computed from the Paris law. These models need to use extra treatments like crack tip tracking algorithms to improve the accuracy of locally extracted energy from the cohesive law.

The novelty of this work is combining the level set method for describing the crack growth with accurate methods of computing the energy release rate. This provides an alternative for the current research approaches which try to improve the cohesive fatigue models. Two different approaches have been followed to develop level set fatigue models. First, in chapter **??** a level set model for delamination has been presented based on a fracture mechanics approach previously developed for quasi-static delamination analysis with large finite elements. This approach is very suitable for embedding the Paris law in a numerical framework because the computed local values of crack growth rate can be directly used to update the level set field. In contrast with the classical fracture mechanics based fatigue approach with the VCCT, the proposed level set model does not require the front to be aligned with the element boundaries. Instead the front is placed inside the elements at the location specified with the level set method. The model is com-

prised of two sub-models: a cracked laminate model and a crack growth model which are solved sequentially. The cracked laminate model provides a mechanical analysis of a structure and calculate the displacement field in a partially delaminated laminate using a special kinematic formulation. The assumption of shell theory in the element formulation removes the stress singularity from the displacement field around the crack front and allows to accurately capture crack growth with a relatively coarse discretization. The second sub-model takes the displacement from the cracked laminate model and computes the energy release rate. The computed energy release rate is used in combination with the Paris law to find the crack growth rate at the crack front. Based on this velocity the level set field is updated. The new level set field implicitly defines the new crack front location. The proposed model accurately predicts the crack growth rate and delamination growth pattern due to the following features:

- Mesh-independent definition of the crack front with the level set method that enables the method to analyze self-similar and non-self similar crack growth
- Accurate computation of the energy release rate and its pure mode components using the modified version of the VCCT method developed in **??**
- Accurate computation of the mode ratio along the crack front
- The possibility to directly impose the crack growth rate computed from the Paris law as level set velocity

The load ratio effect on fatigue crack propagation has been investigated which shows the possibility to include such effects in the model. Although, this fatigue level set model is accurate and the presented front shape is continuous and smooth, the model uses a special element formulation to represent the kinematics of a partially delaminated laminate, which limits the applicability of the model.

The idea of using the level set method for modeling fatigue crack growth was further pursued in chapters **??** and **??** for a second alternative model by developing the thick level set interface approach for modeling delamination and splitting in composites. The proposed method keeps the suitability of the level set model for fatigue modeling of the first model while using interface elements to overcome the limitations of the model proposed in chapter **??**. This provides a discontinuous damage model which can also be applied to multiple delaminations and other failure processes. To develop this new approach the thick level set method (TLS) **?** has been linked to the interface elements using a new definition for damage in the constitutive law of interface elements. Similar to the cohesive zone method there is a damage variable defined which changes gradually from 0 to 1. However, unlike the cohesive zone method damage, this damage is not a direct function of the displacement jump. Instead, the damage variable is defined as a predefined function of the nearest distance to a moving front which results in a band of damage with a predefined length l_c between sane and fully damaged material. Similar to the continuum thick level set method a staggered solution scheme is used in which the displacements and damage growth are computed sequentially. In each time step the finite element model composed of solid elements and interface elements is responsible for mechanical analysis, after which energy release values are computed by solving a

second system of equations defined on only a subdomain of the interface. A non-local fracture mode ratio is also computed, which only varies in direction along the front, not perpendicular to it. This is in contrast with the cohesive zone methods where the locally computed values of mode ratio can vary along the length of the cohesive zone. Finally, the energy release rate and mode ratio are related to the damage development with Paris law. The main features of the developed thick level set interface method are listed below:

- Accurate non-local computation of the energy release rate
- Accurate non-local computation of the mode ratio using the non-local computing of pure mode components of the energy release rate
- Algorithmic robustness of the staggered solution scheme
- Using interface elements this method can be applied to failure processes other than delamination (e.g. splitting or matrix cracking)
- Using the level set method to define the crack growth allows the prediction of delamination growth based on the mechanics of the problem without predefinition of the growth pattern

In chapter **??** the formulation of the thick level set method has been presented and the verification of the method for simulating the initiation and propagation of delamination in composites under quasi-static loading is presented. A strength based initiation criterion has been developed to handle damage initiation under quasi-static loading. The sensitivity analysis of numerical input parameters of the model has been performed. With this analysis the influence of input parameters on the efficiency of the model is investigated and the obtained results are summarized as follows:

- The specifications of an ideal damage function for the thick level set interface method is analyzed and an efficient damage function is proposed based on this analysis
- The effect of the integration scheme on the results is investigated where sub-triangulation of the finite elements that are intersected by the bounds of the damaged zone has been shown to improve the accuracy of the results.
- The effect of the predefined length of the damaged band (l_c) on the results is examined which proves that the model is not sensitive to it. As the required element size is linked to the length of the damage band, the insensitivity to this length provides the freedom to use a coarser mesh. In contrast with cohesive zone models, the size of the numerical fracture process zone can be increased to alleviate mesh requirements without causing spurious initiation of damage, because the initiation criterion does not depend on l_c.

After introducing the formulation of the thick level set interface method and investigating the sensitivity with respect to the model parameters in chapter **??**, the extension of the method for simulating fatigue crack growth has been presented in chapter **??**. The proposed fatigue model has been applied to analysis of delamination and splitting. To

extend the model for fatigue analysis, the Paris law is embedded in the model. Here, the suitability of the thick level set interface method for 3D fatigue analysis becomes evident, because this method provides an accurate input energy release rate for the Paris law and allows to directly impose the computed crack growth rate from the Paris law to update the level set field and the crack front location.

The developed models in this thesis allow for accurate simulation of self-similar and non-self-similar crack propagation under pure and mixed-mode loading conditions. The fracture mechanics level set model presented in chapter **??** is more suitable for delamination modeling in large structures, as it can use large elements for simulation . On the other hand, the thick level set interface model proposed in chapters **??** and **??** enables modeling of other failure mechanisms like splitting and matrix cracking under quasi-static and fatigue loading conditions. Although the presented models in this thesis have been initially developed for composite materials, they can be applied for modeling cracking in adhesive interfaces between metals or in microelectronics (thin film interfaces) where delamination also takes place.

It is envisioned that, developing the numerical frameworks capable of simulating the failure process in composites under fatigue, will allow for prediction of the failure process in composites. This enables engineers to design structures based on the "slow growth" approach **?**, allowing for some growth of damage. Therefore, engineers can consider higher acceptable load levels which results in lighter and cheaper composite structures. Moreover, the developed numerical frameworks can improve the safety of composite structures as the prediction of crack growth pattern facilitates the effective application of preventive methods like Z-pinning **?** and stitching **?**.

5.2. RECOMMENDATIONS FOR FUTURE WORK

THE THICK LEVEL SET INTERFACE MODEL FOR MODELING INITIATION AND ONSET UNDER FATIGUE

In chapter **??** of this thesis modeling crack initiation under quasi-static loading has been addressed. There is also the potential to extend the thick level set interface method for modeling initiation under cyclic loading. One issue regarding this extension is developing a proper initiation criterion for fatigue, considering the fact that under cyclic loading a crack can initiate at a stress lower than the value of quasi-static strength. Moreover, in the transition phase between damage initiation and crack propagation the resistance against damage growth is less than the fracture energy G_c. Substituting the expression for the critical energy, $Y_c(\phi)$, that has been proposed to cover both initiation and propagation under quasi-static conditions into the Paris law could be an elegant solution, but the validity of this idea should be investigated.

COMBINING XFEM WITH THICK LEVEL SET METHOD FOR MODELING MATRIX CRACKING UNDER FATIGUE LOADING

Although there is a possibility to model matrix cracking by inserting interface elements at the possible crack locations in the mesh, a mesh-independent representation of matrix cracks is preferable, because, due to the large number of possible matrix cracks inside a laminate, meshing each of them can become very cumbersome. In the extended finite element method (XFEM) the meshing of possible crack paths is not needed which

provides more flexibility than using interface elements. To model matrix cracking under fatigue loading developing an XFEM thick level set method is a promising direction. To develop this model a free energy formulation needs to be defined for elements inside the damaged band, and based on this formula the local values of energy release rate can be computed for these elements. Combining this XFEM-TLS method with the developed TLS-interface method can provide a fatigue numerical framework in which different failure mechanisms in composite laminate such as delamination, splitting and matrix cracking are efficiently taken into account. Aside from modeling matrix cracks, in a general condition when the interface between two faces of the crack is not a flat surface or in the 2D case when the crack front does not follow a straight path more treatments need to be considered to define and update the damage distribution.

DEVELOPING THE CONTINUUM THICK LEVEL SET FATIGUE MODEL

Considering the suitability of the thick level set method for fatigue analysis shown in this thesis, there is also the possibility for developing a continuum thick level set fatigue model. This model can be used for instance for micromechanical analysis of composite materials. In addition, this model can have applications in homogeneous materials like metals where the crack path is not defined in advance.

COMPARING THE EFFICIENCY AND 3D CAPABILITIES OF THE PROPOSED FATIGUE MODELS AGAINST EXISTING COHESIVE FATIGUE MODELS

Most of the recent developed cohesive fatigue models are only validated against standard experiments like DCB, 4ENF or mixed-mode test and the 3D capability of these models has not been properly investigated. The accuracy and efficiency of these models needs to be compared with the level set fatigue models developed in this thesis, to clarify the advantages and disadvantages of both approaches.

Recently a new method is proposed in **?** which uses the cohesive zone method along with the level set method for simulating delmination growth under fatigue. Thorough evaluation of the performance of this model against 3D cohesive models with crack tip cracking algorithms and the models developed in this thesis is also recommended for future work.

PROVIDING MORE COMPLEX 3D FATIGUE BENCHMARKS

Not many 3D fatigue benchmarks are available in literature for validating the capability of a numerical model to predict the delamination growth pattern. Therefore, there is a need for more experimental work which provides more information about the delamination growth pattern under fatigue loading. Basic experiments should then also be performed to determine the Paris law parameters for the investigated material. The needed parameters for a 3D mixed mode analysis are C_I, C_{II}, C_{mix} and M_I, M_{II}, M_{mix} related to the Eqs. (**??**) and (**??**). The values for each set of C an M (e.g. C_I and M_I) can be extracted from crack growth rate measurements related to each fracture mode, at different levels of energy release rate.

CONSIDERING THE EFFECTS OF ENVIRONMENTAL FACTORS

The effects of environmental factors like humidity or thermal effects are not considered in the model. These could be added by considering their effects on the value of Paris law parameters.

EXTENDING THE VALIDITY OF PROPOSED FATIGUE MODELS TO REGIONS I AND III

The form of the Paris equation used in the developed fatigue models in this thesis only covers region II of the typical crack growth pattern. However, some additions to the general form of the Paris equation have been proposed in order to extend its validity to regions I and III **???**. These variants of the Paris equation can be implemented in the presented fatigue models to extend their applicability. This implementation is straightforward. Any change in the expression used for computing crack growth rate from energy release rate will not affect the general structure of the developed numerical frameworks.

ACKNOWLEDGEMENTS

This period of my life passed in the blink of an eye. Thank you god for everything you gave me and enabled me to successfully progress through this phase of my life. This thesis is the result of four and half years of research at the computational mechanics group of CITG faculty of Delft university of technology. While only my name appears as the author of this book, It is most certainly not the result of individual work.

First of all I would like to express my gratitude to my promoter Prof. Bert Sluys for giving me the opportunity to join his group, and for ideal supervision and continuous support of my PhD. Bert, your positive outlook and your trust in my research inspired me and gave me confidence. Your commitment, guidance and encouragement had a very important role in my research. I would like to express my special appreciation and thanks to my copromotor Dr. Frans van der Meer for advising me on my PhD study. He shared with me a lot of his expertise and research insights. The discussions with him were always fruitful and informative to me. Frans, I am so grateful that I am always welcomed for discussions without any set appointment and I will never forget many times that I left your office with the joy of learning new concepts. Frans, I have enormously benefited from your invaluable scientific support, advice and continuous encouragement.

I would like to thank my thesis committee Prof. Moës, Prof. Benedictus, Prof. van Paepegem, Dr. Turon and Dr. Chen for accepting taking part in this committee.

My sincere thank go to Mehdi musivand and Amin karamnejad who have always been genius friend and supportive colleague. I am thankful to Luis Magalhaes Pereira and Kai Li for being such wonderful friends and colleagues. I would like to thank Frank Everdij for his help and support on the computer related issues. I would also thank our kind secretary Anneke Meijer for her help in administration work. I would like to thank all colleagues and staff members of the computational mechanics group for all collaboration and friendship we had during my PhD: Ali Paknahad, Rafid Al-Khoury, Noori, Mohsen Goudarzi, Marcello Malagu, Liting Qiu, Angelo Simone, Behrouz Arash, Erik Simons, Friborz Ghavamian, Jaap Weerheijm, Jafar Amani, Jitang Fang, Lars Voormeeren, Osvalds Verners, Azam Arefi, Prashanth Srinivasan, Tiziano Li Piani, Wouter Steenstra, Yangyueye Cao, Yaolu Liu.

My appreciation extended to my Iranian friends in the Netherlands who have been a great support for me and my family. With the risk of forgetting someone who I definitely should have mentioned, I would like to to thank families Alemi, Madadi, Mirzaei, Najafi, Shahbazi, Bakhshandeh, Chahardowli, Derakhshani, Abouhamzeh, Abbasi, Saeedi, Fasihi, Ghaemi nia, Bornaee, Tohidian, Hoseini nasab, Ahmadi mehr, Karimian, Behdani, Hesan, Rahimi, Kavian, and all members of Hey' at Mohabban Al-Mahdi.

Most importantly I express my great appreciation to my family. I am extremely grateful to my parents for unconditional love and support. I am really proud of you. In fact, it is beyond my ability to compensate even a small part of your support. I would like to

extend my appreciation to my brother and my sisters. Thank you so much for your kindness and support. I also want to thank my parents in-law, brothers and sisters in-low for their love and always backing me.

Last but not least, I express my deepest thank to my lovely wife who has been incredibly supportive and patient during these years. For sure every achievement of my PhD owes also to your support and dedication. To be honest, I can not express my highest appreciation in only a few words. Thank you very much for everlasting love, infinite support and encouragement. Hosein Jan my beloved son, you are a gift from god to me and your mother. I thank you so much for all great time you have provided to us.

Mohammad Latifi
Delft, May 2017

LIST OF PUBLICATIONS

JOURNAL PAPERS

1. **M. Latifi** , F.P. van der Meer , L.J. Sluys, "A level set model for simulating fatigue-driven delamination in composites", International Journal of Fatigue, 3: 37-48, 2015

2. **M. Latifi** , F.P. van der Meer , L.J. Sluys, "An interface thick level model for simulating delamination in composites", International Journal of numerical methods in engineering, 2016

3. **M. Latifi** , F.P. van der Meer , L.J. Sluys, "Fatigue modeling in composites with the thick level set interface method", Accepted for publication in Composites Part A: Applied Science and Manufacturing

CONFERENCE PROCEEDINGS

1. **M. Latifi** , F.P. van der Meer , L.J. Sluys, "Modeling fatigue -driven delamination using a thick level set interface model", ECCM17: 17^{th} European Conference on Composite Materials, Munich, Germany, 26-30 June, 2016

2. **M. Latifi** , F.P. van der Meer , L.J. Sluys, "A new interface damage model for modeling delamination using thick level set method", VII European congress on numerical methods in applied sciences and engineering, Greece, 5-10 June, 2016

3. F.P. van der Meer , **M. Latifi** , A. Amiri-Rad, "Three level set based models for fatigue crack growth analysis", 6^{th} ECCOMAS Thematic Conference on the Mechanical Response of Composites, Eindhoven, Netherlands, 2017

4. **M. Latifi** , F.P. van der Meer , L.J. Sluys, "A thick level set interface model for simulating fatigue-driven delamination in composites", 5^{th} Intern. Conference on Mechanical Response of Composites (Composites 2015), Bristol, United kingdom, 7-9 September, 2015

5. **M. Latifi** , F.P. van der Meer , L.J. Sluys, "Finite element interface model for simulating delamination using a thick level set approach", CFRAC 2015, the Fourth International Conference on Computational Modeling of Fracture and Failure of Materials and Structures Paris, France, 1-3 June, 2015

6. **M. Latifi** , F.P. van der Meer , L.J. Sluys, "Simulation of delamination growth in laminated composites under high-cycle fatigue using a level set model", 11th World Congress on Computational Mechanics, Barcelona, Spain, 20-25 July, 2014

7. **M. Latifi** , F.P. van der Meer , L.J. Sluys, "A level set model for computational modeling of fatigue-driven delamination in laminated composites", Intern. Conference on Aging of Materials and Structures, Delft, The Netherlands, 26–28 May, 2014